Since 1955

Strojniški vestnik
Journal of Mechanical Engineering

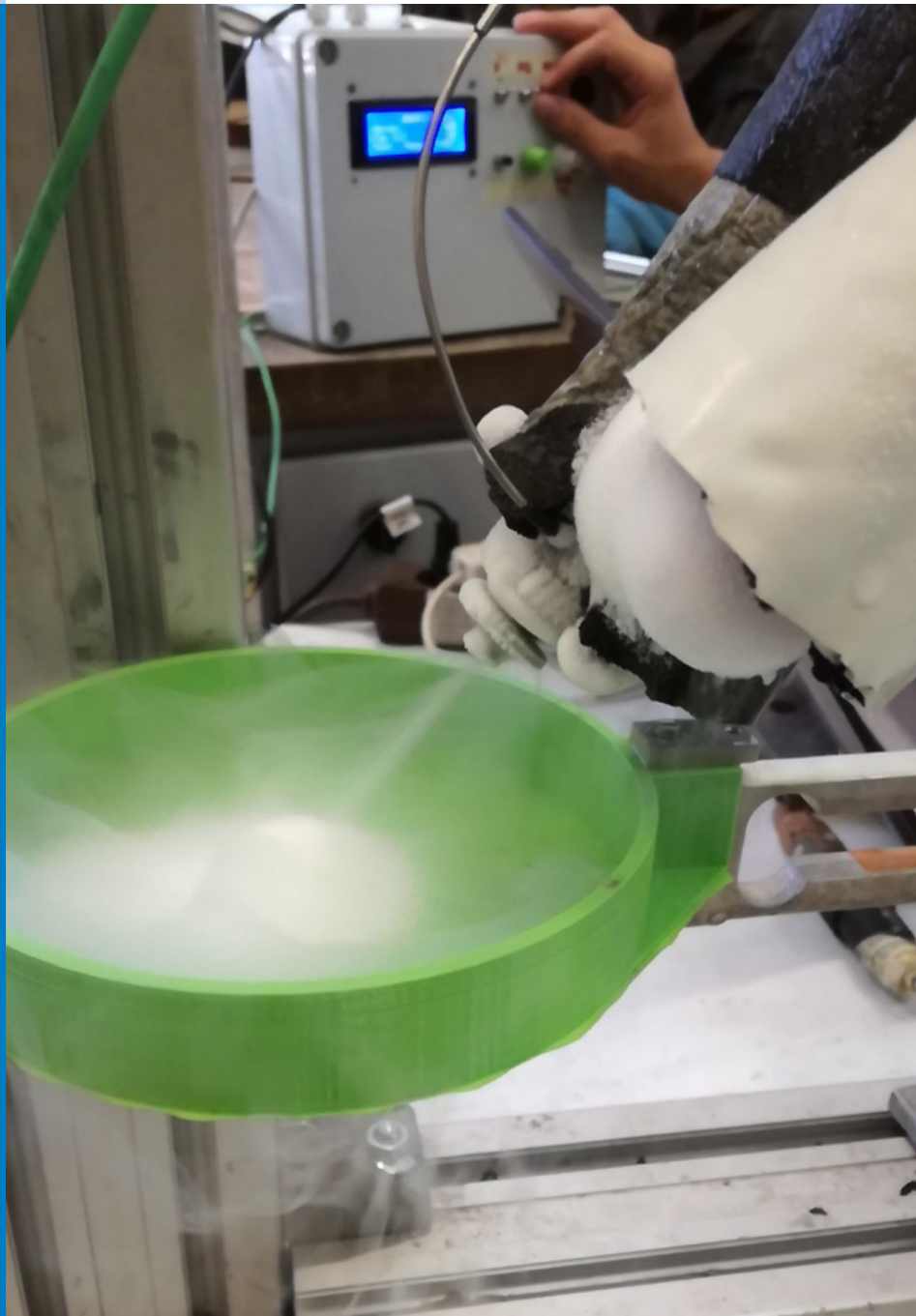

no. 10
year 2017
volume 63

Strojniški vestnik – Journal of Mechanical Engineering (SV-JME)

Aim and Scope
The international journal publishes original and (mini)review articles covering the concepts of materials science, mechanics, kinematics, thermodynamics, energy and environment, mechatronics and robotics, fluid mechanics, tribology, cybernetics, industrial engineering and structural analysis.
The journal follows new trends and progress proven practice in the mechanical engineering and also in the closely related sciences as are electrical, civil and process engineering, medicine, microbiology, ecology, agriculture, transport systems, aviation, and others, thus creating a unique forum for interdisciplinary or multidisciplinary dialogue.
The international conferences selected papers are welcome for publishing as a special issue of SV-JME with invited co-editor(s).

Editorial Office
University of Ljubljana, Faculty of Mechanical Engineering
SV-JME, Aškerčeva 6, SI-1000 Ljubljana, Slovenia
Phone: 386 (0)1 4771 137
Fax: 386 (0)1 2518 567
info@sv-jme.eu, http://www.sv-jme.eu

Print: Papirografika Bori, printed in 300 copies

Founders and Publishers
University of Ljubljana, Faculty of Mechanical Engineering, Slovenia
University of Maribor, Faculty of Mechanical Engineering, Slovenia
Association of Mechanical Engineers of Slovenia
Chamber of Commerce and Industry of Slovenia, Metal Processing Industry Association

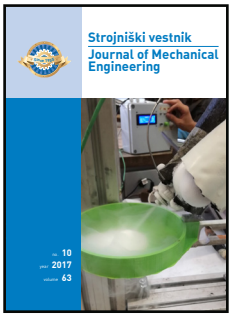

Cover: Ice Abrasive Waterjet process (IAWJ) utilises ice particles as abrasive material mixed in high speed waterjet to cut materials or modify surfaces. Ice particles with temperature below 100 °C have hardness similar to mineral abrasive. The technology attracted interest from food processing industry, medicine and from companies that have to fulfil special requirements when machining advanced materials.

Image Courtesy:
Laboratory for Alternative Technologies, Faculty of Mechanical Engineering, University of Ljubljana, Askerceva 6, 1000 Ljubljana, Slovenia, EU
http://www.fs.uni-lj.si/lat/

General information
Strojniški vestnik – Journal of Mechanical Engineering is published in 11 issues per year (July and August is a double issue).

Institutional prices include print & online access: institutional subscription price and foreign subscription €100,00 (the price of a single issue is €10,00); general public subscription and student subscription €50,00 (the price of a single issue is €5,00). Prices are exclusive of tax. Delivery is included in the price. The recipient is responsible for paying any import duties or taxes. Legal title passes to the customer on dispatch by our distributor.

Single issues from current and recent volumes are available at the current single-issue price. To order the journal, please complete the form on our website. For submissions, subscriptions and all other information please visit: *http://en.sv-jme.eu/.*

You can advertise on the inner and outer side of the back cover of the journal. The authors of the published papers are invited to send photos or pictures with short explanation for cover content.

We would like to thank the reviewers who have taken part in the peer-review process.

ISSN 0039-2480

The journal is subsidized by Slovenian Research Agency.

Strojniški vestnik - Journal of Mechanical Engineering is available on http://www.sv-jme.eu, where you access also to papers' supplements, such as simulations, etc.

Contents

Strojniški vestnik - Journal of Mechanical Engineering
volume 63, (2017), number 10
Ljubljana, October 2017
ISSN 0039-2480

Published monthly

Editorial

The Management and Innovative Technologies (MIT) conference and workshop was held in Fiesa, Slovenia from 5th to 7th of September 2016. The event was a three-day debate on the purpose and practice of technology, innovation and creativity in action. It was human-sized allowing intensive and tailored conversation and connecting, sharing of knowledge and experience, but with enough international and disciplinary diversity to ensure breadth and the opportunity to network and develop potential partnerships and collaborations, with a chance to relax, reflect and gain some inspiration. The scientific part was devoted to new and emerging manufacturing technologies as well as to process modelling, control and automation. This year novelty was a form of presentations; the participants were encouraged to present papers in the form of PechaKucha. Although these from of presentation is mostly used by architects and economists it was well accepted by participants from academia and industry: mechanical and electrical engineers, geologists, physicists, sociologists.

Eight selected papers, published in the conference proceedings, are significantly extended, improved and published in this thematic issue. Three contributions are related to manufacturing of thermoplast, thermoset and metallic products by additive technologies. The papers present approaches to improve the homogeneity of the manufacturing space and the selection of the optimal process parameters. The Fused Deposition Modelling (FDM) has a lack of producing smooth surfaces, thus a hybrid process consisting of FDM and milling is presented. The rest of the selected papers are related to waterjet technology. Pulsating waterjet offers several advantages compared to continuous waterjet technology. The discontinuous sequence of impacts is creating a high momentary stresses in the impingement zone. As a result, the peak pressure acting on the surface is not the stagnation pressure, but the significantly higher water hammer pressure. The erosion effect of both technologies are compared when machining various aluminium alloy with modified surface as well as of concrete and carbon nanotube concrete composite (CNT/concrete composite). Although CNTs are one of the most promising fillers to improve concrete properties, which could lead to further economic and environmental benefits, but we should not forget on the health issues related to nanoparticles. Selective properties of waterjet was sucessfuly used in determination of concrete and concrete composite quality. Another application using selectivity of high-speed waterjet is automatable splicing of steel cord conveyor belts. The waterjet diameter in abrasive waterjet machining depends on the water nozzle and focusing tube diameter, hence also on the wear of both of them. By measuring the abrasive waterjet diameter, the wear of these consumables can be estimated. Furthermore, the measured diameter can be used as an input to the machine control system to adapt the cutting speed and nozzle offset from the contour of the workpiece, therefore enabling quality and accurate cutting regardless of wear of the cutting head components. In order to expand the empirical database of abrasive waterjet technology, the Taguchi method was used and the results are presented in the last paper in this issue.

In addition to the established MIT conference programme, the workshop was run interactively. It was moderated by a sociologist, writer and actor MSc. Paul Levy from University of Brighton. The themes were proposed by participants forming open space sessions. We were discussing about our research and business culture. One of the themes was how far we are ready to cooperate in activities related to military needs.

Joško Valentinčič
guest editor

Strojniški vestnik - Journal of Mechanical Engineering 63(2017)10, 553-558

DOI:10.5545/sv-jme.2017.4365 Original Scientific Paper
Received for review: 2017-01-31
Received revised form: 2017-05-18
Accepted for publication: 2017-05-29

Manufacturing Space Homogeneity in Additive Manufacturing – Electron Beam Melting Case

Alexandre Piaget – Matthieu Museau* – Henri Paris
Univ Grenoble Alpes, CNRS, France

This paper focuses on the manufacturing space homogeneity of the electron beam melting (EBM) technology. An Arcam AB A1 machine is used as tool for experimentations, with titanium (Ti-6Al-4V) as material. The objective of this study is to show the correlation between workpieces geometrical deformations and their position in the manufacturing space. Results show that the position on Z-axis does not affect quality, but there is a strong link in the Z-plane: significant defects appear near the manufacturing space boundaries. First manufactured layers are deformed in the vicinities of the manufacturing space edges. Up to 3 mm of material loss and 8mm of dimensional deformation are measured. Further analyses point that this phenomenon is particularly related to a sintering variation in the powder: there are up to 3 % density difference from the center to borders. To avoid the problem, reduction of the manufacturing space and a supporting strategy are proposed. Defects can also be removed by implementing thermal insulation on the machine or by modifying the beam operation.
Keywords: quality management, additive manufacturing, electron beam melting, manufacturing space homogeneity

Highlights
- *The demonstration of the manufacturing space heterogeneity in the EBM case is presented.*
- *A new method to diagnose the heterogeneity of the manufacturing space and quantify its impacts is experimented.*
- *The homogeneous area in the EBM manufacturing space is identified.*
- *A solution to manufacture parts out of the homogeneous area properly, using supports, is developed.*
- *Solutions to improve the machine in order to make the whole manufacturing space homogeneous are proposed.*

0 INTRODUCTION

The additive manufacturing technologies have become essential tools for modern industry [1] and [2]. Among the different additive manufacturing technologies, electron beam melting (EBM) is able to manufacture a wide range of metallic parts (massive, topologically optimized, lattice structure) [3] and [4]. Compared to selective laser melting (SLM), the EBM technology is still poorly studied [5]. However, there is a strong need to further master this technology. Aeronautic, spatial and also medical fields are particularly interested in mastering the quality provided by this process [6] to [9].

In order to control the quality, without destruction of manufactured parts, test specimens are manufactured simultaneously [10]. By testing those specimens, information about the quality of manufactured parts is obtained. Design for Additive Manufacturing has been studied and provides some information (as swaying, supporting, etc.) for the manufacturing accuracy depending on desired shapes [11] and [12]. Most of the time, specimens are arranged in the edges of the manufacturing space. Previously, several parts showed defects when they were manufactured within certain areas of the manufacturing space. Thus, a question arises about the homogeneity of the manufacturing space. Indeed, heterogeneity could lead to errors in the manufacturing and control processes. This key point that is not addressed in the literature, is the topic of this paper.

Does the position of a part in the manufacturing space have an impact on the final part quality? This problem is approached by studying the geometrical deformation which is the main defect. As defect already occur, there is a need to characterize this space and its heterogeneity, and the way it impacts on the manufactured parts. These characteristics are related to the machine used (described below), but the experimental method can be applied to other machines.

The scope of this study focuses just on the manufacturing space homogeneity. It won't look after the effect of different electron beam set of parameters neither after the CAD effect on manufacturing quality. Parameters that guarantee the quality are known [11] and [12], they are selected for this work and maintained during the study.

1 METHOD

The method consists in manufacture several iteration of a part at different location and observe the differences between every iteration. The first objective of this study is to evaluate the impact of the position in the manufacturing space on the final workpiece

*Corr. Author's Address: Institute of Engineering Univ. Grenoble Alpes, Laboratoire G-SCOP, 46 Avenue Félix Viallet, Grenoble, France, matthieu.museau@g-scop.fr

geometry. Thus, 25 locations of the manufacturing space will be tested during the experimentation.

For the experimentation, the largest manufacturing space available with the machine is needed. But the manufacturing space is limited by the use of software Magics® (Materialise), Build Assembler® (Arcam AB) that reduce the initial manufacturing space (200 mm × 200 mm × 180 mm) to 195 mm in length, 195 mm in width and 180 mm in height.

Otherwise, workpieces will be built without any supporting strategy. Indeed, EBM technology doesn't necessarily involve a supporting strategy to build workpieces [13]. Based on Vayre et al. [11], there is no need to add support to the experimental workpieces because of the experimented workpieces thinness.

1.1 Design of Workpieces

Two kinds of workpieces have been selected for the test (Fig. 1). The first one is a massive workpiece. The second one is a lattice structure. Thus, those workpieces represent the two kinds of geometry cases encountered.

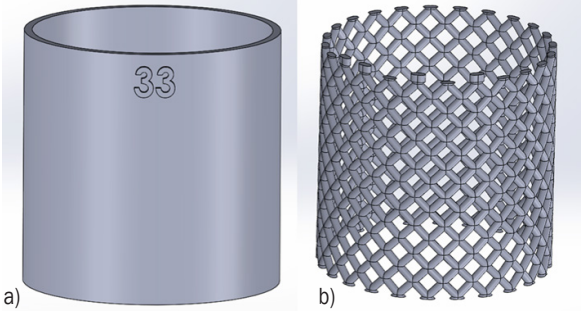

Fig. 1. *Experimentation workpieces; a)massive and b) lattice structure*

The height and the diameter of the pipes are 30 mm. The thickness of the wall for the massive pipe and of the beam for the lattice one is 1 mm. Inside each pipe, two other pipes with different diameters (Ø20 mm and Ø10 mm) are integrated to the experimentation in order to have different thermal conditions. Indeed, the Ø10 mm workpiece always has a Ø20 mm and a Ø30 mm pipes for neighbors while the Ø30 mm workpiece has a number of neighbors depending on its position.

Those parts were designed and converted to stl files with SOLIDWORKS® 2015. The stl tolerance is 3 µm for the deviation parameter and 0.5 degree for the angle parameter.

1.2 Manufacturing Process

The Arcam AB A1 machine [14] and [15] uses an electron beam to melt powder (Fig. 2). The powder from the hoppers is spread over a platform in 50 µm thick layers with a rake. The electron beam sinters the whole of the introduced powder. This increases the thermal and electrical conductivity. Then it locally melts the powder to manufacture the desired geometry. The platform finally goes down of the thickness of a layer and this cycle can be repeated. The accuracy of the electron beam is far lower than the size of the powder (~0.1 mm) [16].

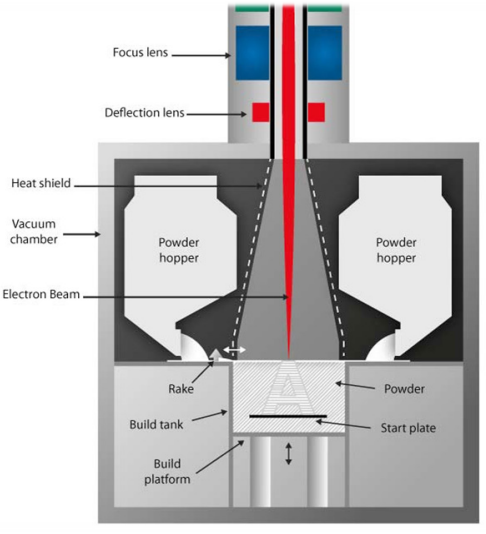

Fig. 2. *Arcam EBM systems, schematic architecture* [11]

In order to qualify the geometric defect, some parameters have to be chosen. Ti-6Al-4V powder from Arcam AB is used for the study as it's the most used material in EBM [16]. Arcam theme melt 50 µm for Ti-6Al-4V is selected for the whole experimentation.

The experimentation consists in testing 25 locations of the manufacturing space. Grouped by three, workpieces will be repeated on each locations of a unique altitude of the manufacturing space in order to avoid scan length problems [17]. By measuring each workpieces, defects are characterized and linked to the location.

Our calibration process fits with ARCAM recommendations [18] and was done before manufacturing.

1.3 Measurement of Printed Workpieces

Observations show that the defect appears in first layers: the bottom of some parts is deformed. Thus,

the objective is to measure the first layer distortion. Note that, as the lower part of the workpieces is analyzed, the workpieces are represented upside down later in the document.

In order to measure the first layer distortion, a three-dimensional optical control machine (Vertex from Micro-vu) is used. This equipment is able to focus on a specific point and calculate the height of this point from the focal range. The surface is controlled at 24 points (every 15 degrees) distributed all along the surface. The measurement precision is ± 9 µm. From this, we recovered the difference between the nominal height and the measured one (Fig. 3a).

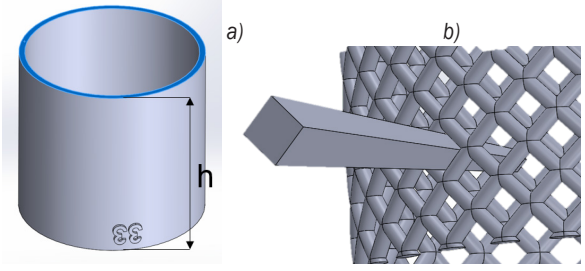

Fig. 3. *Representation of the measurement processes: a) massive and b) lattice workpieces*

Measuring the first layer deformation does not provide information on the deformation of the following layers. With the lattice structure, the target is to measure the defect spread through several layers. Consequently, the measurement protocol has to be adapted. A tool has been created to control the external geometry of the lattice pipe (Fig. 3b). This tool is a checking gauge calibrated to detect a ±10 % change in the shape of every cell of the part. Errors may occur depending on the surface quality and local deformation, in such case, the cell is also declared defective. This way, we may have information about the defect on the workpiece: its angular position and altitude.

2 RESULTS

Measures are presented in a radar chart in order to represent the size and the angular position of the defect. So, in the diagrams, the more a point is far from the middle, the more the defect is important. As shown in Fig. 4, defect occurs on some workpieces (on both pictures, the left workpiece fits the CAD model and the right one includes a deviation from the model). The defect is materialized in two forms: material loss and geometric deformation. Lattice structures show both failure (Fig. 4b): between the well-shaped and the defective workpiece, deformations are observed in first layers (missing) and in diamond meshes (misshapen).

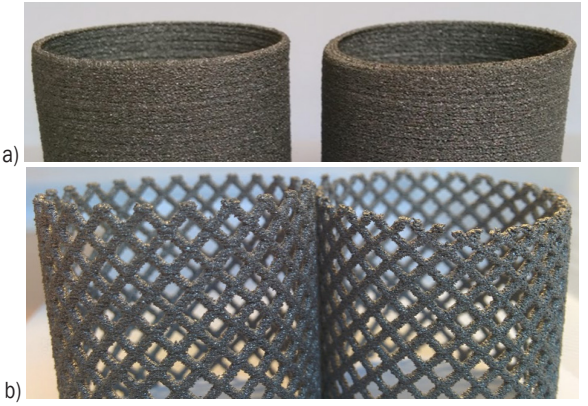

Fig. 4. *a) Massive and b) lattice workpieces placed upside down*

Fig. 5 presents the results for the massive workpiece. From these results, occurrences of defects on nearby workpieces of borders are observed. Furthermore, the defect is more critical as the point observed on a workpiece is close to the boarders. The biggest gap measured between the nominal and the manufactured surface is 3 mm high. Whereas, for the inner workpieces, measured defects are smaller than 0.8 mm. This value corresponds with the 50 µm roughness owned by the material resource **[17]**.

Fig. 6 presents results for the lattice workpieces in numbers of defective cells (±10 % change in the shape) for an angular position and starting from the bottom of a workpiece. The same conclusion can be drawn as there is no defect in the inner workpieces and the external workpieces have an outwardly directed defect. In addition, the highest number of defective cells for one angular position is four, it is equivalent to 8 mm high from the first layer.

Another interesting point is that a group of workpieces has undergone a 2 mm mechanical shifting (Fig. 7). The 3 corresponding curves are overlapping (located at the bottom left in Fig. 6) because workpieces cells are all affected in the same way.

What is interesting in this point is that it brings other elements to explain and understand the sources and consequences of the deformation phenomenon, although this shifting is not repeatable.

Fig. 7 is a photography that shows the encountered problem. This shifting is in the movement direction of the rake.

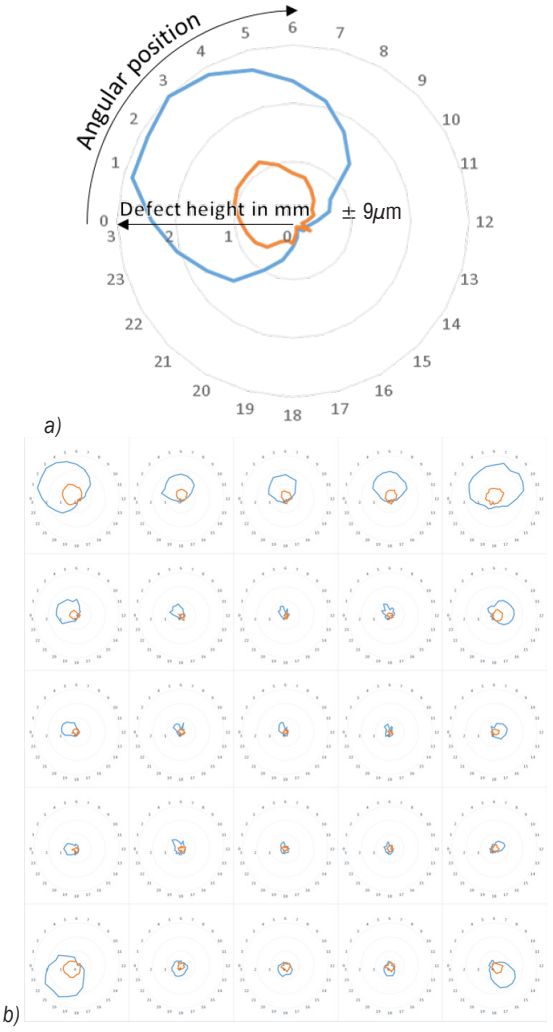

Fig. 5. *a) Example and b) defect cartography of the massive workpieces (blue: Ø30 mm, orange: Ø20 mm)*

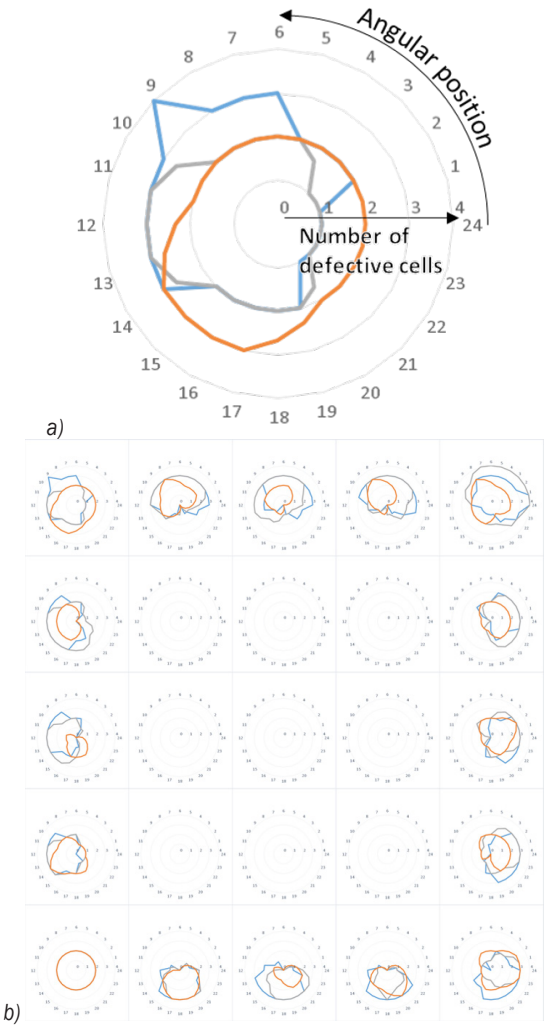

Fig. 6. *a) Example and b) defect cartography of the lattice workpieces (blue: 30 mm, orange: 20 mm, grey: 10 mm)*

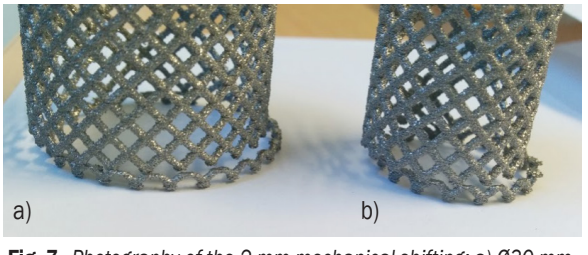

Fig. 7. *Photography of the 2 mm mechanical shifting: a) Ø30 mm, and b) Ø20 mm*

Finally, observations and measures show that only the workpieces near the boarders of the manufacturing space are reached by the defects.

In corners, the defect reaches its highest value: the maximal height of the defect is 8mm from the first layer. Those defects are significant enough to justify a thorough study with the aim to master and avoid this problem.

3 DISCUSSION

3.1 Hypothesis

To explain the phenomenon, several hypotheses have been expressed. First, the electron beam hypothesis has been selected. Indeed, to reach boarders, the electron beam has to undergo an important deflection that leads to change the shape of the beam from a circle to an ellipse. The energy broadcasted to the powder is lower as the surface of transmission gets bigger. It generates a decrease in the temperature that prevents the melting of the powder. This decrease

might explain the location of the defect and the defect type also.

The second hypothesis concerns the workspace in the machine. At the borders of the manufacturing space, next to the sintered powder, there are cold powder and the metal enclosure that might absorb the energy of the sintered powder and thereby generate a loss of temperature. As Ti-6Al-4V is a bad thermal conductor [19], this phenomenon might just take place at the border between the sintered powder and the cold powder. Lowering temperature locally leads to the same conclusion as the electron beam hypothesis.

A third hypothesis arises from the mechanical shifting (Fig. 7). As a portion of the workpiece has been moved in the rake direction, this hypothesis involves the rake: when the rake spreads the powder out, it can move the matter underneath by the thrust applied on the powders. That might cause deformation and matter loss in the workpiece.

The first and the second hypothesis might explain the difference between the workpieces but they don't solve the matter shifting. On its side, the third hypothesis elucidates the shifting but there is no reason for the non-homogeneity of that phenomenon.

The hypothesis we kept is a combination of the previous ones: the contact area shape of the electron beam is circular on the powder bed center, but away from the center, it becomes elliptical and provides less energy to the powder. In addition, the energy leaks with the proximity to cold powders and metal enclosure. This makes the sintering of the powder weaker near the boarders. Then, the rake passage might easily move the poorly sintered powder and the molten material suspended in the powder. This might lead to a loss of material as well as deformation for the manufactured parts. In addition, the sintering weakness modifies the thermal conductivity, the cooling of the manufactured parts is no more homogeneous and it generates additional deformation.

3.2 Analysis

In order to validate the hypothesis, an analysis of the sintered powder is made. This analyze was conducted with an X-ray microtomography machine. The machine is able to reconstruct a 3D model of the studied sample with voxels. This reconstruction aims to display and measure the size of the necks binding in the sintered powder. A difference of necks size between the powders in the center and in the periphery of the manufacturing space would indicate a significant difference of the sintering [20].

The samples of powders are one centimeter side cube. This size allows observation of a large number of powder grain that limits the impact of defects in the powder. Due to the titanium opacity to X-ray, getting a 1µm resolution with titanium parts requires more power than supplied by the machine [21]. Resolution has been reduced to 5 µm in order to provide a clear tomography of the samples. Despite a clear tomography, it becomes impossible to measure necks because of the resolution. However, [20] show there is a link between density and sintering progress with spherical powders. Thereby, measuring density permits comparison of the two samples sintering.

Table 1 presents the results of the analysis. With more than 3 % difference, assumptions about the difference of sintering are justified. Indeed, according to OLMOS [20], 3 % are significant enough to make a difference of sintering. This difference impacts the powder stiffness and its heat conductivity. This generates a harmful heterogeneity in the manufacturing space that might have bad effects on manufactured parts [22].

Table 1. *Porosity measured from the tomography reconstruction*

Samples	Center	Periphery
Porosity [%]	37.84	41.29
Standard deviation [%]	1.36	1.92

4 CONCLUSION

The observed defect has an impact on geometry of manufactured parts with EBM technology. According to their position, parts may undergo geometric deformation and matter loss. It can be inferred from this study that the manufacturing space is heterogeneous.

In the worst case, the 8 first millimeters are affected by this defect. The closest defect to the center is 86 mm distant from the center. The more the defect is far from the center, the more important it is. With this information, a first strategy can be used to bypass the defect. Indeed, creating supports 8 mm (or more) long all along the first layer permits to transfer the defect from the part to supports. A manufacturing space reduction to an 86 mm radius cylinder can also be a solution to avoid the defect apparition. Those 2 strategies have been validated with the workpieces.

These results are a fitting complement to rules and specifications of the Design for Additive Manufacturing applied to the EBM technology. In addition, the proposed methods can be applied to different technologies such as SLM or SLS.

As well, modification could be made to change the machine operation and more precisely the electron beam. By bringing more energy, the powder sintering would be homogenized. Improve the insulation of the powder bath with the machine will also limit the energy loss.

5 REFERENCES

[1] Gibson, I., Rosen, D., Stucker; B. (2015). Development of additive manufacturing technology. *Additive Manufacturing Technologies*, p. 19-42, **DOI:10.1007/978-1-4939-2113-3_2**.

[2] Gao, W., Zhang, Y., Ramanujan, D., Ramani, K., Chen, Y., Williams, C.B., Wang, C.C.L., Shin, Y.C., Zhang, S., Zavattieri P.D. (2015) The status, challenges, and future of additive manufacturing in engineering. *Computer-Aided Design*, vol. 69, p. 65-89, **DOI:10.1016/j.cad.2015.04.001**.

[3] Hrabe, N., Quinn, T. (2013). Effects of processing on microstructure and mechanical properties of a titanium alloy (Ti-6Al-4V) fabricated using electron beam melting (EBM), part 1: Distance from build plate and part size. *Materials Science and Engineering: A,* vol. 573, p. 264-270, **DOI:10.1016/j.msea.2013.02.064**.

[4] Novak, N., Vesenjak, M., Ren Z. (2016) Auxetic Cellular Materials – a Review. *Strojniški vestnik - Journal of Mechanical Engineering*, vol. 62, no. 9, p. 485-493, **DOI:10.5545/sv-jme.2016.3656**.

[5] Sing, S.L., An, J., Yeong, W.Y., Wiria, F.E. (2016). Laser and electron-beam powder-bed additive manufacturing of metallic implants: A review on processes, materials and designs. *Journal of Orthopaedic Research*, vol. 34, no. 3, p. 369-385, **DOI:10.1002/jor.23075**.

[6] Daneshmand, S., Aghanajafi, C. (2012). Description and modeling of the additive manufacturing technology for aerodynamic coefficients measurement. *Strojniški vestnik - Journal of Mechanical Engineering*, vol. 58, no. 2, p. 125-133, **DOI:10.5545/sv-jme.2010.238**.

[7] Waller, J.M., Parker, B.H., Hodges, K.L., Burke, E.R., Walker, J.L. (2014). *Nondestructive Evaluation of Additive Manufacturing. National Aeronautics and Space Administration*, Hampton.

[8] Budzik, G., Burek, J., Bazan, A., Turek, P. (2016). Analysis of the accuracy of reconstructed two teeth models manufactured using the 3DP and FDM technologies. *Strojniški vestnik - Journal of Mechanical Engineering*, vol. 62, no. 1, p 11-20, **DOI:10.5545/sv-jme.2015.2699**.

[9] Petrovic, V., Haro, J.V., Blasco, J.R., Portolés, L. (2012). Additive manufacturing solutions for improved medical implants. *Biomedicine*, Lin, C. (ed.), *InTech*, **DOI:10.5772/38349**.

[10] CCT MAT – STR, CNES: (2016). *PRINTtemps de la Fabrication Additive (Spring of Additive Manufacturing).* Toulouse.

[11] Vayre, B., Vignat, F., Villeneuve, F. (2013). Identification on some design key parameters for additive manufacturing: application on electron beam melting. *Procedia CIRP*, vol. 7, p. 264-269, **DOI:10.1016/j.procir.2013.05.045**.

[12] Vayre, B., Vignat, F., Villeneuve F. (2012). Designing for Additive Manufacturing. *Procedia CIRP*, vol. 3, p. 632-637, **DOI:10.1016/j.procir.2012.07.108**.

[13] Obaton, A.-F., Bernard, A., Taillandier, G., Moschetta J.-M. (2016). Fabrication additive: Etat de l'Art et Besoins Métrologiques Engendrés. (Additive manufacturing: state of the art and generated metrological needs) *Revue Francaise de Métrologie*, vol. 2016-1, n° 41.

[14] Arcam AB (2016). Creating new opportunitites in design and production. From *www.arcam.com/wp-content/uploads/justaddbrochure-web.pdf*, accessed on 2016-09-01.

[15] Arcam AB (2010). Arcam A1, the future in implant manufacturing. From *http://www.arcam.com/wp-content/uploads/Arcam-A1.pdf*, accessed on 2016-09-01.

[16] Vayre, B. (2014) *Conception pour la Fabrication Additive, Application à la Technologie EBM (Design for Additive Manufacturing, Application to the EBM Technology)*. PhD Thesis, University of Grenoble Alpes, Grenoble.

[17] Safdar, A. (2012). A study on electron beam melted Ti-6Al-4V. From *http://lup.lub.lu.se/record/2543181*, Lund University, accessed on 2016-08-25.

[18] Arcam AB (2011), *Arcam EBM System, User Manual*, A1 A2. Mölndal.

[19] Slotwinski, J.A., Garboczi, E.J., Stutzman, P.E., Ferraris, C.F., Watson, S.S., Peltz, M.A. (2014). Characterization of metal powders used for additive manufacturing. *Journal of Research of the National Institute of Standards and Technology*, vol. 119, **DOI:10.6028/jres.119.018**.

[20] Olmos, L. (2009). *Etude du Frittage de Poudres par Microtomographie in situ et Modélisation Discrète (Study of sintering powders by in situ microtomography and discrete simulations)*. PhD Thesis. Institut National Polytechnique de Grenoble – INPG, Grenoble.

[21] Thiery, C. (2013). *Tomographie à Rayons X (X-Ray Tomography)*. Techniques de l'Ingénieur, art. p950.

[22] Zou, C.-M., Liu, Y., Yang, X., Wang, H.-W., Wei Z.-J. (2012). Effect of sintering neck on compressive mechanical properties of porous titanium. *Transactions of Nonferrous Metals Society of China*, vol. 22, sup. 2, p. s485-s490, **DOI:10.1016/S1003-6326(12)61750-6**.

Strojniški vestnik - Journal of Mechanical Engineering 63(2017)10, 559-566

DOI:10.5545/sv-jme.2017.4591 Original Scientific Paper
Received for review: 2017-05-19
Received revised form: 2017-06-29
Accepted for publication: 2017-07-19

Low Cost Printer for DLP Stereolithography

Joško Valentinčič[1,*] – Matej Peroša[1] – Marko Jerman[1] – Izidor Sabotin[1] – Andrej Lebar[1,2]
[1]Faculty of Mechanical Engineering, University of Ljubljana, Slovenia
[2]Faculty of Health Sciences, University of Ljubljana, Slovenia

A general research direction of stereolithography based on digital light processing (DLP) is to reduce the production time and to increase manufacturing accuracy. Compared to fused deposition modelling (FDM) machines, machines for DLP stereolithography are expensive and thus not available to a broad range of users as it is the case with FDM 3D printers. Comparing technologies, DLP stereolithography offers quicker and more accurate production. In this paper, performances of a low cost DLP stereolithographic printer is presented. Three main challenges are treated: an uneven illumination of commercial DLP projectors, a direction of illumination and a selection of optimal 3D printing parameters. Uneven illumination of DLP projector results in smaller usable working area and poor printing quality. The problem is solved by implementing an appropriate software mask, thus the product quality is not influenced by its position on a working table. The direction of illumination has a key role in DLP stereolithography. It is shown that constrained surface (illumination through a transparent bottom of the vat) gives better 3D printing accuracy compared to free surface (illumination of the photopolymer surface) stereolithography. To further improve the product quality, the optimal process parameters are determined. Using the Taguchi based surface response methodology optimal process parameters are defined and by using them, the deviation of the actual dimensions from the specified dimensions is less than 80 μm.
Keywords: DLP stereolithography, software mask, illumination, surface response method

Highlights
- *An illumination intensity on the whole projection surface can be achieved by using an appropriate software mask, but the required exposure time increases significantly.*
- *Using Taguchi based surface response methodology, optimal process parameters were defined: exposure time 16.5 s, layer thickness 0.06 mm and time between two consecutive exposures 4.1 s.*
- *A low cost DLP stereolithography printer is able to print part which actual dimensions deviate from the nominal dimensions in x and y direction for 30 μm and 10 μm respectively, and 80 μm in z direction.*

0 INTRODUCTION

Additive manufacturing (AM) is a formal expression for a process which belongs to a class of technologies used to be called rapid prototyping technologies (RP). Several other terms are, or used to be, in use as well: automated fabrication, freeform fabrication or solid freeform fabrication, layer-based manufacturing, stereolithography or 3D printing **[1]**. There are numerous ways to classify AM technologies, but recently accepted ISO/ASTM 52900 standard **[2]** classifies AM processes regarding type of material, principle applied for fusion or bonding, feedstock that is used for adding the material and machine architecture, i.e. how the material is brought together.

Stereolithography is a liquid-based AM process for 3D parts by curing a photosensitive polymer kept in a vat, thus the term vat photopolymerization process is often used. Various light sources are used for photopolymerization **[1]**. Shorter the light wavelength higher the curing rate. Controlled light irradiation induces a curing reaction, forming a highly cross-linked polymer. Compared to other polymer-based AM technologies such as the extrusion or jetting based processes, the stereolithographic process can produce parts with fine features and good accuracy by using various polymers **[3]**.

In the last years, the resolution of digital light processing (DLP) projector has been significantly improved due to the use of new low cost digital micromirror devices (DMD). In contrast to other light sources, the use of DLP projector enables building the whole layer at the same time. A DLP stereolithography is used in various fields including medical applications, where biocompatible and biodegradable materials must be used **[4]** and **[5]**, and oceanography **[6]** for a better understanding and restoration of fragile marine ecosystems.

Two types of DLP stereolithography systems are distinguished, namely free surface and constrained surface stereolithography. In free surface (also denoted as top-down stereolithography), the layer is cured on the photopolymer surface and the product is sunk in the liquid from the surface towards the bottom of the vat. On the other hand, in constrained surface (also denoted as bottom-up) stereolithography, the layer is cured through the optically clear bottom of the vat, and a non-stick layer so that the printed structure does not adhere to the substrate. Thus, the product grows up from the vat and out of the liquid. The

*Corr. Author's Address: Faculty of Mechanical Engineering, University of Ljubljana, Slovenia, jv@fs.uni-lj.si

constrained surface stereolithography offers several advantages over a free surface based system. The main one is that the curing of liquid resin is sealed from the oxygen-rich environment [7]. By eliminating the oxygen inhibition effect, the liquid photopolymer resin can be cured faster. The diffusion effects of oxygen were investigated to have significant effects on the size, shape and properties of parts fabricated by stereolithography [8]. However, a cured layer is sandwiched between the previous layer and the bottom surface of the vat. The solidified material may adhere strongly to the bottom of vat causing the object to break or deform when the build platform moves up from the vat during the building process [9].

The state-of-the-art is continuous liquid interface production (CLIP) where DMD is moved continuously over the area of the medium while the projected image is updated accordingly. CLIP is using an oxygen-permeable window below the ultraviolet image projection plane, which creates a "dead zone" (persistent liquid interface) where photopolymerization is inhibited between the window and the polymerizing part [10]. Such printers are already available on the market for around 250,000 €.

A printing resolution that can be achieved by DLP stereolithography depends on the size of micromirrors in DMD and an optical system. In general, higher printing resolution is easier to achieve on smaller printing area by the use of suitable optics, but the smallest feature size that can be produced depends on the resin, too. Kinetics of photoinitiated multi-vinyl polymerisations have been discussed in an extensive review in [11], but in practice much simpler equations are used to describe the polymerisation kinetics in the fabrication of structures by stereolithography [4]. They can be used to determine optimal process parameters for the given resin, but the rest of the influential parameters such as machine and DMD performances should be considered, too. Here, the established design of experiments (DOE) techniques can serve well.

A low cost desktop stereolithographic printer using a commercial DLP projector as a light source was built and tested. All material costs to build the printer were below 1,500 €. The projector has only a small bandwidth in the optical spectrum close to ultraviolet light; the majority is in visible spectrum. Since photopolymerization is faster when photopolymer is illuminated by shorter wavelengths, one cannot expect high productivity using such light source in DLP stereolithography. Additionally, the luminance was not equal on the whole projected area. To improve printing accuracy, the equal luminance over all projection area was achieved by developing an appropriate software mask. Further on, the influence of illuminance from bottom and top of the photopolymer vat was examined, i.e. a constrained surface method and a free surface method. At last but not least, the optimal process parameters were defined by Taguchi based surface response methodology.

1 EXPERIMENTAL SETUP

All experiments were performed on custom made DLP stereolithographic printers. A printer utilizing the free from surface method is shown in Fig. 1 and printer utilising the constrained surface method is shown in Fig. 2. Both printers are using the same software and hardware. The NC-code is prepared by Creation Workshop (DataTree3D Ltd., USA) installed on a laptop computer. The computer is connected to Arduino Mega 2560 microcontroller which is further connected to Gecko drive (Geckodrive Inc., USA) and a stepper motor. A stepper motor is used to rotate the threaded spindle. The motor has resolution of 1.8° and the spindle with a pitch of 2 mm is used, therefore the resolution of Z stage is 0.01 mm.

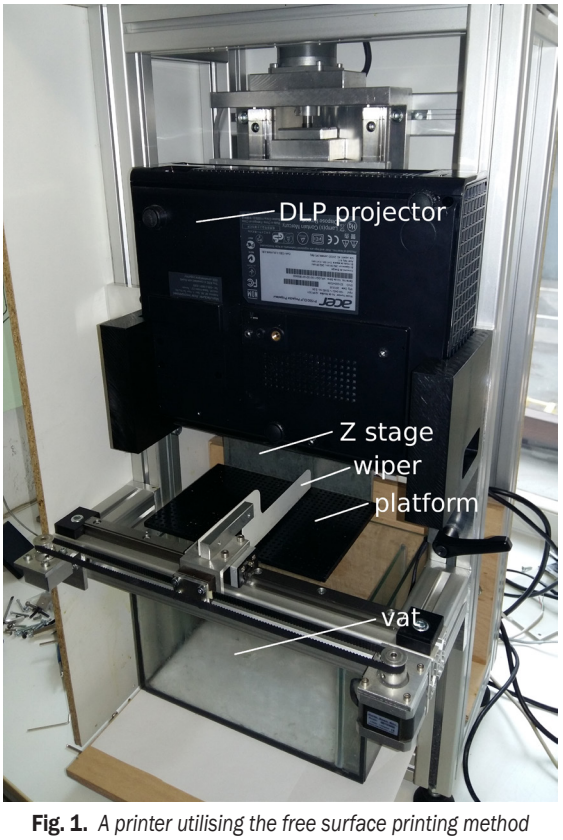

Fig. 1. *A printer utilising the free surface printing method also denoted as top-down DLP stereolithography*

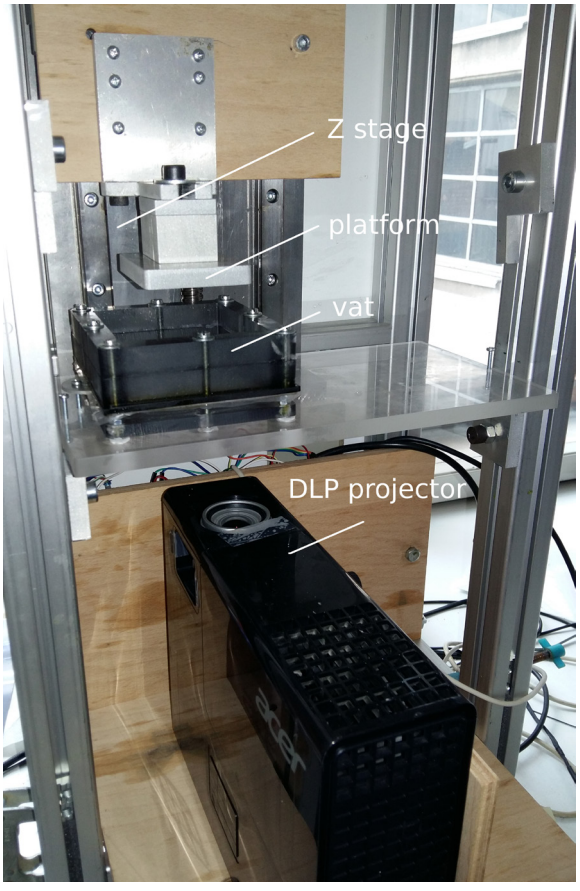

Fig. 2. *A printer utilising the constrained surface printing method also denoted as bottom-up DLP stereolithography*

In free form surface method, two gecko drives and two stepper motors are used. The second stepper motor is used to move mechanical wiper over the surface of photopolymer in order to avoid dipping and to redistribute the resin after curing each layer. In the case of constrained surface method, the mechanical wiper is not needed. In both cases, photopolymerisation was initiated by a DLP projector Acer P1500 having 1920 × 1080 pixels and 3000 lumen. The printing area was 88 mm by 50 mm, thus the pixel size was 46 µm. The photopolymer used in this research was Deep Black (Fun To Do, Netherlands).

To build a software mask to compensate for uneven illumination, a testing site to capture the DLP projector image was build. The site consists of a computer connected to the DLP projector, a screen on which a white image was projected and a camera used to capture the image. The camera was a Canon 30D with 50 mm lens, 1/125 s shutter speed and f/4.5 aperture.

2 COMPENSATION OF UNEVEN ILLUMINATION

Commercial DLP projectors are not made to be used as a light source in DLP stereolithography, but with certain limitations they can do the job. The main drawback is the light spectrum. In preliminary tests of custom built DLP printer, it was observed that at certain locations of the printing area the test pieces were not entirely printed. The cause was the lack of uniformity in the DLP projector's illumination. The objective was to improve the printing area and printing quality by reducing the DLP projector's uneven illumination. The method, which is described in this article, uses a software mask to improve the DLP projector's illumination and printing quality. A mask is numerically applied over an image of projecting layer, thus the luminance of each pixel can be altered.

The projector was projecting the white light image to the screen and the picture of the image was taken by the camera. The screen had black border that was used to focus the camera (as shown in Fig. 3).

Fig. 3. *A captured image of the DLP projector illumination with a size of 88 mm by 50 mm; the image was modified for an easier presentation of areas with lower illumination*

In the next steps the borders were cropped. The cropped image was then resized to 1920 × 1080 pixels and converted to a greyscale 8-bit PNG format, which is needed for image processing. The image was inverted i.e. the value of each pixel was subtracted from the brightest value which is 255. The result was a rather dark image. Finally, a 50 % transparency was set by changing the alpha channel value of each pixel on the dark image in Creation Workshop software. The result was a grey image that was used as a mask. The resizing, image conversion, image inversion and transparency setting were performed with a computer programme written in Microsoft Visual studio C++.

3 DIRECTION OF ILLUMINATION

A study was performed to find out which setup is better for the given printer: constrained surface method, i.e. building the part on the bottom of the vat, or free surface method, i.e. building the part on polymer surface. Both setups were evaluated by comparing the dimensions and visual inspection of test parts. In both cases the same focal length was used. In free surface method, the starting volume of the photopolymer in the vat was kept the same for all tests. When building product on the bottom of the vat, the photopolymer volume does not have a significant influence on the building process.

The test part given in Fig. 4 has external dimensions of 20 mm × 22 mm × 4 mm. Five test parts were built by each method. Dimensions of several features were measured in *x*, *y* and *z* axis. Each measurement was repeated five times. Altogether, more than 1000 measurements were performed. All measurements were performed using camera with mounted appropriate lenses and custom made software developed in Matlab to measure the dimensions on recorded images.

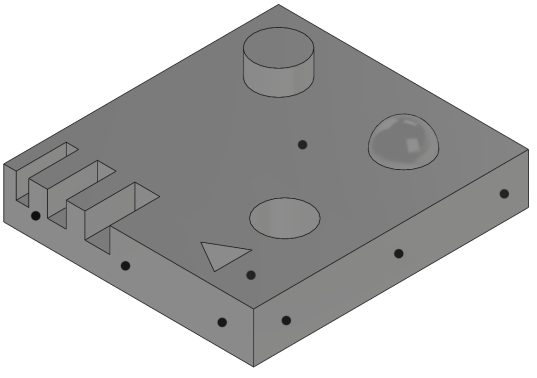

Fig. 4. *Test part geometry with external dimensions 20 mm × 22 mm × 4 mm; black dots indicate the measuring points in x, y and z direction*

4 PROCESS PARAMETERS

DOE method is used to increase our understanding and knowledge of DLP stereolithography. For continuous improvement in product/process quality, it is fundamental to understand the process behaviour, the amount of variability and its impact on processes [12].

Based on preliminary tests, three printing parameters were selected, namely exposure time, layer thickness and time between the consecutive exposures with their maximum (+1), mid (0) and minimum (-1) values. Thus, three parameters (factors) on three levels were used for the design of experiments. The factors and their values are shown in Table 1.

An L_{18} (2^1 3^7) orthogonal array was chosen for DOE by the Taguchi based surface response methodology. The orthogonal array allows the design of experiments of one factor at two levels and seven factors at three levels. The factors that were not needed were removed with the help of a linear graph of the orthogonal array. The L_{18} requires 15 experiments to be conducted.

Table 1. *Process parameters and their levels*

Factor	Level		
	–1	0	+1
A: Exposure time [s]	8.5	12.5	16.5
B: Layer thickness [mm]	0.01	0.06	0.1
C: Time between two consecutive exposures [s]	3.6	4	4.4

The experiments were carried out in random order. In preliminary tests it was noted that the residence time of the photopolymer in the vat influences the quality of the part, thus the photopolymer was well shaken before it was poured into the vat. After each test, the vat was emptied and cleaned. After each test the printed test sample was measured using a micrometer.

The test sample has several features that served for visual inspection. It was noticed that visually good parts have also good dimensional accuracy, thus only the measured dimensions were used in optimization procedure. The dimensions in *x*, *y* and *z* directions were measured at the measuring points shown in Fig. 4. At each measuring point, the measurements were repeated three times.

5 RESULTS AND DISCUSSION

5.1 Compensation of Uneven Illumination

An image of the DLP projector illumination with the mask applied was captured and compared with the image without the mask. The results of the comparison are presented in Figs. 5 and 6.

For better visualisation, the intensity of white light is presented in colours. The discrepancy of white colour is significantly reduced when software mask is used as can be observed by comparing both figures.

It has to be noted that the intensity of the light by using mask is reduced, thus longer exposure time must be used and consequently the manufacturing time increases. The mask could be made to completely

reduce discrepancy, i.e. the area in the lower left corner in Fig. 6 would not deviate from the rest of the image, but then the brightness of all pixels would equal to the brightness of the least bright pixel. Using such mask, the required exposure time would increase even more. In order to find the right balance between even illumination and exposure time, the unevenness cannot be completely eliminated.

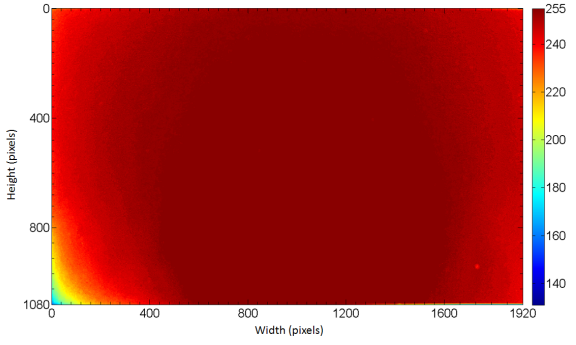

Fig. 5. *Characteristics of DLP illumination without mask*

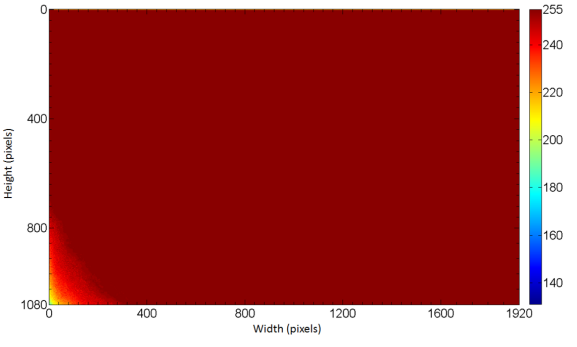

Fig. 6. *Characteristics of DLP illumination with mask*

5.2 Direction of Illumination

Two types of illumination were investigated, namely constrained surface method and free surface method. All together 1128 measurement data were collected and analysed separately regarding accuracy in *x*, *y* and *z* axis. Further on, measurements of inner dimensions are distinguished from measurements of outer dimensions. In *z* axis only outer dimension measurements were performed. The average values are very close to nominal values (Table 2). One can notice that parts built by constrained surface method better meets the nominal values than the part built by free surface which is in agreement with the findings in literature [7] to [9], [13] and [14]. The same conclusion can be drawn when comparing standard deviations, which are gathered in the Fig. 7.

Although the average values of these dimensions are close to the nominal values (Table 2), standard deviations of dimensions around 0.07 mm in the case of constrained surface method (Fig. 7) indicate that the precision could be improved.

Table 2. *Average deviations from nominal dimensions in mm; where A is a constrained surface method and B is a free surface method*

	x axis		y axis		z axis
	outer	inner	outer	inner	
A	0.00	0.03	–0.01	0.03	–0.01
B	–0.14	0.16	–0.18	0.08	0.31

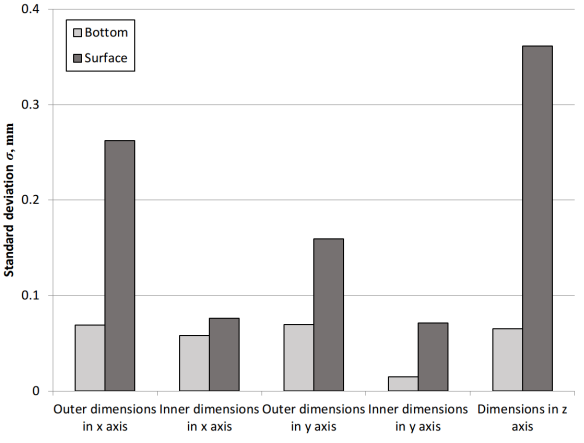

Fig. 7. *Standard deviation of part dimensions; where OUTx is outer dimensions in x axis, INx inner dimensions in x axis, OUTy outer dimensions in y axis, INy inner dimensions in y axis, and z dimensions in z axis*

5.3 Process Parameters Optimization

Since constrained surface method gives better results than free surface method, only the former is further examined. According to L_{18} (2^1 3^7) orthogonal array the experiments were performed as given in Table 3, where the results of experiments are given, as well.

An analysis of the measurements is done according to the Taguchi based surface response methodology. The regression models are developed for each response, namely measured dimensions in *x*, *y* and *z* direction and are given in Eqs. (1) to (3) respectively.

$$x = 22.04 + 5.57 \cdot A - 6.49 \cdot B - 10^{-3} \cdot C + 2 \cdot 10^{-9} \cdot A \cdot B - \\ - 2 \cdot 10^{-9} \cdot A^2 + 20.57 \cdot B^2 + 10^{-7} \cdot C^2 , \quad (1)$$

$$y = 21.55 + 3 \cdot 10^{-5} \cdot A - 4.68 \cdot B + 4 \cdot 10^{-5} \cdot C + \\ + 10^{-4} \cdot A \cdot B = 10^{-9} \cdot A^2 + 14.81 \cdot B^2 , \quad (2)$$

$$z = 4.72 - 8 \cdot 10^{-6} \cdot A - 5.04 \cdot B - 8 \cdot 10^{-5} \cdot C + \\ + 22.22 \cdot B^2 . \quad (3)$$

Table 3. *Experimental values and results; where A is exposure time, B layer thickness and C the time between two consecutive exposures*

Factor			Response		
A	*B*	*C*	*x* [mm]	*y* [mm]	*z* [mm]
8.5	0.01	3.6	20.16	21.91	4.17
12.5	0.06	4.0	20.08	21.83	4.09
16.5	0.10	4.4	20.21	21.93	3.95
8.5	0.01	4.0	20.15	21.90	4.41
12.5	0.06	4.4	20.14	21.90	3.97
16.5	0.10	3.6	20.12	21.89	3.97
8.5	0.06	3.6	20.01	21.78	4.16
12.5	0.10	4.0	20.07	21.84	3.97
16.5	0.01	4.4	20.20	21.98	4.18
8.5	0.10	4.4	19.99	21.77	3.97
12.5	0.01	3.6	20.24	21.97	4.24
16.5	0.06	4.0	20.15	21.93	4.00
8.5	0.06	4.4	20.10	21.87	4.02
12.5	0.10	3.6	20.10	21.86	4.01
16.5	0.01	4.0	20.19	21.98	4.17
8.5	0.10	4.0	19.98	21.75	4.07
12.5	0.01	4.4	20.27	21.98	4.17
16.5	0.06	3.6	20.11	21.87	4.12

The significance of the developed models is given by *F*-value, coefficient of determination (R^2), adjusted coefficient of determination (R_{adj}^2), predicted coefficient of determination (R_{pred}^2) and adequate precision (*AP*). These values are given in Table 4.

Table 4. *Significance of the models*

	Direction		
	x	*y*	*z*
F-value	20.54	25.69	11.66
R^2	0.93	0.93	0.78
R_{adj}^2	0.88	0.89	0.71
R_{pred}^2	0.78	0.83	0.57
AP	16.47	16.30	10.73

The F-values of all models imply that the models are statistically significant. The predicted R-squared is in both cases in reasonable agreement with the adjusted R-squared (the difference has to be less than 0.2). The adequate precision estimates the signal to noise ratio, where a ratio greater than 4 is desirable. In our case, all models indicate an adequate signal and all models are valid. The models for dimension in *x* and *y* direction are highly significant whereas model for *z* direction is still acceptable. A plausible cause could be

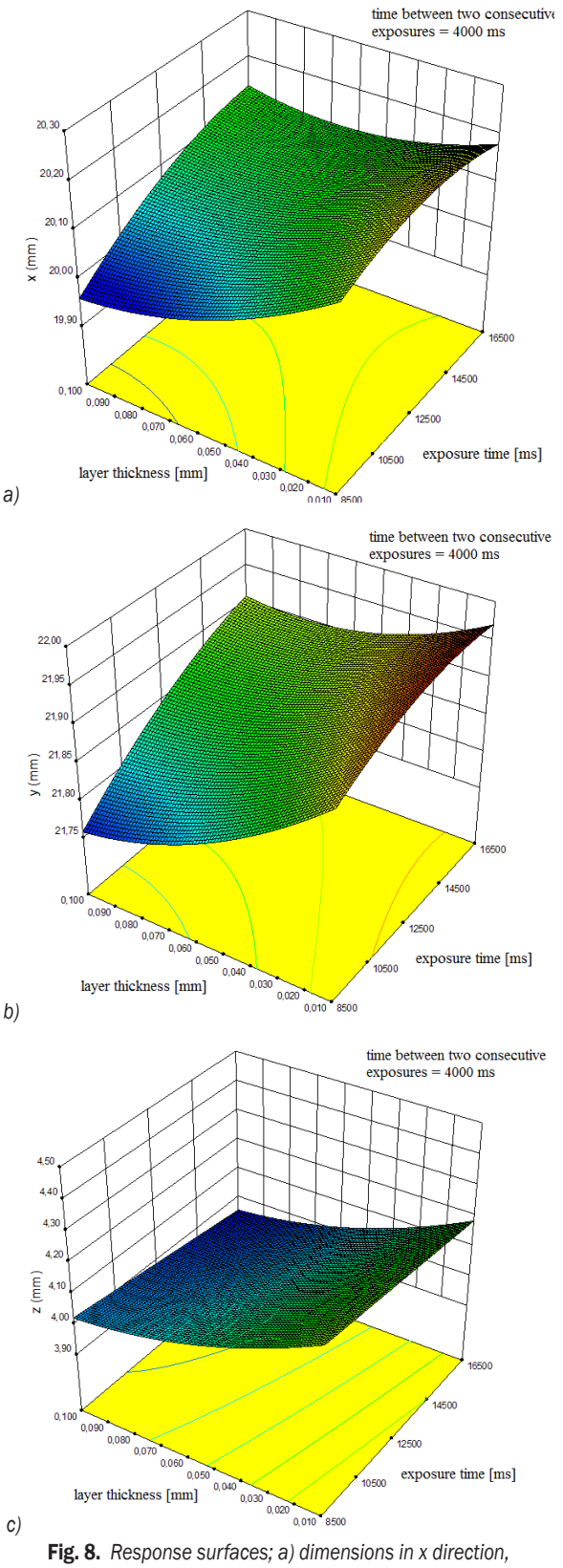

Fig. 8. *Response surfaces; a) dimensions in x direction, b) dimensions in y direction, and c) dimensions in z direction, as a function of process parameters*

in the positioning of the platform. After each test the printing platform had to be separated from the printer to safely remove the test sample. When the platform was put back on its place, the positioning accuracy could not be compromised, thus the spacing between the printing platform and the bottom of the vat might not be the same as in the previous experiment trial.

The response surfaces are given in Fig. 8. One can notice that the dimensions in x direction tend to be greater than the nominal value (20 mm) whereas the dimensions in y axis tend to be smaller than the nominal one (22 mm). Thus, it is difficult to find process parameters that satisfy both requirements. This could be due to the misalignment of the projected image, the transparent bottom of the vat and the build platform which is mounted on the z stage.

After the analysis of the responses x, y and z, a numerical optimization followed. The aim of the optimization is to determine the input parameters values in such a way that the responses are as close as possible to the nominal dimensions of the test sample (x = 20 mm, y = 22 mm and z = 4 mm). These are the three optimization criteria. The boundary condition is set as well: optimization is done within the limits of the input parameters values that were set during the planning phase of DOE.

The optimal input parameters, obtained with numerical optimization are: exposure time 16.5 s, layer thickness 0.06 mm, time between two consecutive exposures 4 s. In the final phase, a series of confirmation tests were performed to verify whether the optimal parameters give the results that were predicted with the regression models.

Table 5. *Results of confirmation tests and discrepancy between predicted and measured dimensions (Δ)*

Response	Predicted [mm]	Measured [mm]	Δ [mm]
x	20.12 ± 0.06	20.15	0.03
y	21.91 ± 0.04	21.92	-0.01
z	4.02 ± 0.14	3.94	-0.08

A total of three confirmation tests were performed and the report is given in Table 5. The predicted response values, i.e. dimensions of the part build by constrained surface method using the optimal parameters, lies within the determined confidence interval (α = 0.05) and the dimensions of the part build by constrained surface method using the optimal parameters lies within the confidence interval. One of the test samples printed during the confirmation tests are shown in Fig. 9.

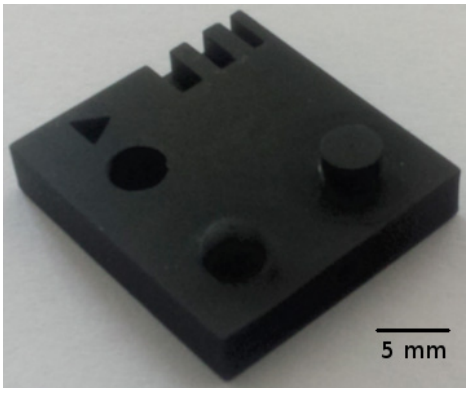

Fig. 9. *Test sample manufactured for model confirmation test*

5 CONCLUSIONS

Based on the results presented in this paper, the following conclusions can be drawn.

- The implementation of the mask successfully reduces the unevenness of the DLP projector's illumination and thereby the parts of the same quality are built in the entire printing area. But using the mask the exposure time increases significantly.
- A better printing accuracy is obtained when the photopolymer is illuminated through a transparent bottom of the vat, i.e. using the constrained surface method.
- The optimal printing parameters for the custom build 3D printer with applied software mask and photopolymer Deep Black were obtained: exposure time 16.5 s, layer thickness 0.06 mm, time between two consecutive exposures 4 s. Using these parameters, the deviation of the actual dimensions from the nominal dimensions in x and y direction is 30 μm and 10 μm respectively, and 80 μm in z direction.
- The material costs of the developed DLP stereolithography printer are less than 1500 €. The printer is not suitable for professional work due to very long exposure time. A better illumination system with light spectrum closer to ultraviolet light and with even luminance over all projected area is needed, but then the stereolithographic printer is not a low cost machine any more.

With the illumination compensation and printing parameter optimization the printing quality of the prototype 3D printer was significantly improved, but there is still a few possibilities for improvements, e.g. to reduce the pixel size by reducing the area of illumination and to improve the parallelism between

building stage, transparent bottom of the vat and the projected image.

6 ACKNOWLEDGEMENTS

The authors would like to thank to the Slovenian Research Agency for supporting the work in the frame of Research programme Innovative production systems (P2-0248).

7 REFERENCES

[1] Gibson, I., Rosen, D., Stucker, B. (2015). *Additive Manufacturing Technologies*, Springer, New York, **DOI:10.1007/978-1-4939-2113-3**.

[2] ISO/ASTM 52900:2015, *Additive manufacturing – General principles – Terminology*, International Organization for Standardization, Geneva

[3] Pan, Y., Chen, Y. (2016). Meniscus process optimization for smooth surface fabrication in Stereolithography. *Additive Manufacturing*, vol. 12, part B, p. 321-333, **DOI:10.1016/j.addma.2016.05.004**.

[4] Melchels, F.P.W., Feijen, J., Grijpma, D.W. (2010). A review on stereolithography and its applications in biomedical engineering. *Biomaterials*, vol. 31, no. 24, p. 6121-6130, DOI:10.1016/j.biomaterials.2010.04.050.

[5] Gauvin, R., Chen, J.-C., Lee, J.W., Soman, P., Zorlutuna, P., Nichol, J.W., Bae, H., Chen, S., Khademhosseini, A. (2012). Microfabrication of complex porous tissue engineering scaffolds using 3D projection stereolithography. Biomaterials, vol. 33, no. 15, p. 3824-3834, **DOI:10.1016/j.biomaterials.2012.01.048**.

[6] Mohammed, J.S. (2016). Applications of 3D printing technologies in oceanography. *Methods in Oceanography*, vol. 17 p. 97-117, **DOI:10.1016/j.mio.2016.08.001**.

[7] Pan, Y., Zhou, C., Chen, Y. (2012). A fast mask projection stereolithography process for fabricating digital models in minutes. *Journal of Manufacturing Science and Engineering*, vol. 134, no. 5, **DOI:10.1115/1.4007465**.

[8] Jariwala, A.S., Jones, H., Kwatra, A., Rosen, D.W. (2013). Process planning method for exposure controlled projection lithography. *Proceedings of the 24th Solid Freeform Fabrication Symposium*, Austin, p. 95-110.

[9] Waheed, S., J.M. Cabot, N.P. Macdonald, t. Lewis, R.M. Guijt, B. Paull, M.C. Breadmore, (2016). 3D printed microfluidic devices: enablers and barriers. *Lab on a Chip*, vol. 16, no. 11, p. 1993-2013, **DOI:10.1039/C6LC00284F**.

[10] Tumbleston, J.R., Shirvanyants, D, Ermoshkin, N, Janusziewicz, R, Johnson, A.R., Kelly, D., Chen, K., Pinschmidt, R., Rolland, J.P.1, Ermoshkin, A., Samulski, E.T., DeSimone, J.M. (2015). Continuous liquid interface production of 3D objects, *Science*, vol. 347, no. 6228, p. 1349-1352, **DOI:10.1126/science.aaa2397**.

[11] Andrzejewska, E. (2001) Photopolymerization kinetics of multifunctional monomers. *Progress in Polymer Science*, vol. 26, no. 4, p. 605-665, **DOI:10.1016/S0079-6700(01)00004-1**.

[12] Antony, J. (2003). *Design of experiments for engineers and scientists*, Butterworth-Heinemann, Oxford.

[13] Huang, Y.-M., Kuriyama, S., Jiang, C.-P. (2004). Fundamental study and theoretical analysis in a constrained-surface stereolithography system. *The International Journal of Advanced Manufacturing Technology*, vol. 24, no. 5-6, p. 361-369, **DOI:10.1007/s00170-003-1627-9**.

[14] Jariwala, A.S., Ding, F., Boddapati, A., Breedveld, B., Grover, M.A., Henderson C.L., Rosen, D.W. (2011). Modeling Effects of Oxygen Inhibition in Mask-based Stereolithography. *Rapid Prototyping Journal*, vol. 17, no. 3, p. 168-175, **DOI:10.1108/13552541111124734**.

Strojniški vestnik - Journal of Mechanical Engineering 63(2017)10, 567-576

DOI:10.5545/sv-jme.2017.4396 Original Scientific Paper
Received for review: 2017-02-14
Received revised form: 2017-06-27
Accepted for publication: 2017-09-14

Optimization of Hybrid Manufacturing for Surface Quality, Material Consumption and Productivity Improvement

Damir Grguraš* – Davorin Kramar
University of Ljubljana, Faculty of Mechanical Engineering, Slovenia

This paper presents hybrid manufacturing process of 3D printing and milling. Fused deposition modeling (FDM) has been applied to improve product manufacturing performance, afterwards, milling was used to improve outer surface roughness. Today's FDM systems rely on the use of standard nozzle size with a diameter of D_1 = 0.4 mm. To achieve shorter production times a bigger nozzle size (diameter D_2 = 1.1 mm) has been used in this research. Optimization of technological parameters of hybrid manufacturing was carried out according to the minimal time of production, a minimal final surface roughness and minimal usage of material. In addition, these results were compared with optimal results obtained with the standard nozzle size. Significantly shorter production time, without affecting surface quality, was achieved when using bigger nozzle size.

Keywords: hybrid manufacturing, fused deposition modeling, milling, PLA material, design of experiments – DOE, empirical modeling and optimization, response surface methodology – RSM

Highlights

- *Hybrid manufacturing of fused deposition modeling and milling is presented.*
- *Two different extruder nozzle sizes were used for fused deposition modeling.*
- *The optimization of technological parameters of hybrid manufacturing, according to the minimal production time, minimal surface roughness and minimal usage of material, has been carried out for both extruder nozzle sizes.*
- *Optimal technological parameters obtained with standard and nonstandard extruder nozzle size are revealed by comparison.*

0 INTRODUCTION

Fused deposition modeling (FDM) is an additive manufacturing technology commonly used for modeling, prototyping, and production applications. Due to the relatively low manufacturing cost, it is one of the most commonly used 3D printing technique. Nevertheless, dimensional accuracy, surface roughness and manufacturing times are highly dependent on the process parameters. In some cases, FDM products do not meet desirable dimensional accuracy and surface roughness despite the well-selected process parameters. Thereby, in order to improve product quality, hybrid manufacturing with additional machining can be applied. Thus, FDM process can be applied for product creation, while machining, e.g. milling can be used to improve dimensional accuracy and overall surface roughness. The aim of applying both selected technologies (FDM and milling) in combination is to remove drawbacks of individual one. The milling process has its limitations in the type of geometry where close surface production is required, since the cutting tool by itself cannot produce them. On the other hand, FDM technology almost does not pose any limitations regarding generating complex geometry shapes, but lacks in produced surface quality. These drawbacks can be minimized with the use of both technologies in combination [1] and [2].

Few studies can be found, where additive and subtractive technologies are combined, while most of them present studies of metal parts processing. In the work of Song et al. [3] and [4], 3-axis CNC milling centre was upgraded with two welding guns vertically attached to the spindle housing. For parts creation the welding process gas metal arc welding (GMAW) has been applied followed by significant improvement of dimensional accuracy by machining. In the Norway – Slovenian collaborative research [5], new working hybrid cell for hybrid manufacturing has been developed. A commercial machine for additive manufacturing has been combined with a machining centre into one working cell and both processes were integrated into one unified controlled system. The position accuracy has been ensured with the usage of fixtures on standard pallets and therefore the dimensional accuracy of the products improved. Furthermore, Yamazaki [6] developed hybrid multi – tasking machine tool by equipping laser metal deposition functionality in addition to existing integrated turning and milling capabilities. This machine tool concept enables a further evolution of done-in-one processes enabling building near-net shape components to be produced by additive manufacturing and then quickly generating the

*Corr. Author's Address: University of Ljubljana, Faculty of Mechanical Engineering, Aškerčeva 6, 1000 Ljubljana, Slovenia, damir.grguras@fs.uni-lj.si

net shape through high-precision finish machining operations. Lee et al. [7] developed hybrid rapid prototyping system using FDM and 5-axis machining. One of the innovative features of the system involved installing the cutter spindle on one end and the FDM extruder on the other end of the rotary B axis. Thus, allowing the machine to switch between the two activities without any extra actuation system, thereby simplifying the mechanism complexity and reducing the time to find the position of the cutter relative to the FDM part for subsequent machining. Having five axis on this machine resulted in several benefits, e.g. five-axis machine could make the overhang feature without using the support material. All of these studies are showing current trend in upgrading existing machine tools or developing completely new hybrid machine tools for combination of additive and subtractive machining. Additionally, few studies were made for FDM process parameters optimization for better dimensional accuracy. Mohamed et al. [8] used l-optimality criterion for the optimization of FDM process parameters in order to address the limitations of the commonly used traditional designs. In the same study mathematical models of nonlinear relationships between process parameters and dimensional accuracy were also developed. Kaveh et al. [9] presented a newly developed experimental method to determine the optimum quantity of each effective printing parameters for high impact polystyrene material. Rao and Rai [10] used teaching-learning-based optimization (TLBO) algorithm and non-dominated Sorting TLBO for FDM optimization procedure. Further, in study [11], multi objective optimization was used for sustainable manufacturing. Three-dimensional statistical approach for determining the manufacturing tolerances has been used in study [12]. In this study, in order to achieve optimal technological parameters settings of hybrid manufacturing, i.e. 3D printing and milling parameters, a response surface methodology has been applied.

1 PROCESS PRINCIPLE AND EXPERIMENTAL SETUP OF 3D PRINTING AND MILLING

The CNC machine for hybrid manufacturing has been developed for this research. It combines a 3D printing and milling system, as shown in Fig. 1. The 3D printing system relies on FDM technique where the plastic filament is led to the heating body and is afterwards deposited through the nozzle down onto a build platform. The milling system consists of a Kress milling motor with nominal rated input power of 800 W. The spindle speed can be set between 10.000 to 29.000 rpm. The specimens, i. e. cubes (dimensions 22 mm × 22 mm × 22 mm) from PLA material, were manufactured by the FDM process. Afterwards, milling process has been applied in order to achieve better surface roughness.

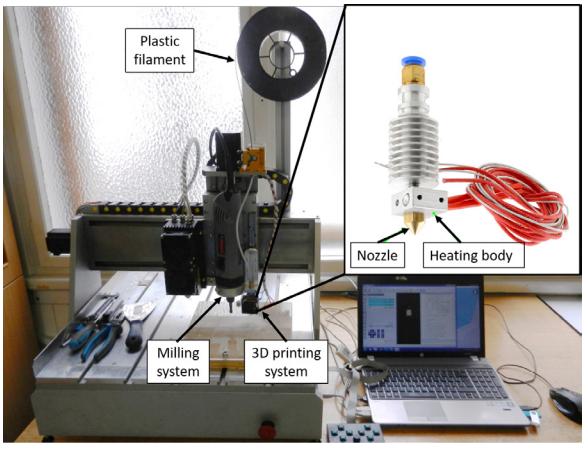

Fig. 1. *Machine for hybrid manufacturing consists of 3D printing (FDM) and milling systems* [1]

2 EXPERIMENTAL APPROACH AND RESULTS

2.1 Technological Parameters of Hybrid Manufacturing

The following technological parameters, which were determined based on the previous knowledge and preliminary experiments of hybrid manufacturing, were chosen:

- spindle speed of milling tool n [min^{-1}],
- layer height h [mm],
- material compensation flow Φ [%],
- printing speed v [mm/s],
- feed speed of milling tool v_f [mm/min],
- milling depth a_p [mm].

For hybrid manufacturing two different nozzle sizes were used; standard (diameter, D_1 = 0.4 mm) and nonstandard size (diameter, D_2 = 1.1 mm). The limit values (minimal and maximal values) of the technological parameters were determined based on pilot experiments and with the integration of proposed values of a 3D printing control software CURA.

2.2 Design and Execution of Experiments

Because, technological parameters for nozzle sizes D_1 = 0.4 mm and D_2 = 1.1 mm differ, two separate experiment designs had to be created. Each technological parameter was examined on three levels. For the level –1 the minimum values of the parameters were considered, and for the level +1 the maximum

values. Values of a mid-level 0 represent the average between levels –1 and +1. For both nozzles, the parameter values at each level are shown in the Tables 1 and 2.

Table 1. *Values of technological parameters at each level for nozzle size D_1 = 0.4 mm*

Level	Technological parameter					
	n [min–1]	h [mm]	Φ [%]	v [mm/s]	v_f [mm/min]	a_p [mm]
–1	10000	0.10	55.0	15	200	0.10
0	15500	0.20	67.5	40	400	0.20
+1	21000	0.30	80.0	65	600	0.30

Table 2. *Values of technological parameters at each level for nozzle size D_2 = 1.1 mm*

Level	Technological parameter					
	n [min–1]	h [mm]	Φ [%]	v [mm/s]	v_f [mm/min]	a_p [mm]
–1	10000	0.30	60.0	10	200	0.41
0	15500	0.55	70.5	25	400	0.55
+1	21000	0.80	80.0	40	600	0.69

For the design of experiments (DOE) with 6 technological parameters on three levels, Taguchi orthogonal array L_{27} has been applied and two parallel DOEs for both nozzle sizes were created using Design-Expert software. The DOEs for both nozzle sizes are presented in the next Chapter 2.3 in Tables 4 and 5 (left of the thick line).

Table 3. *List of output parameters*

Output parameter	Unit	Parameter description
Ra_h	[μm]	Arithmetic deviation profile in the direction perpendicularly to the loading material
Ry_h	[μm]	Maximal surface roughness in the direction perpendicularly to the loading material
Ra_l	[μm]	Arithmetic deviation profile in the direction of loading material
Ry_l	[μm]	Maximal surface roughness in the direction of loading material
MD	[m]	Material deposition - used material for FDM process
t	[s]	Time for hybrid manufacturing

The output parameters, which are listed and described in Table 3, represent responses of hybrid

Table 4. *Design of experiments and corresponding results; nozzle size D_1 = 0.4 mm*

	n [min–1]	h [mm]	Φ [%]	v [mm/s]	v_f [mm/min]	a_p [mm]	Ra_h [μm]	Ry_h [μm]	Ra_l [μm]	Ry_l [μm]	MD [m]	t [s]
1	10000	0.10	55.0	15	200	0.10	5.69	47.35	4.97	44.15	1.02	8066
2	10000	0.10	67.5	40	400	0.20	5.05	42.40	6.57	48.02	1.21	7324
3	10000	0.10	80.0	65	600	0.30	5.86	45.63	6.62	50.40	1.48	7191
4	10000	0.20	55.0	40	400	0.30	3.89	45.11	5.85	47.16	1.02	3715
5	10000	0.20	67.5	65	600	0.10	2.43	22.18	4.19	37.27	1.24	3647
6	10000	0.20	80.0	15	200	0.20	5.55	40.55	5.71	43.97	1.48	4100
7	10000	0.30	55.0	65	600	0.20	1.93	25.18	2.39	23.58	1.01	2477
8	10000	0.30	67.5	15	200	0.30	5.82	41.24	6.28	44.95	1.24	2776
9	10000	0.30	80.0	40	400	0.10	4.71	50.47	5.50	38.99	1.48	2522
10	15500	0.10	55.0	40	600	0.20	5.45	48.25	5.68	46.61	1.02	7313
11	15500	0.10	67.5	65	200	0.30	3.53	27.65	4.05	29.91	1.24	7210
12	15500	0.10	80.0	15	400	0.10	5.33	45.29	5.80	41.53	1.48	8053
13	15500	0.20	55.0	65	200	0.10	7.96	82.49	5.62	48.47	1.02	3668
14	15500	0.20	67.5	15	400	0.20	5.68	45.58	5.47	41.10	1.24	4082
15	15500	0.20	80.0	40	600	0.30	6.06	46.26	6.69	52.11	1.48	3714
16	15500	0.30	55.0	15	400	0.30	6.13	50.70	6.62	47.77	1.01	2761
17	15500	0.30	67.5	40	600	0.10	5.29	42.10	5.54	45.38	1.24	2516
18	15500	0.30	80.0	65	200	0.20	5.37	41.39	5.30	40.88	1.48	2496
19	21000	0.10	55.0	65	400	0.30	5.29	42.82	5.71	44.66	1.02	7202
20	21000	0.10	67.5	15	600	0.10	6.71	48.43	6.33	45.22	1.24	8043
21	21000	0.10	80.0	40	200	0.20	2.88	26.48	2.67	19.78	148	7337
22	21000	0.20	55.0	15	600	0.20	6.20	48.38	5.76	45.69	1.02	4079
23	21000	0.20	67.5	40	200	0.30	5.37	52.67	5.58	47.86	1.24	3736
24	21000	0.20	80.0	65	400	0.10	5.14	47.09	5.44	43.72	1.48	3657
25	21000	0.30	55.0	40	200	0.10	6.56	70.75	5.61	49.68	1.01	2540
26	21000	0.30	67.5	65	400	0.20	6.26	52.78	5.52	48.43	1.23	2482
27	21000	0.30	80.0	15	600	0.30	6.27	47.76	6.93	53.11	1.48	2759

Table 5. *Design of experiments and corresponding results; nozzle size D_2 = 1.1 mm*

	n [min^{-1}]	h [mm]	Φ [%]	v [mm/s]	v_f [mm/min]	a_p [mm]	Ra_h [μm]	Ry_h [μm]	Ra_l [μm]	Ry_l [μm]	MD [m]	t [s]
1	10000	0.30	60.0	10	200	0.41	5.10	47.26	4.91	41.65	2.09	2330
2	10000	0.30	70.0	25	400	0.55	5.64	47.73	6.92	52.15	2.43	1977
3	10000	0.30	80.0	40	600	0.69	4.83	45.01	5.82	45.32	2.78	1901
4	10000	0.55	60.0	25	400	0.69	4.81	49.14	6.26	50.37	2.05	1102
5	10000	0.55	70.0	40	600	0.41	9.19	114.12	4.33	43.31	2.39	1061
6	10000	0.55	80.0	10	200	0.55	16.08	162.03	10.90	73.92	2.73	1312
7	10000	0.80	60.0	40	600	0.55	1.18	8.44	3.75	27.50	2.04	721
8	10000	0.80	70.0	10	200	0.69	2.24	17.52	3.64	24.02	2.38	900
9	10000	0.80	80.0	25	400	0.41	2.57	18.40	3.57	21.06	2.72	763
10	15500	0.30	60.0	25	600	0.55	4.30	33.67	4.43	33.19	2.09	1973
11	15500	0.30	70.0	40	200	0.69	24.75	198.15	9.61	75.19	2.43	1921
12	15500	0.30	80.0	10	400	0.41	7.47	61.69	8.65	57.98	2.78	2319
13	15500	0.55	60.0	40	200	0.41	14.65	171.67	5.64	40.99	2.05	1079
14	15500	0.55	70.0	10	400	0.55	7.56	55.75	8.94	60.33	2.39	1293
15	15500	0.55	80.0	25	600	0.69	9.07	120.38	6.09	54.23	2.73	1103
16	15500	0.80	60.0	10	400	0.69	2.97	26.14	5.25	38.50	2.04	882
17	15500	0.80	70.0	25	600	0.41	3.64	31.49	4.07	34.31	2.38	752
18	15500	0.80	80.0	40	200	0.55	8.98	65.07	8.11	60.07	2.72	752
19	21000	0.30	60.0	40	400	0.69	10.63	158.18	6.20	42.14	2.09	1907
20	21000	0.30	70.0	10	600	0.41	7.76	56.27	6.78	48.55	2.43	2311
21	21000	0.30	80.0	25	200	0.55	8.09	55.75	9.48	68.24	2.78	1989
22	21000	0.55	60.0	10	600	0.55	5.73	42.42	7.87	53.77	2.05	1282
23	21000	0.55	70.0	25	200	0.69	25.00	154.25	11.12	95.37	2.39	1121
24	21000	0.55	80.0	40	400	0.41	6.30	54.83	6.22	49.46	2.73	1068
25	21000	0.80	60.0	25	200	0.41	9.60	98.97	8.04	61.24	2.04	771
26	21000	0.80	70.0	40	400	0.55	3.40	43.69	7.06	48.81	2.38	730
27	21000	0.80	80.0	10	600	0.69	6.82	51.13	5.39	42.63	2.72	888

manufacturing and were followed and measured for each experiment set. Surface roughness of the machined parts was measured with contact surface roughness measuring device Mitutoyo Surftest SJ 301.

2.3 Evaluation and Analysis of Result

In Tables 4 and 5 (right of the thick line) the results for both nozzle sizes (D_1 = 0.4 mm and D_2 = 1.1 mm) conducted after carrying out all of the 27 experiments are given. This results were further used to analyse the influence of the technological parameters on the output responses as well as to obtain mathematical models for their final optimisation.

The mathematical models were obtained and evaluated by deployment of a computer program Design-Expert, which develops and analyses regression models using analysis of variance (ANOVA). Those acquired models have been evaluated on the basis of F-value, p-value, R^2, adjusted R^2 (Adj – R^2), predicted R^2 (Pred – R^2) and S/N ratio (signal to noise ratio). Please see Table 6 and 7.

2.4 Regression Models and Their Interpretation

In the following chapter, the regression models for the different responses and both nozzle sizes are presented through mathematical equations as well as 3D response surface graphs.

Regression models for roughness Ra_h:

- Nozzle size D_1 = 0.4 mm:

$$\begin{aligned} Ra_h = {} & 12.07961 + 3.2641 \cdot 10^{-4} \cdot n + \\ & 18.38333 \cdot h - 0.15542 \cdot \phi - 0.030158 \cdot v_f + \\ & 8.49242 \cdot 10^{-7} \cdot n \cdot v_f - 0.042417 \cdot h \cdot v_f + \\ & 3.67 \cdot 10^{-4} \cdot \phi \cdot v_f - 1.83104 \cdot 10^{-8} \cdot n^2. \end{aligned} \quad (1)$$

- Nozzle size D_2 = 1.1 mm:

$$\begin{aligned} \ln\left(Ra_h\right) = {} & 0.54592 + 8.93868 \cdot h + 0.056732 \cdot v - \\ & 5.08715 \cdot 10^{-3} \cdot v_f - 1.28640 \cdot 10^{-4} \cdot v \cdot v_f - \\ & 9.38239 \cdot h^2 + 8.21082 \cdot 10^{-6} \cdot v_f^2. \end{aligned} \quad (2)$$

The main influence on surface roughness in the direction perpendicular to the loading material flow, for both nozzle sizes, has layer height h and feed speed

Table 6. *Evaluation of regression models; nozzle size D_1 = 0.4 mm*

Output parameter	F-value	p-value	Regresor-influential parameter	Atypical hierarchical parameter	R^2	Adj-R^2	Pred-R^2	S/N
Ra_h	9.03	<0.0001	$n, n\times v_f, h\times v_f, \phi\times v_f$	n_2, h, ϕ, v_f	0.801	0.712	0.5379	12.48
Ry_h	5.83	0.0011	*	*	0.811	0.672	0.164	10.88
Ra_l	8.99	<0.0001	$a_p, n\times v_f, h\times v_f, \phi\times v_f, v_{f2}$	$n, h, \phi, v_f, n\times h$	0.849	0.755	0.597	12.28
Ry_l	12.27	<0.0001	$n, v_f, a_p, n\times h, n\times v_f, h\times v_f, \phi\times v_f, v_2$	$h, \phi, v, \phi\times v, h_2$	0.925	0.849	0.668	15.04
MD	39259.52	<0.0001	ϕ	/	0.999	0.999	0.999	343.19
t	3121.86	<0.0001	h, v	/	0.996	0.996	0.995	123.40

* Useless model because Adj-R^2 and Pred-R^2 differ more than 0.2.

Table 7. *Evaluation of regression models for hybrid; nozzle size D_2 = 1.1 mm*

Output parameter	F-value	p-value	Regresor-influential parameter	Atypical hierarchical parameter	R^2	Adj-R^2	Pred-R^2	S/N
Ra_h	7.97	0.0002	$h, v_f, v\times v_f, h^2$	v	0.705	0.617	0.427	10.90
Ry_h	5.90	0.0012	*	*	0.835	0.693	0.344	9.95
Ra_l	12.50	<0.0001	$n, \phi, v_f, v\times a_p, h^2, a_p{}^2$	h, v	0.902	0.830	0.669	12.11
Ry_l	14.40	<0.0001	$n, \phi, v_f, a_p, n\times h, n\times v, \phi\times v_f, v\times a_p, v_f\times a_p, h^2$	h, v	0.935	0.870	0.673	15.68
MD	246000	<0.0001	$h, \phi, h\times\phi, h^2, \phi^2$	/	1.000	1.000	1.000	1190.27
t	1157.56	<0.0001	h, v	/	0.990	0.989	0.987	80.32

*Useless model because Adj-R^2 and Pred-R^2 differ more than 0.2.

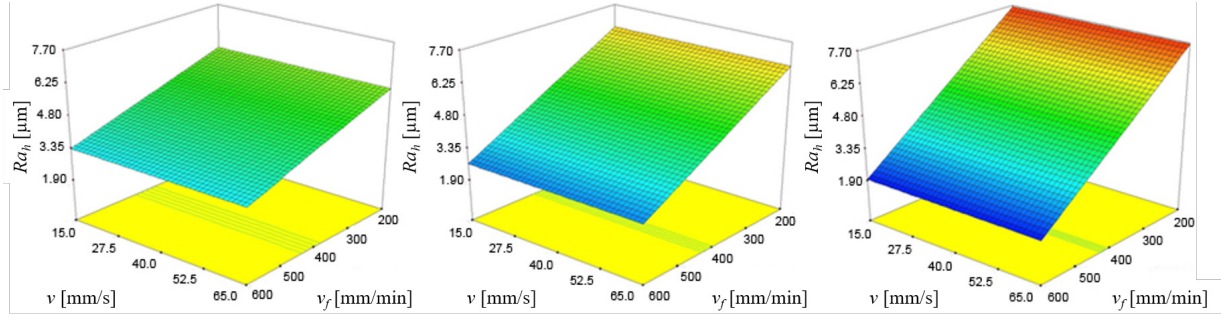

Fig. 2. *Influence of printing speed v and feed speed of milling tool v_f on surface roughness Ra_h by different layer heights h using nozzle size D_1 = 0.4 mm, n = 10000 min^{-1}, Φ 55 %, a_p = 0.1 mm; a) h = 0.1 mm, b) h = 0.2 mm, and c) h = 0.3 mm*

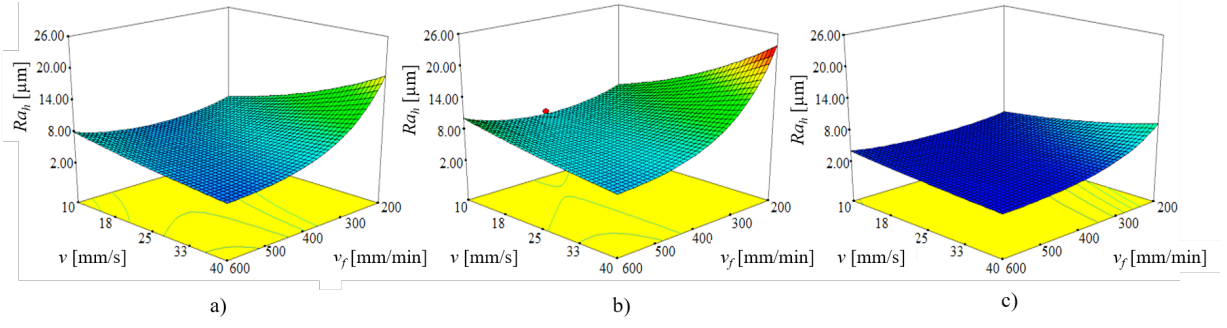

Fig. 3. *Influence of printing speed v and feed speed of milling tool v_f on surface roughness Ra_h by different layer heights h using nozzle size D_2 = 1.1 mm; a) h = 0.3 mm, b) h = 0.55 mm, and c) h = 0.8 mm*

of the milling tool v_f. It can be concluded (see Figs. 2 and 3) that the minimal roughness Ra_h can be obtained through higher layers. That leads to fewer passages or gaps in between layers, which might be detected with the tip of the measuring device stylus. The models for both nozzles show that printing speed v has only marginal effect on the surface roughness. However the best results (minimal roughness), especially with larger nozzle D_2, can be achieved, when maximal feed speed v_f and printing speed are applied. Experimental observations have also revealed that otherwise, slow feeds in combination with high spindle speed of milling tool cause material overheating, which leads to winding of material on the tools' surface and therefore to poor surface quality.

Regression models for roughness Ra_l:

- Nozzle size D_1 = 0.4 mm:

$$Ra_l = 10.85149 - 3.71616 \cdot 10^{-4} \cdot n + 7.16414 \cdot h - 0.082622 \cdot \phi - 7.27924 \cdot 10^{-3} \cdot v_f + 2.96111 \cdot a_p + 5.80808 \cdot 10^{-4} \cdot n \cdot h + 6.75758 \cdot 10^{-7} \cdot n \cdot v_f - 0.038625 \cdot h \cdot v_f + 2.33778 \cdot 10^{-4} \cdot \phi \cdot v_f - 1.25556 \cdot 10^{-5} \cdot v_f^2. \quad (3)$$

- Nozzle size D_2 = 1.1 mm:

$$Ra_l = -28.06072 + 3.78833 \cdot 10^{-4} \cdot n + 49.56052 \cdot h + 0.18399 \cdot \Phi - 0.26487 \cdot v - 7.98704 \cdot 10^{-3} \cdot v_f + 58.95257 \cdot a_p - 7.85634 \cdot 10^{-6} \cdot n \cdot v - 0.21452 \cdot h \cdot \Phi + 0.66534 \cdot v \cdot a_p - 31.67556 \cdot h^2 - 66.1281 \cdot a_p^2. \quad (4)$$

The conclusions obtained with previous regression models (Ra_h) can be applied also for the models of the surface roughness in the direction of the loading material Ra_l. To achieve minimal roughness, the tool spindle speed n must be set at level –1, as shown in Fig. 4. Higher spindle speed values cause material overheating and similar problems with material winding around tool, as found by interpretation of the feed speed v_f in the perpendicular direction. The regression models also reveal that at the highest value of layer h, minimal surface roughness Ra_l can be achieved using minimal material compensation flow Φ (Figs. 5 and 6).

Regression models for roughness Ry_l:

- Nozzle size D_1 = 0.4 mm:

$$Ry_l^{2.68} = 71475.11377 - 3.97046 \cdot n + 86279.98635 \cdot h - 613.28730 \cdot \phi + 1212.98635 \cdot v - 158.1637 \cdot v_f + 22158.41371 \cdot a_p + 10.87269 \cdot n \cdot h + 5.37597 \cdot 10^{-3} \cdot n \cdot v_f - 295.27319 \cdot h \cdot v_f - 6.99385 \cdot \phi \cdot \mathrm{v} + 2.15472 \cdot \phi \cdot \mathrm{v}_f - 3.08891 \cdot 10^{-5} \cdot h^2 - 8.9001 \cdot v^2. \quad (5)$$

- Nozzle size D_2 = 1.1 mm:

$$Ry_l = -129.23439 - 7.37746 \cdot 10^{-4} \cdot n + 265.11886 \cdot h + 2.13655 \cdot \Phi - 1.19240 \cdot v + 0.22008 \cdot v_f - 3.26786 \cdot a_p + 7.46030 \cdot 10^{-3} \cdot n \cdot h - 8.17239 \cdot 10^{-5} \cdot n \cdot v - 1.26044 \cdot h \cdot \Phi - 2.44771 \cdot 10^{-3} \cdot \Phi \cdot v_f + 4.41349 \cdot v \cdot a_p - 0.19900 \cdot v_f \cdot a_p - 270.54667 \cdot h^2. \quad (6)$$

The models in form of response surface diagrams presented in Figs. 7 and 8 give the same conclusions as in the case of the *Ra* roughness. The lowest spindle speed value has the lowest influence on heating of the workpiece material and its winding around the tool for both nozzle sizes. The higher feed speed v_f leads to better roughness in both cases, while the milling depth a_p has almost no influence on roughness Ry_l when

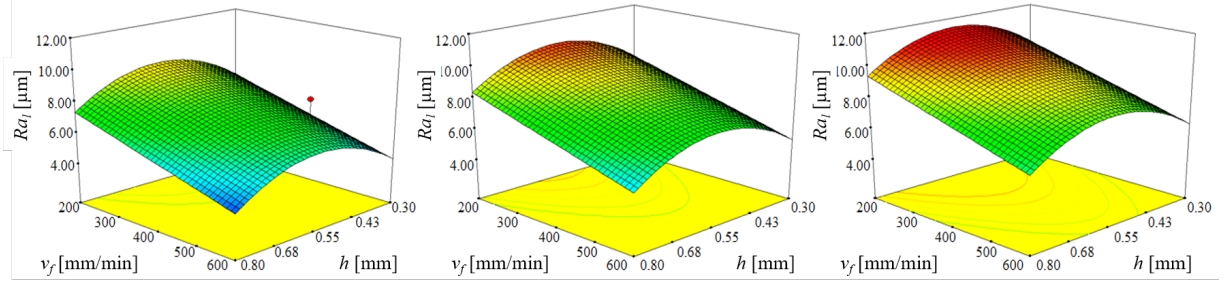

Fig. 4. Influence of feed speed of milling tool v_f and layer height h on surface roughness Ra_l by different spindle speed of milling tool n using nozzle size D_2 = 1.1 mm, Φ = 70 %, v = 25 mm/s, a_p = 0.55 mm; a) n = 10000 min^{-1}, b) n = 15500 min^{-1}, and c) n = 21000 min^{-1}

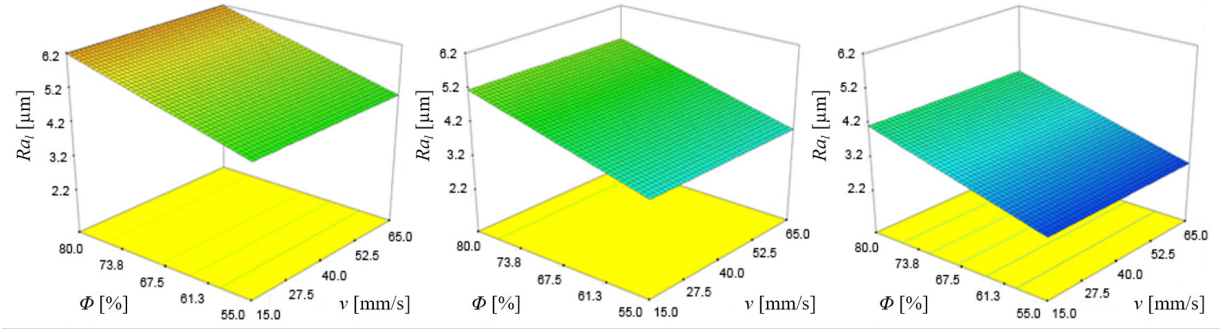

Fig. 5. Influence of material compensation flow Φ and printing speed v on surface roughness Ra_l by different layer heights h using nozzle size D_1 = 0.4 mm, n = 10000 min^{-1}, v_f = 600 mm/min, a_p = 0.1 mm; a) h = 0.1 mm, b) h = 0.2 mm, and c) h = 0.3 mm

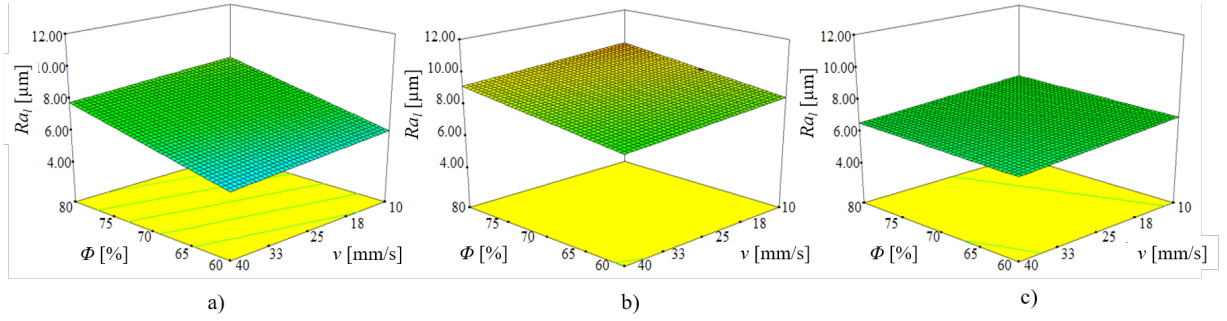

Fig. 6. *Influence of material compensation flow* Φ *and printing speed* v *on surface roughness* Ra_l *by different layer heights* h *using nozzle size* D_2 *= 1.1 mm,* n *= 15500 min*$^{-1}$*,* v_f *= 400 mm/min,* a_p *= 0.55 mm; a)* h *= 0.3 mm, b)* h *= 0.55 mm, and c)* h *= 0.8 mm*

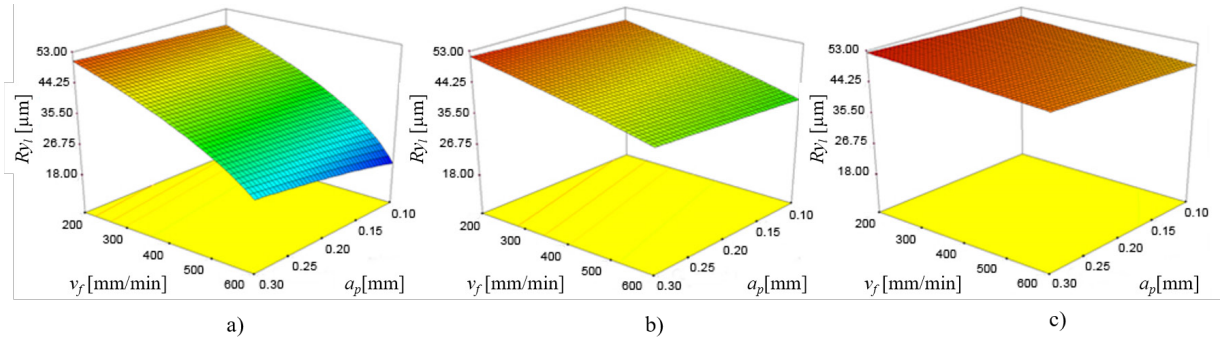

Fig. 7. *Influence of feed speed of milling tool* v_f *and milling depth ap on surface roughness* Ry_l *by different spindle speed of milling tool* n *using nozzle size* D_1 *= 0.4 mm,* h *= 0.3 mm,* Φ *= 55 %,* v *= 65 mm/s; a)* n *= 10000 min*$^{-1}$*, b)* n *= 15500 min*$^{-1}$*, and c)* n *= 21000 min*$^{-1}$

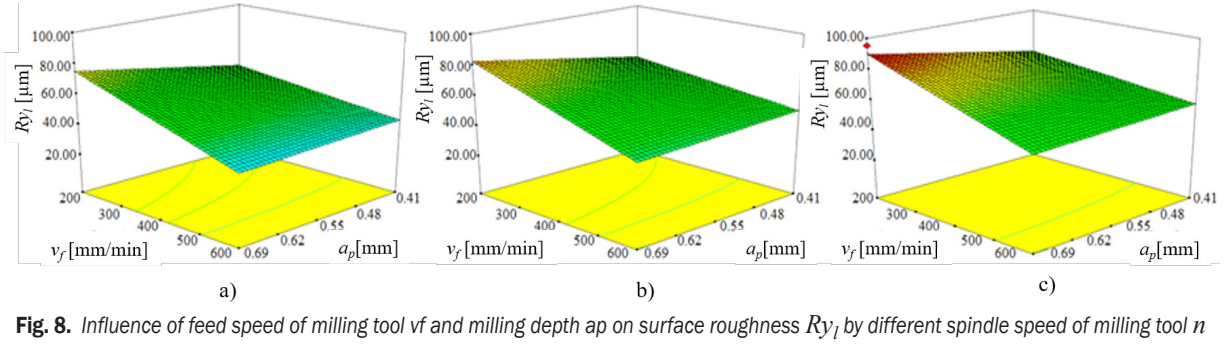

Fig. 8. *Influence of feed speed of milling tool vf and milling depth ap on surface roughness* Ry_l *by different spindle speed of milling tool* n *using nozzle size* D_1 *= 1.1 mm,* h *= 0.55 mm,* Φ *= 70 %,* v *= 25 mm/s; a)* n *= 10000 min*$^{-1}$*, b)* n *= 15500 min*$^{-1}$*, and c)* n *= 21000 min*$^{-1}$

the larger nozzle is applied. In the case of nozzle size D_1 = 0.4 mm, milling depth a_p is proportional to the roughness Ry_l (see Fig. 7). The finest roughness can be achieved by the use of minimal values of the milling depth a_p.

Regression models for material deposition MD:

- Nozzle size D_1 = 0.4 mm:

$$\sqrt{MD} = 0.54968 + 8.32623 \cdot 10^{-3}. \quad (7)$$

- Nozzle size D_2 = 1.1 mm:

$$\ln(MD) = -0.53217 - 0.18252 \cdot h + 0.027546 \cdot \Phi + 2.39521 \cdot 10^{-4} \cdot h \cdot \Phi + 0.11018 \cdot h^2 - 9.53869 \cdot 10^{-5} \cdot \Phi^2. \quad (8)$$

As can be observed from *MD* models in form of equations the main influence on material deposition *MD* for both nozzle sizes has material compensation flow Φ with proportional effect. In addition, as seen from the response surface diagram for the nozzle size D_2 = 1.1 mm (Fig. 9) if the minimal material flow is used the layer height *h* has no big influence on the material deposition.

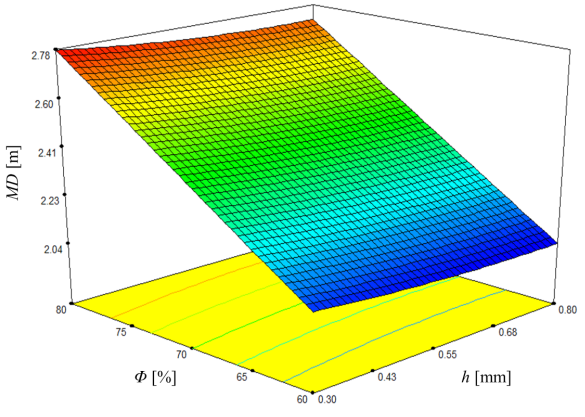

Fig. 9. *Influence of layer height h and material compensation flow Φ on material deposition MD using nozzle size D_2 = 1.1 mm*

Regression models for hybrid manufacturing time t:

- Nozzle size D_1 = 0.4 mm:

$$1/t = -1.488 \cdot 10^{-5} + 1.2647 \cdot 10^{-3} \cdot h + 5.61659 \cdot 10^{-7} \cdot v. \quad (9)$$

- Nozzle size D_2 = 1.1 mm:

$$\frac{1}{\sqrt{t}} = 0.011849 + 0.027023 \cdot h + 9.22941 \cdot 10^{-5} \cdot v. \quad (10)$$

The biggest influence on hybrid manufacturing time *t* has a layer height *h*. Shorter production times and minimal surface roughness are achieved by higher layer implementations. Response surface diagrams for both nozzle sizes (Figs. 10 and 9) show that at maximal layer height *h* printing speed *v* has no big influence on the hybrid manufacturing time.

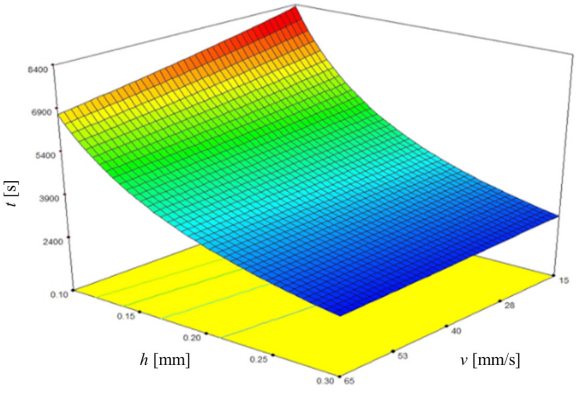

Fig. 10. *Influence of layer height h and printing speed v on time for manufacturing t for nozzle size D_1 = 0.4 mm*

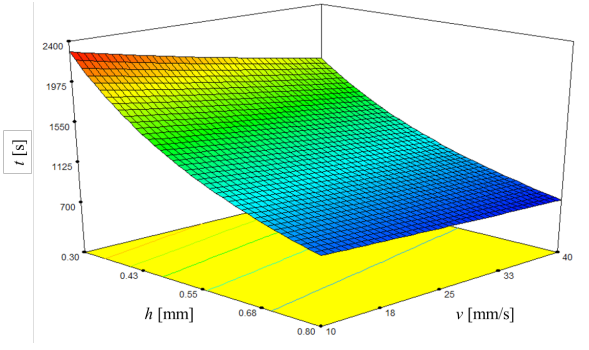

Fig. 11. *Influence of layer height h and printing speed v on time for manufacturing t for nozzle size D_2 = 1.1 mm*

2.5 Optimization of Parameters in the Hybrid Manufacturing

Faster production, with lower production costs and improved product quality, is what it is usually striving for. Accordingly, obtained regression models presented in chapter 2.4, were further deployed for hybrid manufacturing optimization according to three equally-weighted criteria: the minimal surface roughness *Ra* and *Ry* (in both directions), minimal material deposition *MD* and shortest production time *t*. The parameters settings for optimal technological solution for both nozzle sizes are shown in Table 8.

The optimal technological parameters settings, presented in the Table 8, match with the conclusions obtained during interpretation of the regression models. Nevertheless, the obtained optimal

parameters were checked with the confirmation test (Tables 9 and 10). The results of the measured output parameters after the confirmation test fit well with the optimization predicted values for both nozzle sizes as shown in the Tables 9 and 10.

Table 8. *Optimal technological parameters settings for both nozzle sizes*

	Nozzle size	
	D_1 = 0.4 mm	D_2 = 1.1 mm
n [mm–1]	10000	10000
h [mm]	0.3	0.8
Φ [%]	55	60
v [mm/s]	65	40
v_f [mm/min]	600	600
a_p [mm]	0.10	0.46

Table 9. *Results of confirmation test obtained with nozzle size D_1 = 0.4 mm*

	With optimization predicted values	After confirmation test measured values
Ra_h [μm]	1.96	2.05
Ry_h [μm]	Useless model	Not measured
Ra_l [μm]	2.71	2.74
Ry_l [μm]	18.56	19.24
MD [m]	1.02	1.01
t [s]	2494	2496

Table 10. *Results of confirmation test obtained with nozzle size D_2 = 1.1 mm*

	With optimization predicted values	After confirmation test measured values
Ra_h [μm]	2.18	2.16
Ry_h [μm]	Useless model	Not measured
Ra_l [μm]	2.69	2.60
Ry_l [μm]	18.05	18.18
MD [m]	2.04	2.04
t [s]	724	723

Comparison of parameters settings for both nozzle sizes reveals that the same conclusions can be applied for both of them. For the achievement of optimal conditions according to required criteria, maximal layer height h, maximal printing speed v, minimal material compensation flow Φ, minimal spindle speed of milling tool n, maximal feed speed of milling tool v_f, and milling depth a_p at minimal level should be selected.

For the consideration of the minimal surface roughness, the size of the nozzle bears no importance. Furthermore, a noticeable difference in the material consumption between the two nozzle sizes has minor importance due to the affordable material price. However, when the hybrid manufacturing time t is important, then it is better to use bigger nozzle size D_2 = 1.1 mm which allows for three times shorter manufacturing time.

3 CONCLUSIONS

A statistical approach has been applied to investigate the influence of the technological parameters on the surface roughness, material deposition and hybrid manufacturing time.

Based on the analysis of regression models, the optimal spindle speed of the milling tool n, layer height h, material compensation flow Φ, printing speed v, feed speed of the milling tool v_f and milling depth a_p have been identified. Conclusions obtained with optimal results by both nozzle sizes can be interpreted in the same manner:

1. Surface roughness after hybrid manufacturing: the main influence on roughness has layer height h. With the highest layer, minimal roughness (Ra and Ry) can be achieved in both directions of measurement. At such layer height, material compensation flow Φ has no influence on roughness. The high spindle speed of the milling tool n can cause material winding on the tools surface. Therefore, the optimal value for this parameter is selected as a minimal value. The feed speed of the milling tool v_f affects inversely proportional the roughness. A smaller milling depth a_p assures better roughness when the smaller nozzle is being applied, while in the case of larger nozzle the depth of milling has only marginal influence.
2. Material deposition in the hybrid manufacturing: the main influence on material deposition MD has material compensation flow Φ, which effects proportionally.
3. Hybrid manufacturing time: the shortest manufacturing time can be achieved and the highest surface quality can be obtained when both, the fastest printing and the highest layer, are applied.

Main conclusion: with the application of the bigger nozzle size (D_2 = 1.1 mm) the same final surface roughness can be achieved as with smaller (standard, D = 0.4 mm) nozzle size, but at three times higher productivity.

4 REFERENCES

[1] Grguraš, D. (2015). *Preparation of the CNC-Code and Optimization of the Technological Parameters in the Hybrid Manufacturing. MSc thesis,* University of Ljubljana, Faculty of Mechanical Engineering, Ljubljana. (in Slovene)

[2] Kozan, Ž. (2016), *Optimization of the Technological Parameters in Hybrid Manufacturing.* BSc thesis, University of Ljubljana, Faculty of Mechanical Engineering, Ljubljana. (in Slovene)

[3] Song, Y.-A., Park, S., Choi, D., Jee, H. (2005). 3D welding and milling: Part I – a direct approach for freeform fabrication of metallic prototypes. *International Journal of Machine Tools and Manufacture*, vol. 45, no. 9, p. 1057-1062, **DOI:10.1016/j.ijmachtools.2004.11.021**.

[4] Song, Y.-A., Park, S., Choi, D., Chae, S.-W. (2005). 3D welding and milling: Part II – optimization of the 3D welding process using an experimental design approach. *International Journal of Machine Tools and Manufacture*, vol. 45, no. 9, p. 1063-1069, **DOI:10.1016/j.ijmachtools.2004.11.022**.

[5] Boivie, K., Homar, D., Dolinšek, S., Broetan V. (2012). The hybrid manufacuring cell: an integrated solution for additive manufacturing with CNC machining. *4th International Conference on Additive Technologies*, Maribor, p. 1-15.

[6] Yamazaki, T. (2016). Development of a Hybrid Multi-tasking Machine Tool: Integration of Additive Manufacturing Technology with CNC Machining. *Procedia CIRP*, vol. 42, p. 81-86, **DOI:10.1016/j.procir.2016.02.193**.

[7] Lee, W.-C., Wei, C.-C., Chung, S.-C. (2014). Development of a hybrid rapid prototyping system using low-cost fused deposition modeling and five-axis machining. *Journal of Materials Processing Technology*, vol. 214, no. 11, p. 2366-2374, **DOI:10.1016/j.jmatprotec.2014.05.004**.

[8] Mohamed, O.A., Masood, S.H., Bhowmik, J.L. (2016). Optimization of fused deposition modeling process parameters for dimensional accuracy using I-optimality criterion. *Measurement*, vol. 81, p. 174-196, **DOI:10.1016/j.measurement.2015.12.011**.

[9] Kaveh, M., Badrossamay, M., Foroozmehr, E., Etefagh, A.H. (2015). Optimization of the printing parameters affecting dimensional accuracy and internal cavity for HIPS material used in fused deposition modeling processes. *Journal of Materials Processing Technology*, vol. 226, p. 280-286, **DOI:10.1016/j.jmatprotec.2015.07.012**.

[10] Rao, R.V., Rai, D.P. (2016). Optimization of fused deposition modeling process using teaching-learning-based optimization algorithm. *Engineering Science and Technology, an International Journal*, vol. 19, no. 1, p. 587-603, **DOI:10.1016/j.jestch.2015.09.008**.

[11] Hassine H., Barkallah M., Bellacicco A., Louati J., Riviere A., Haddar M. (2015). Multi Objective Optimization for Sustainable Manufacturing, Application in Turning. *International Journal of Simulation Modelling*, vol. 14, no. 1, p. 98-109, **DOI:10.2507/IJSIMM14(1)9.292**.

[12] Barkallah M., Louati J., Haddar M. (2012). Evaluation of Manufacturing Tolerance Using a Statistical Method and Experimentation. *International Journal of Simulation Modelling*, vol. 11, no. 1, p. 5-16, **DOI:10.2507/IJSIMM11(1)1.194**.

Strojniški vestnik - Journal of Mechanical Engineering 63(2017)10, 577-582

DOI:10.5545/sv-jme.2017.4356 Original Scientific Paper
Received for review: 2017-01-26
Received revised form: 2017-04-14
Accepted for publication: 2017-06-06

Influence of Variously Modified Surface of Aluminium Alloy on the Effect of Pulsating Water Jet

Jiri Klich* – Dagmar Klichova – Vladimir Foldyna – Petr Hlavacek – Josef Foldyna
Institute of Geonics of the CAS, Czech Republic

Erosion effects of a pulsating water jet impinging the surface of aluminium alloy samples pre-treated by various techniques (rough and fine milling, planing and rolling) were studied. The influence of the initial surface topography on the final topography of the sample exposed to the pulsating water jet was investigated. Based on roughness parameter Ra erosion of surface layers was analysed and discussed in relation to the traversing speed of the jet. It was found that initial surface pre-treatment have a significant impact on the final topography of the surface affected subsequently by pulsating water jet. Surfaces, whose properties are significantly affected by the action of some machining processes (i.e. milling) show much greater resistance to pulsating water jet than unpaved surfaces (i.e. rolling) and surfaces have smaller roughness. While milled (rough or fine) or planed surface roughness has approximately the same increase of Ra parameter, only rolled surfaces are up to 150 times rougher after pulsating water jet treatment. This is due to the small hardening of the surface layers and reduced durability against pulsating water jet in comparison with others investigated techniques. The highest roughness was achieved on all pre-treated surfaces at the lowest speeds, because the pulsating water jet affects the surface for a longer time.
Keywords: pulsating water jet, surface topography, material erosion

Highlights
- *Surface parameters were obtained after PWJ treatment.*
- *Different influence of PWJ was found on various modified surfaces.*
- *Hardened surface layer during milling, which results in its greater resistance to the impact of the PWJ.*
- *The parameter Raratio was used to compare the roughness of surfaces before and after treatment.*

0 INTRODUCTION

Over hundred years, researchers have been interested in the interaction of a liquid with a solid. One of the first researchers dealing with this subject was Cook [1] who wrote his article on the surface erosion in 1928. He clearly recognized the importance of the water hammer pressure.

Pulsating water jet (PWJ) has been successfully used for several industrial applications. Pulsating water jet is an extension of the conventional (continuous) jet, consisting of an array of high-speed water pulses. When a pulsating water jet impinges a target, the momentum flux through the nozzle is not transmitted to the target material as a steady force, but as a discontinuous sequence of impacts, creating high momentary stresses in the impingement zone. As a result, the peak pressure acting on the surface is not the stagnation pressure, but the significantly higher water hammer pressure [2] and [3].

There are several ways how to create the pulsating water jet as shown, for instance, in [4]. It can be done using mechanical interrupters, self-resonating systems, jets modulation by the piezoelectric magnetostrictive effects, jet disruption by electric discharge, laser based pulsating of water jets, etc. In our case, the system for the generation of acoustic pulsations developed at the Institute of Geonics of the ASCR, v. v. i. was used [5] to [7].

The high-speed pulsating water jets are generated by sufficiently high pressure pulsations in pressure water in the upstream direction to the nozzle exit. In the nozzle, the pressure pulsations change into speed pulsations and the jet emerges from the nozzle exit as a continuous jet with variable axial speed. Owing to the variable speed, the jet is formed into pulses at a certain stand-off distance towards the nozzle exit (so called forced break-up length of the jet) and it starts acting as a pulsating jet. Exploitation of effects related to the water pulses impingement on solids in the field of the high-speed water jet technology should result in considerable improvement of its performance, better adaptation to progressively more demanding environmental requirements and, consequently, more cost-saving use of the technology from the economical point of view [8].

Unlike classical continuous water jet, pulsating water jet is able to create different final texture in surface treatment and it is several times more effective [2].

The objective of the paper is to determine erosion effects of the pulsating water jet impinging the surface of aluminium alloy samples treated by various techniques (rough and fine milling, planing

*Corr. Author's Address: Institute of Geonics of the ASCR, v. v. i., Ostrava, 70800, Czech Republic, jiri.klich@ugn.cas.cz

and rolling) and to discuss the influence of the initial surface topography on the final topography of the sample exposed to the pulsating water jet.

1 METHODS

Kerfs were formed successively with pulsating water jet on test samples. These aluminium alloy samples were pre-treated with various technological processes. Subsequently, surface roughness was obtained. We suppose that surface pre-treatment by various forming and machining techniques has significant influence on disintegration ability of subsequently applied pulsating water jet due to surface strengthening by particular technique ([9] and [10]).

The facility used for the experiment consisted basically of a high-pressure water supply system, pulsating water jet generator, robotic manipulator ABB IRB 6640-180/2.55 Master for traversing the jet over test samples and optical surface profilometer MicroProf FRT for the evaluation of surface characteristics of the samples [11].

The high-pressure water was supplied to the generator of pulsating water jet by a plunger pump Hammelmann HDP 253 able to deliver up to 65 l·min^{-1} of water at the operating pressure up to 160 MPa. The generator was equipped with a commercially available fan nozzle with the equivalent orifice diameter of 2.0 mm and the spraying angle of 10°.

The generator of pulsating water jet was designed for the maximum operating pressure of 150 MPa. It consisted of a piezoelectric transducer vibrating at the operating frequency of about 20 kHz and it was driven by an ultrasonic generator Ecoson with the maximum output power of 800 W.

Test samples were manufactured from the aluminium alloy from Alfun Company known as EN AW 5083 H111 (Table 1). This alloy was chosen, because it is frequently used in construction. Industry often requires surface treatment of this material.

Table 1. *Aluminium alloy EN AW 5083 H111*

Chemical composition [wt. %]			
Al	Mg	Mn	
94.8	4.5	0.7	
Mechanical properties			
Yield strength $\sigma_{0.2}$ [MPa]	Tensile strength σ_{Pt} [MPa]	Elongation A_{50} [mm]	Hardness Brinell [HB]
125	275	12	75

Firstly, the abrasive water jet technology was used to cut the samples from 10 mm thick sheet in order to eliminate thermal effects on the properties of samples [12] to [14]. Dimensions of the test samples were 10 mm × 60 mm × 100 mm (Fig. 1). Secondly, the samples surface was treated by rough milling, fine milling and planing. One sample remained untreated; its surface was only affected by rolling during the aluminium sheet manufacturing. Parameters of the used technological operations are presented in Table 2. Then, surfaces were scanned by an optical profilometer to determine the initial surface roughness of the prepared samples (before their exposition to the pulsating water jet) [15] and [16].

To compare the roughness of surfaces before and after treatment of the PWJ, the parameter Ra_{ratio} (Eq. (1)) was used, where Ra represents the roughness of surface after the PWJ treatment and Ra_{ini} represents the roughness of initial surface untreated by the PWJ:

$$Ra_{ratio} = \frac{Ra}{Ra_{ini}}. \quad (1)$$

Table 2. *Parameters of technological operations*

Surface treatment	Technological parameters
Rough milling	Milling cutter Ø63 mm, 12 cutting edges, 360 RPM, traversing speed 65 mm·min^{-1}
Fine milling	Milling cutter Ø63 mm, 12 cutting edges, 1500 RPM, traversing speed 470 mm·min^{-1}
Planing	Planing machine 52 strokes per minute, feed rate 0.12 mm per stroke
Rolling	N/A

2 EXPERIMENTS

To enable to expose the sample surface to the effect of the pulsating water jet, the following testing procedure was developed (Fig. 2). A robotic arm ensured the nozzle movement with an exactly programmed trajectory. During experiments, the traversing speed of the nozzle was set to (0.5, 0.75, 1.0, 2.0 and 4.0) mm·s^{-1}; the stand-off distance was set to 55 mm. This stand-off distance was determined as optimal for experimental conditions based on previous tests [8]. The angle of incidence was set to 90°.

The tests were performed at the operating pressure of 20 MPa (the corresponding jet speed was approx. 180 m·s^{-1}). Pressure pulsations were generated in a pulsating water jet generator at the frequency of 20.09 kHz (the readout displayed by the ultrasonic generator); the amplitude of vibration of the ultrasonic sonotrode tip was set to 7 μm.

Each sample was exposed to the action of the pulsating jet in five areas according to a predefined

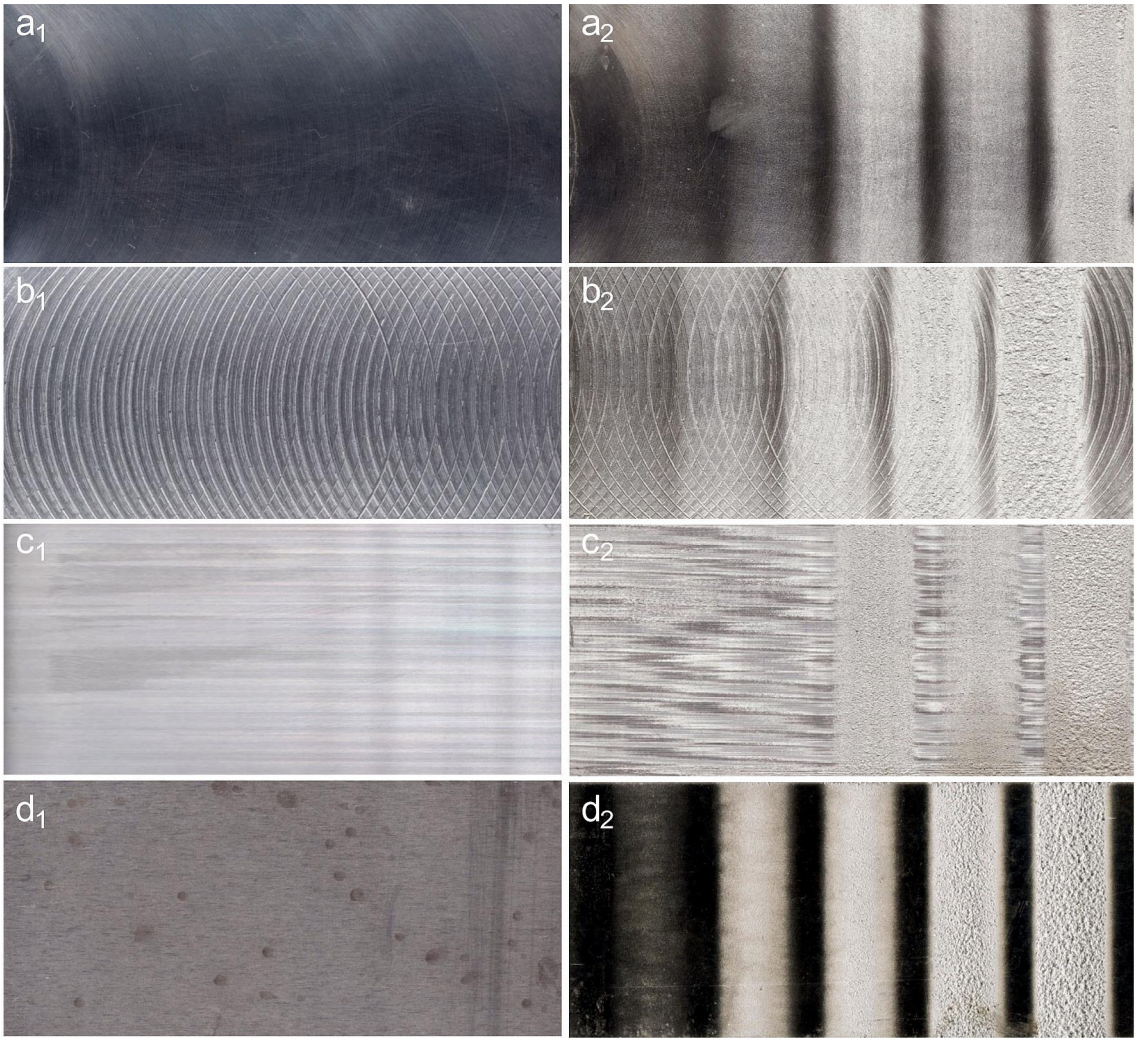

Fig. 1. *Appearance of initial surfaces of EN AW 5083 H111 samples after treatment by various technologies: a1) fine milling, b1) rough milling, c1) planing, d1) rolling; traces formed by PWJ on pre-treated surfaces: a2) fine milling, b2) rough milling, c2) planing, d2) rolling; traversing velocities on samples a2, b2, c2, d2: 4.0, 2.0, 1.0, 0.75 and 0.5 mm·s^{-1} (from left to right)*

experimental plan based on variations of the traversing speed of the pulsating water jet (Fig. 1).

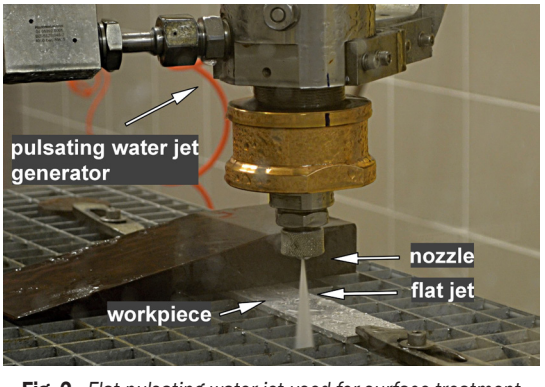

Fig. 2. *Flat pulsating water jet used for surface treatment*

Subsequently, the optical profilometer MicroProf FRT was used for the 3D determination of sample surfaces (Fig. 3).

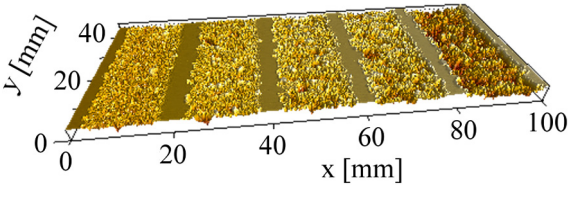

Fig. 3. *3D visualization of pre-treated (planed) surface*

Measured data were processed using the SPIP software. Fig. 4 shows the areas of 40 mm × 5 mm measured on tested surfaces.

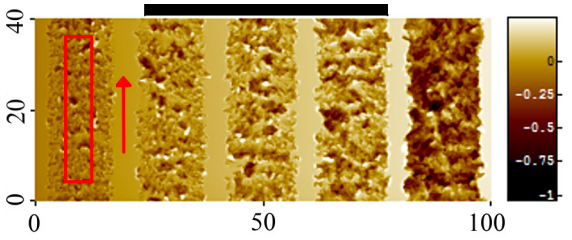

Fig. 4. *Designation of measured areas and profile direction on pre-treated surface*

The distance of measurement points for every tested surface profile was set to 4 µm in *y* direction and 250 µm in *x* direction. Then, five profiles in each kerf of the obtained topography were analysed. After averaging, the profile was analysed and the 2D surface parameter *Ra* was finally determined. It is the most commonly used parameter for assessing surface roughness. This parameter is included in the accuracy of the standards used in technical drawings and blueprints when not set a specific roughness of the surface. Statistically, this is a very stable and repeatable parameter.

3 RESULTS

The values of the parameter *Ra* in relation to the traversing speed of the jet *v* and the initial surface treatment of a material are presented in Fig. 5.

The least roughened initial surface with an average value of *Ra* = 0.5 µm was achieved on a surface affected by the rolling technology. This value was measured in a direction perpendicular to the rolling direction. The roughness of *Ra* = 0.9 µm was achieved on a fine milled surface. The planing technology showed the roughness of *Ra* = 2.6 µm in a direction perpendicular to the direction of the cutter. The roughest surface with the value of *Ra* = 4.5 µm was created using the rough milling technology.

Obtained results indicate that the surface pre-treatment of a material has a significant effect on the surface topography after the application of the pulsating water jet. Fig. 5 shows the surface roughness *Ra* in relation to the traversing speed *v* on various tested surfaces. It can be observed that at the traversing speed v = 4.0 mm·s^{-1}, the roughness *Ra* does not really differ from its initial values. The roughest surface is the rough milled surface, followed by the planed surface, then the rolled surface and finally the surface treated by the fine milling. At the traversing speed v = 2.0 mm·s^{-1}, the PWJ has even stronger effect and roughness order of the rolled surface is changed. At the traversing speed v = 1.0 mm·s^{-1}, the PWJ effect on material surface is very strong and the roughness of the rolled surface increases rapidly. In contrast, the parameter *Ra* does not change considerably on both roughly and finely milled surfaces. At the traversing speed v = 0.75 mm·s^{-1}, the value of *Ra* for fine milled surface is still low. The *Ra* value increases significantly in case of other surfaces. At the lowest traversing speed v = 0.5 mm·s^{-1}, very large volume removal occurs on every surface. Accordingly, the value *Ra* increases significantly on all surfaces.

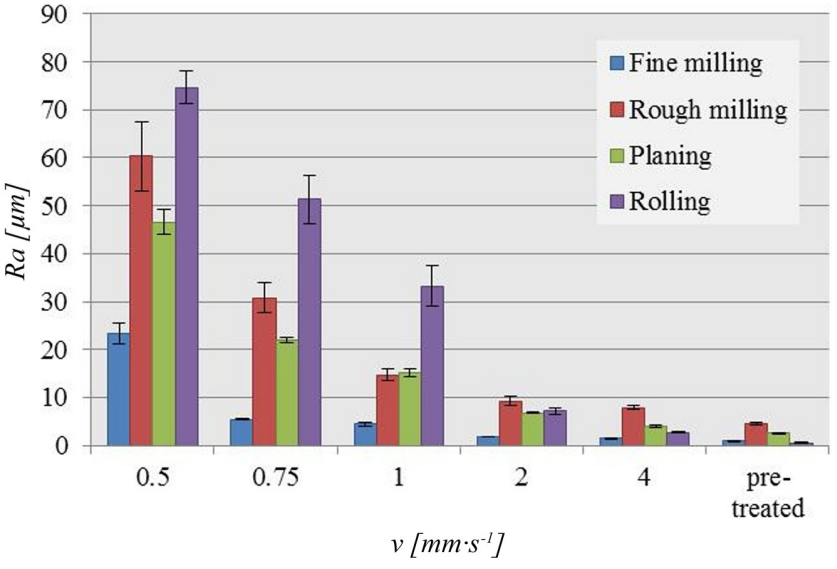

Fig. 5. *Effect of traversing speed v on arithmetical mean of profile Ra*

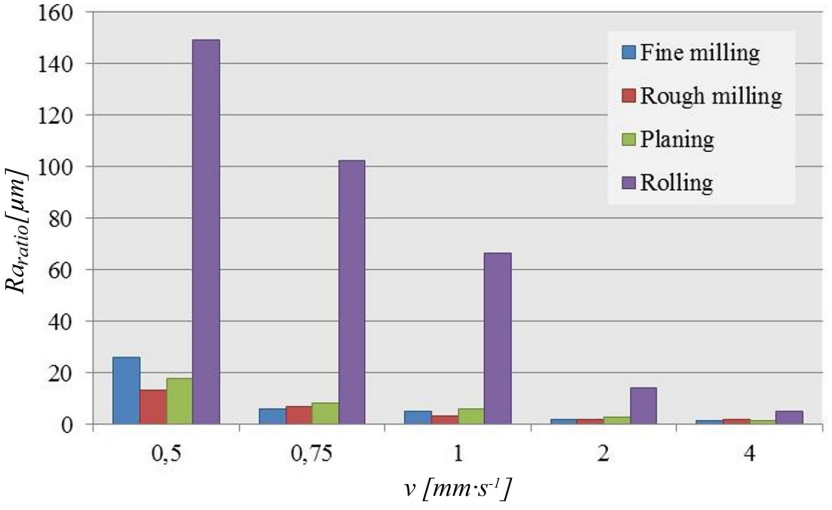

Fig. 6. *Relative roughness Raratio between original surfaces and the surfaces affected by PWJ at different traversing speed v*

If we look at Fig. 6 showing the ratio of the roughness *Ra* before and after the PWJ action, we can realize that the roughness of the rolled surface treated by the PWJ at the traversing speed v = 0.5 mm·s^{-1} has increased 150 times, by other surfaces only approximately 20 times.

4 DISCUSSION

The assumptions that surfaces with significant roughness (after rough milling) disrupt the effect of the PWJ and that the radial flow of the liquid along the surface aligns peaks created by rough milling were confirmed. Values of roughness *Ra* are very similar to the values of the rolled and milled surfaces before the PWJ action. However, significant difference between these two surfaces occurs after using the PWJ. This could be caused by hardening of the surface layer during milling, which results in its greater resistance to the impact of the PWJ.

Surfaces treated by pulsating jets show larger effective area compared to those treated by continuous jet [17]. This knowledge could be utilized in applications where good adhesion of coating layer or new overlay material to substrate surface both in tension and shear is needed.

This feature of pulsating jets was confirmed by tests on repair of concrete structures. Generally speaking, repair materials better adhere to rough surface. Toutanji and Ortiz [18] reported that surface treatment by water jet produces a better bonding strength than surface treatment by sander. It was found [19] that the pulsating jet produces more "rough" surface with larger effective surface area compared to continuous one. During standard pull-off tests average bonding strength in the cases of the pulling off carried out on the contact between mortar and concrete was by about 38 % higher in the case of surfaces treated with pulsating water jet than in the cases of surfaces treated with continuous water jet [20].

5 CONCLUSIONS

Experimental work oriented on the evaluation of effects of the pulsating water jet on surfaces treated by different technologies shows that the erosion caused by repeated impacts of water pulses depends on the initial conditions of a material surface.

Generally, the highest values of roughness after the pulsating water jet application were achieved on surfaces pre-treated by the rolling and consequent annealing which relieved stresses in surface layer. In contrast, other surface treatments based on various machining methods strengthened surface layers and thereby hindered the jet from easy penetration into the material.

Practical meaning of this experiment is to determine which kind of surface is optimal for subsequent using of pulsating water jet. This could help to optimize the process and reduce costs in production. During the subsequent treatment of the surface, the parameters are intended by the pre-treatment technology. For example, travel speed or water pressure, which affects the economy significantly.

Next steps of the research in this area will be oriented at the study of the influence of the surface layer hardness on the erosion process caused by effects of the pulsating water jet and the investigation of changes of properties of surface layers due to impacts of the water pulses.

6 ACKNOWLEDGEMENTS

Presented work has been supported by the ASCR project No. AV0Z30860518 and by the Ministry of Industry and Trade of the Czech Republic project No. FV 10446 and the project Institute of Clean Technologies for Mining and the Utilization of Raw Materials for Energy Use – Sustainability program, reg. no. LO1406 financed by the Ministry of Education, Youth and Sports of the Czech Republic.

7 REFERENCES

[1] Cook, S.S. (1928). Erosion by water-hammer. *Proceedings of the Royal Society A Mathematical, Physical and Engineering Science*, vol. 119, no. 783, p. 481-488, **DOI:10.1098/rspa.1928.0107**.

[2] Foldyna, J., Sitek, L., Ščučka, J., Martinec, P., Valíček, J., Páleníková., K. (2009) Effects of pulsating water jet impact on aluminium surface. *Journal of Materials Processing Technology*, vol. 209, no. 20, p. 6174-6180, **DOI:10.1016/j.jmatprotec.2009.06.004**.

[3] Bai, C., Chandra, S., Daniels, B., Ren, B., Yan, W., Tieu, A., Vijay, M. (2006). Abrasive-Entrained High-Frequency Pulsed Waterjet: Basic Study and Applications. *Proceedings of the 18th International Conference on Water Jetting*, p. 325-336.

[4] Bach, F.W., Schenk, A., Kremer, G., Biskup, C., Meier, O., Fargas, M., Bunte, J., Jäschke, P. (2006). Increase of erosive potential of water jets by laser pulsing. *Proceedings of the 18th International Conference on Water Jetting*, p. 357-366.

[5] Foldyna, J., Švehla, B., (2008). *Method of Generation of Pressure Pulses and Apparatus for Making the Same*. CZ patent 299412, Industrial Property Office, Praque.

[6] Sitek, L., Foldyna, J., Martinec, P., Ščučka, J., Bodnárová, L., Hela, R. (2011). Use of pulsating water jet technology for removal of concrete in repair of concrete structures. *Baltic Journal of Road and Bridge Engineering*, vol. 6, no. 4, p. 235-242, **DOI:10.3846/bjrbe.2011.30**.

[7] Riha, Z., Foldyna, J. (2012). Ultrasonic pulsations of pressure in water jet cutting tool. *Tehnicki Vjesnik - Technical Gazette*, vol. 19, no. 3, p. 487-491.

[8] Foldyna, J., Klich, J., Hlaváček, P., Zeleňák, M., Ščučka, J. (2012). Erosion of metals by pulsating water jet. *Tehnicki Vjesnik - Technical Gazette*, vol. 19, no. 2, p. 381-386.

[9] Asad, M., Mabrouki, T., Girandin, F., Yhang, Z., Rigal, J.-F. (2011). Towards a physical comprehension of material strengthening factors during macro to micro-scale milling. *Mechanics*, vol. 17, no. 1, p. 97-104, **DOI:10.5755/j01.mech.17.1.210**.

[10] Rao, S., Shunmugam, M.S. (2012). Analytical modelling of micro end-milling forces with edge radius and material strengthening effects. *Machining Science and Technology*, vol. 16, no. 2, p. 205-227, **DOI:10.1080/10910344.2012.673966**.

[11] Lehocka, D., Klich, J., Foldyna, J., Hloch, S., Krolczyk, J.B., Carach, J., Krolczyk, G.M. (2016). Copper alloys disintegration using pulsating water jet. *Measurement*, vol. 82, p. 375-383, **DOI:10.1016/j.measurement.2016.01.014**.

[12] Hreha, P., Hloch, S., Monka, P., Monková, K., Knapčíková, L., Hlaváček, P., Zeleňák, M., Samardžić, I., Kozak, D. (2014). Investigation of sandwich material surface created by abrasive water jet (AWJ) via vibration emission. *Metalurgija*, vol. 53, no. 1, p. 29-32.

[13] Hreha, P., Radvanská, A., Cárach, J., Lehocká, D., Monková, K., Krolczyk, G., Ruggiero, A., Samardzić, I., Kozak, D., Hloch, S. (2014). Monitoring of focusing tube wear during abrasive waterjet (AWJ) cutting of AISI 309. *Metalurgija*, vol. 53, no. 4, p. 533-536.

[14] Hreha, P., Radvanská, A., Hloch, S., Peržel, V., Królczyk, G., Monkova, K. (2014). Determination of vibration frequency depending on abrasive mass flow rate during abrasive water jet cutting. *The International Journal of Advanced Manufacturing Technology*, vol. 77, no. 1, p. 763-774, **DOI:10.1007/s00170-014-6497-9**.

[15] Krolczyk, G., Legutko, S. (2014). Experimental analysis by measurement of surface roughness variations in turning process of duplex stainless steel. *Metrology and Measurement Systems*, vol. 21, no. 4, p. 759–770, **DOI:10.2478/mms-2014-0060**.

[16] Wojciechowski, S., Twardowski, P., Wieczorowski, M. (2014). Surface texture analysis after ball end milling with various surface inclination of hardened steel. *Metrology and Measurement Systems*, vol. 21, no.1, p. 145-156. **DOI:10.2478/mms-2014-0014**.

[17] Sitek, L., Foldyna, J., Martinec, P., Ščučka, J., Bodnárová, L., Hela, R. (2011). Use of pulsating water jet technology for removal of concrete in repair of concrete structures. *The Baltic Journal of Road and Bridge Engineering*, vol. 6, no. 4, p. 235-242, **DOI:10.3846/bjrbe.2011.30**.

[18] Toutanji, H., Ortiz, G. (2001). The effects of surface preparation on the bond interface between FRP sheets and concrete members. *Composite Structures*, vol. 53, no. 4, p. 457-462, **DOI:10.1016/S0263-8223(01)00057-5**.

[19] Sitek, L., Foldyna, J., Ščučka, J., Mlynarczuk, M., Sobczyk, J. (2002). Quality of bottom surface of kerfs produced by modulated jets. *Proceedings of the 16th International Conference on Water Jetting*, p. 359-368.

[20] Sitek, L., Foldyna, J., Klich, J., Bodnárová, L., Wolf, I. (2012). Aplications of oscilating waterjets to in situ removing of decomposed surface layers of concrete. *Tunel*, vol. 21, no. 2, p. 16-26.

Strojniški vestnik - Journal of Mechanical Engineering 63(2017)10, 583-589

DOI:10.5545/sv-jme.2017.4357 Original Scientific Paper
Received for review: 2017-01-26
Received revised form: 2017-05-19
Accepted for publication: 2017-06-13

Effects of Continuous and Pulsating Water Jet on CNT/Concrete Composite

Vladimir Foldyna[1, 2,*] – Josef Foldyna[2] – Dagmar Klichova[2] – Jiri Klich[2] – Petr Hlavacek[2] – Lenka Bodnarova[3] – Tomas Jarolim[3] – Katerina Mamulova Kutlakova[1]

[1] VSB-Technical University of Ostrava Nanotechnology Centre, Czech Republic
[2] Institute of Geonics of the ASCR, Department of Material Disintegration, Czech Republic
[3] Brno University of Technology, Faculty of Civil Engineering, Czech Republic

This paper presents first results of the study of the resistance of carbon nanotube concrete composite (CNT/concrete composite) to the action of continuous and pulsating water jets. The experiments oriented at the determination of erosion effects of pulsating and continuous water jets impinging the surface of reference (concrete) and CNT/concrete composite samples were performed. Tested samples were characterized by X-ray powder diffraction and scanning electron microscope. Samples were exposed to pulsating and continuous water jets at various operating parameters. Erosion effects of pulsating and continuous jets were evaluated in terms of material removal rate. The possible influence of addition of CNTs to the concrete on its resistance to the action of continuous and pulsating water jets is discussed in the paper. The experiments proved that CNT/concrete composite exhibits higher resistance than reference concrete to the action of both pulsating and continuous water jet under the given testing conditions.

Keywords: pulsating and continuous water jet, CNT/concrete composite, material removal

Highlights

- *Results of physical-mechanical properties of CNT/concrete composite after 7 days of hydration.*
- *Higher resistance of CNT/concrete composite to the action of pulsating water jet.*
- *Higher resistance of prepared sample to the action of continuous water jet.*
- *Characterization of the sample by X-ray powder diffraction and scanning electron microscopy.*

0 INTRODUCTION

In past years, concrete was used worldwide in the field of civil engineering [1]. The main advantages of cement based composites are ease for construction, room temperature setting, low cost and the ready availability of properties and performance data for design and construction [2] and [3]. The major weaknesses of traditional cement based material is low tensile strength and the fact that it can be easily cracked, which affect durability, safety and strength of concrete structures [4] and [5]. Tensile strength of plain concrete is between 2 MPa to 8 MPa [6]. Many types of fillers were used to improve cement based composites properties, especially its toughness [7]. Used fillers increased tensile strength, but has only slight effect on initiation of micro-cracks because of volumetric changes due to high autogenous shrinkage stresses and delaying only macro-cracks [8]. Therefore, there is a big effort to adapt to the flexural and tensile mechanical properties of the matrix in order to improve the fracture and damage resistance of concrete. To deal with disadvantages of reinforcement of cementitious material mentioned above the reinforcement is typically provided at the micro and milli-scale using microfibers and macrofibers. Concrete matrix however exhibit flaws at the nanoscale, where traditional fillers are not effective [9].

With spreading of nanotechnology into various technologies, it comes also its application in concrete composites [10]. Nanomaterials provide unique multifunction properties due to their size. New types of reinforced polymers, nanoparticles (TiO_2, Fe_2O_3, SiO_2) and especially carbon nanotubes (CNTs) are suitable micro-fillers for these composites, because of their high strength at atomic scale [11].

Nanomaterials can have following beneficial effects on the microstructure and properties of cement based composites:

- filling in free space between cement grains and preventing flow of water,
- forming crystallic centers and speeding up cement hydration process,
- supporting creation of small crystals such as $Ca(OH)_2$ and uniform agglomeration of C-S-H products,
- speeding up pozzolanic reactions, which consume $Ca(OH)_2$ and produce additional C-S-H gel,
- enhancing contact area, which increase bonding strength between aggregates and cement compound.

*Corr. Author's Address: Nanotechnology Centre, VSB-Technical University of Ostrava, 17. listopadu 15/2172, 70833 Ostrava-Poruba, Czech Republic, vladimir.foldyna@vsb.cz

CNTs are one of the most promising fillers to improve concrete nanocomposite properties. Carbon nanotubes are hexagonal nets formed from rolled up graphene into cylindrical nanostructured tubes. Some of them are ended with fullerene hemispheres. There are two main groups of CNTs: single-walled carbon nanotubes (SWCNTs) and multi-walled carbon nanotubes (MWCNTs). SWCNTs consist from single rolled up graphene sheet and MWCNTs are composed of two or more layers of graphene. MWCNTs are cheaper to prepare so they are used more often than SWCNTs [12]. Moreover, MWCNTs offer better reinforcement in cement composites. MWCNTs have many applications in industry (such as electronic materials, medicine and chemistry) due to their exceptional chemical and physical properties (thermal conductivity, electrical conductivity, low specific weight, and high resistance to corrosion) [13] and [14].

The possible improvement in both physical and mechanical properties of cement-based nanocomposites could lead to the new generation of ultra-high performance concretes that would, for example, allow reduction of the dimensions of structural elements, which would lead to further economic and environmental benefits. Therefore, the joint research program was started at the Institute of Geonics and Brno University of Technology to investigate the influence of nanoparticles on properties of cement based composites.

The technology of a high-speed water jet is commonly used in repair of concrete structures due to its selectivity; if properly adjusted, it removes only a corroded or degraded layer of concrete and saves any compacted material. The selective properties of water jets can also be used in determination of concrete quality. The measure of concrete quality can be its resistance to effects of high speed water jets. This property is common to both pulsating and continuous water jets; however, a higher volume of concrete can be removed by pulsating jet under the same working conditions [15].

First results of the study aimed at determination of possible influence of addition of CNTs to the concrete on its resistance to the action of continuous and pulsating water jets are presented and discussed in the paper.

1 METHODS

1.1 Preparation of Testing Samples

Multi-walled carbon nanotubes from Yurui (Shanghai) Chemical Co., Ltd. were used for preparation of CNT/concrete composite in presented work. They were prepared by chemical vapour deposition with purity more than 95 %. Their properties are summarized in Table 1.

Table 1. *Properties of MWCNTs*

Properties	
Internal diameter	approx. 5 nm to 12 nm
Outer diameter	approx. 30 nm to 50 nm
Length	10 μm to 20 μm
Bulk density	0.22 g·cm^{-3}
True density	2.1 g·cm^{-3}

Defined volume (0.564 g) of naphthalene-based superplasticizer with polymeric chain, which was used as a surfactant, was mixed with 0.1 liter of water and 0.141 g of CNTs (0.003 wt. % of cement weight) in rosette vessel. Then, the suspension was ultrasonified for 10 min and, after homogenization, the solution was added into 2.3 liters of water. The mixture of small quarry stone sand 0/4 mm (locality Zabcice), rough-crushed stone 4/8 mm (locality Olbramovice), rough-crushed stone 8/16 mm (locality Olbramovice) and Portland cement CEM I 42.5 R from cement plant Mokra (Heidelberg Cement Czech Republic) was added into mixer and mixed for 1 min without addition of water.

Then, prepared solution of water, superplasticizer and CNTs was added to the mixture and mixed for another 2 minutes. Total volume of prepared concrete with CNTs was 15 dm^3 in Table 2. Reference material was prepared same way only without CNTs. The composition of reference and CNT concrete is given in Table 2.

Table 2. *Composition of reference and CNT/concrete*

Material	Reference	CNT/concrete
CNTs	-	0.141 g
Superplasticizer	0.564 g	0.564 g
Cement	4.7 kg	4.7 kg
Small quarry stone sand 0/4 mm	10.6 kg	10.6 kg
Rough-crushed stone 4/8 mm	4.7 kg	4.7 kg
Rough-crushed stone 8/16 mm	12.5 kg	12.5 kg
Water	2.4 kg	2.4 kg

1.2 Characterization of Samples

Concrete was not fully hydrated, hydration was stopped after 7 days and selected physical and mechanical properties of samples were determined. In addition, their characterization by scanning electron

microscopy (SEM) and X-ray powder diffraction (XRPD) was also performed.

1.2.1 Physical and Mechanical Properties

Tests of consistency of fresh concrete and compressive strength and flexural strength of hardened concrete after 7 days were carried out. The test of consistency was performed in accordance with the standard EN 12350-2 [16]. The compressive strength of hardened concrete was measured in accordance with EN 12390-3 [17], and flexural strength in accordance with EN 12390-5 [18]. Measured physical-mechanical properties of reference and CNT/concrete test specimens are summarized in Table 3.

Table 3. *Physical-mechanical properties of reference and CNT/concrete sample*

Properties	Reference	CNT/concrete
Consistency [mm] - degree	20 – S1	10 – S1
Flexural strength [MPa]	8.98	8.38
Compressive strength [MPa]	42.29	43.75

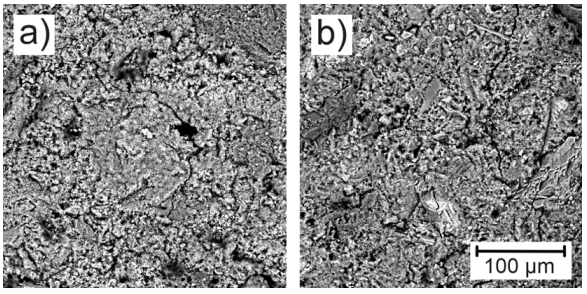

Fig. 1. *SEM image of a) reference, and b) CNT/concrete*

1.2.2 Scanning Electron Microscopy

SEM analysis and characterization of testing specimens by ASPEX PSEM Explorer did not reveal any significant differences in the structure of reference and CNT/concretes. The only conclusion made from the SEM analysis is that the samples were not fully hydrated, as can be seen in Fig. 1. Again, the influence of the CNTs on the hydration process should be studied using SEM on cement paste with addition of CNTs only.

1.2.3 X-Ray Powder Diffraction

Samples were characterized by XRPD patterns measured under CoKα irradiation (λ = 1.789 Å) using the Bruker D8 Advance diffractometer (Bruker AXS) equipped with a fast position sensitive detector VÅNTEC 1.

As one can see in Fig. 2, quartz and non-hydrated phases of Portland cement overshadowed the hydrated phases.

Presence of tricalcium and dicalcium silicate indicates that concrete samples were not fully hydrated. However, the results indicate that the influence of the CNTs on the hydration process has to be studied on cement paste with addition of CNTs

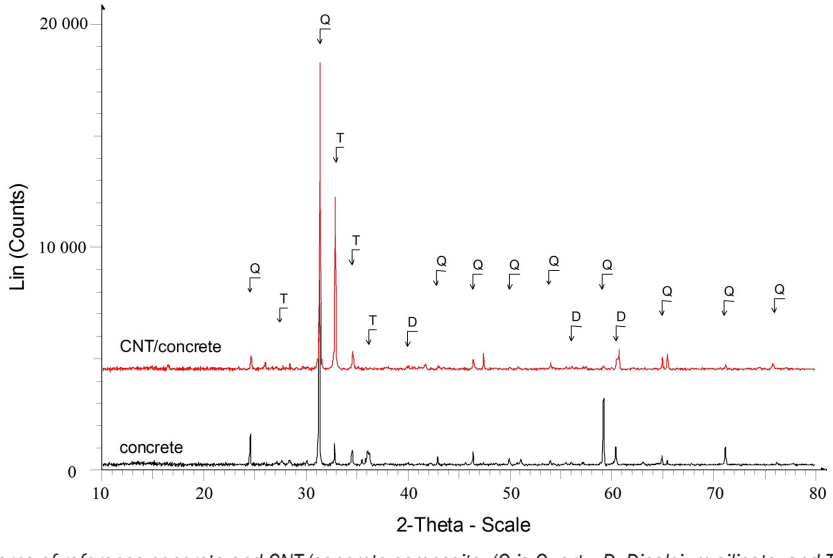

Fig. 2. *XRPD patterns of reference concrete and CNT/concrete composite. (Q is Quartz, D Dicalcium silicate, and T Tricalcium silicate)*

only to avoid overshadowing of hydrated phases by quartz.

2 EXPERIMENTAL

The experiments oriented at the determination of erosion effects of pulsating (PWJ) and continuous (CWJ) water jet impinging the surface of reference (concrete) and CNT/concrete composite samples were performed in the Waterjet laboratory of the Institute of Geonics. Disintegration effects of high-speed water jets were tested and evaluated to compare their effects on CNT/concrete composite and reference samples.

2.1 Laboratory Equipment and Testing Conditions

The experimental assembly for water jetting tests consisted of the high-pressure plunger pump Hammelmann HDP 253 (delivering up to 67 l·min^{-1} at the maximum operating pressure of 160 MPa), a pulsating water jet head (with a 20 kHz ultrasonic generator) installed on the arm of the ABB IRB 6640 robot. The PWJ head (high-speed water jet) was moved over the tested sample by the robot using various traversing velocities. The commercially available nozzle StoneAge Attack (nozzle diameter d was 1.9 mm) was used in the experiment to generate both continuous and pulsating jets. Two values of operating pressure p 20 MPa and 40 MPa were used in experiments. Standoff distances *SOD* of 25 mm (at 20 MPa) and 35 mm (at 40 MPa) were determined in previous experiments to be optimal for given testing conditions. Traversing velocity v_{TR} was changed from 10 mm·s^{-1} to 80 mm·s^{-1} during tests at 20 MPa and from 50 mm·s^{-1} to 160 mm·s^{-1} during tests at 40 MPa. Proprietary method of the generation of the pulsating liquid jet based on the generation of acoustic waves by the action of the acoustic transducer on the pressure liquid and their transmission via pressure system to the nozzle (so called acoustic generator of pressure pulsations) was used to generate PWJ. Acoustic generator of pressure pulsations used in experiments generated pressure pulsations at the frequency of about 20 kHz (exact frequency depends on the actual geometrical configuration of the generator), amplitude of vibrations of the acoustic transducer was set to 7 μm. More details on the method of PWJ generation used in the experiments can be found elsewhere **[19]** and **[20]**. Schematic drawing of the experimental setup is given in Fig. 3.

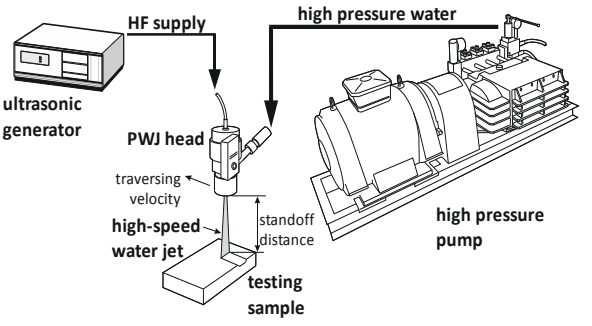

Fig. 3. *Schematic drawing of the experimental setup*

2.2 Experimental Procedure

Erosion effects of PWJ and CWJ on CNT/concrete composite and reference (concrete) samples exposed to their action under various operating parameters were evaluated in terms of material removal rate. Grooves created by the action of the jets were measured using MicroProf FRT optic profilometer. Subsequently, 2D and 3D images of grooves were created and the volume of removed material V was determined using SPIP software. Evaluated length of the groove l was 20 mm, 56 grooves were processed in total. The resistance of the samples to the action of PWJs and CWJs was evaluated in terms of material removal rate ΔV (see in Eq. (1)) which was determined using following formula:

$$\Delta V = \frac{V \cdot v_{TR}}{l} \quad [\text{mm}^3 \cdot \text{s}^{-1}]. \tag{1}$$

3 RESULTS

Results of evaluation of erosion effects of PWJ and CWJ on CNT/concrete composite and reference samples are presented in form of graphs in Figs. 4 and 5. Material removal rate is dependent on a type of water jet. Material removal rate of CWJ remains almost constant with increasing traversing velocity in given range, whereas PWJ exhibits increasing of material removal rate at higher traversing velocities in given range, which can be seen in Figs. 4 and 5.

Photographs and 3D images of selected examples of grooves created by the CWJ and PWJ in reference and CNT/concrete composite samples can be seen in Figs. 6 to 9. Concrete with carbon nanotubes exhibits higher resistance to CWJ and PWJ than reference samples. Major difference between material removal rates can be observed in Fig. 7.

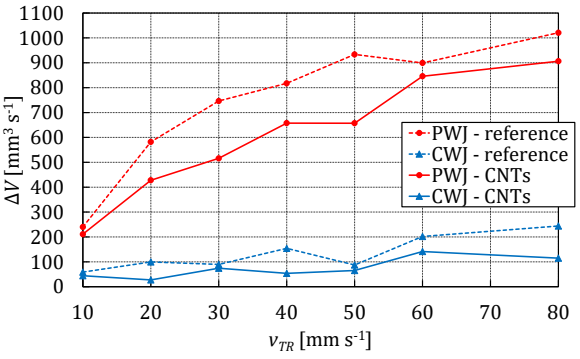

Fig. 4. *Influence of traversing velocity v_{TR} on the material removal rate ΔV in CNT/concrete composite and reference concrete exposed to CWJ and PWJ generated at 20 MPa*

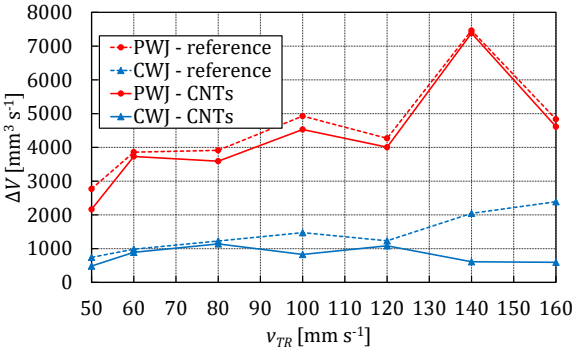

Fig. 5. *Influence of traversing velocity v_{TR} on the material removal rate ΔV in CNT/concrete composite and reference concrete exposed to CWJ and PWJ generated at 40 MPa*

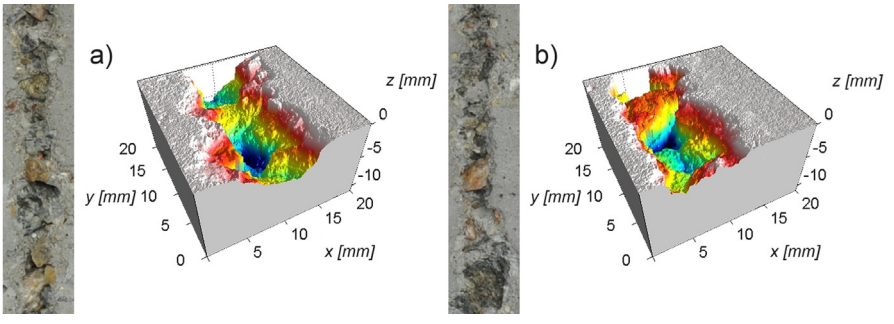

Fig. 6. *Photograph and 3D view of the groove created by a) the PWJ in reference and b) CNT/concrete composite sample (operating pressure p = 20 MPa, traversing velocity v_{TR} = 30 mm·s^{-1})*

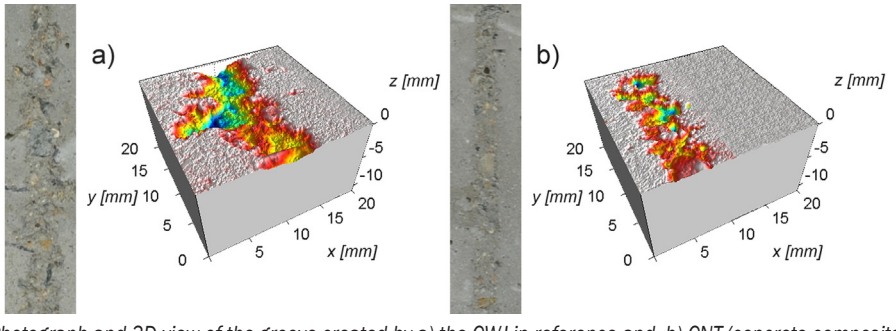

Fig. 7. *Photograph and 3D view of the groove created by a) the CWJ in reference and, b) CNT/concrete composite sample (operating pressure p = 20 MPa, traversing velocity v_{TR} = 40 mm·s^{-1})*

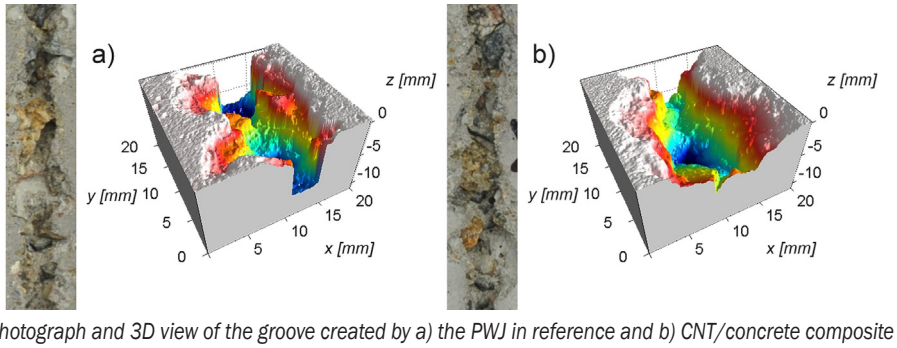

Fig. 8. *Photograph and 3D view of the groove created by a) the PWJ in reference and b) CNT/concrete composite sample (operating pressure p = 40 MPa, traversing velocity v_{TR} = 100 mm·s^{-1})*

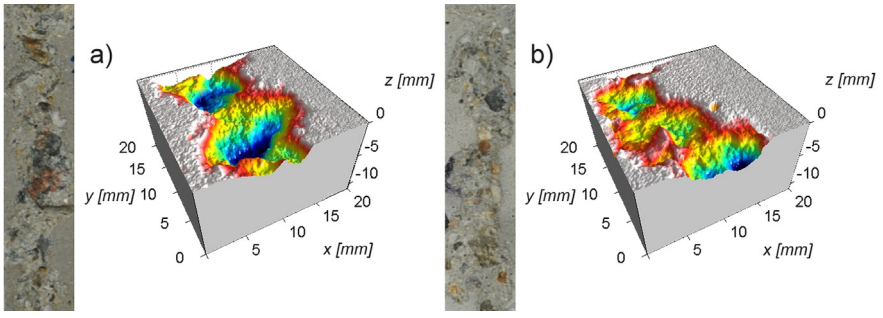

Fig. 9. *Photograph and 3D view of the groove created by a) the CWJ in reference and, b) CNT/concrete composite sample (operating pressure p = 40 MPa, traversing velocity v_{TR} = 100 mm·s^{-1})*

4 DISCUSSION

Generally, higher differences in the resistance of tested samples to the action of both PWJs and CWJs can be observed at operating pressure of 20 MPa. Material removal rate obtained in CNT/concrete composite samples was ranging from 69 % to 94 % compared to reference in case of PWJs. Reference material removal rate (obtained in reference sample) at certain traversing velocity was taken as 100 %. Results of material removal rate for CWJs was ranging from 27 % to 83 %. Whereas PWJs created deeper grooves and was able to remove also larger stone grains from the cement matrix, CWJs was able to remove only upper layer of cement matrix and only some small stone grains.

Similar results were observed at the operating pressure of 40 MPa. Material removal rate for PWJs in CNT/concrete composite samples was within the range 78 % to 99 % compared to reference. Results of material removal rate for CWJs was ranging from 25 % to 93 % at this pressure. Again, PWJs created deeper grooves and was able to remove also larger stone grains from the cement matrix compared to CWJs.

Results obtained in the above described experiment seems to indicate that the CNT/concrete composite exhibits higher resistance than reference concrete to the action of both PWJs and CWJs under the given testing conditions. This can be ascribed most likely to the fact that adding of CNTs to the cement matrix changes its properties in a way, which results in its higher resistance to the action of both PWJs and CWJs. Because no significant changes in properties of the CNT/concrete composite with respect to the reference samples were observed (see above), additional tests performed using cement paste and cement paste with CNTs will be necessary to verify that addition of CNTs into the cement paste can significantly change its resistance to the action of water jets.

5 CONCLUSIONS

First results of the study aimed at the determination of possible influence of addition of CNTs to the concrete on its resistance to the action of continuous and pulsating water jets presented in the paper lead to following conclusions:

- Physical-mechanical properties of reference and CNT/concrete did not differ significantly after 7 days. In addition, test specimens characterization using X-ray powder diffraction and scanning electron microscopy did not reveal any significant differences in the structure of reference and CNT/concretes.
- Regardless the above-mentioned facts, the experiments proved that CNT/concrete composite exhibits higher resistance than reference concrete to the action of both PWJs and CWJs under the given testing conditions. This indicate that adding of CNTs to the cement matrix changes its properties in a way, which results in its higher resistance to the action of both PWJs and CWJs.
- To be able to explain this higher resistance of CNT/concrete composite compared to reference concrete, upcoming studies should be oriented at the determination of the influence of the CNTs on the hydration process XRPD and SEM/TEM on cement paste with addition of CNTs only before continuation of tests on concrete samples after 28 days. In addition, water-jetting tests will be performed on CNTs/cement paste samples to verify findings of the presented study.

6 ACKNOWLEDGEMENTS

The work was performed under the support of the project of the Czech Science Foundation "Study of methods of nanoparticles dispersion, determination of conditions for preventing their re-agglomeration for application in cement composites", reg. no. 15-23219S, the Institute of Clean Technologies for Mining and the Utilization of Raw Materials for Energy Use – Sustainability program, reg. no. LO1406 financed by the Ministry of Education, Youth and Sports of the Czech Republic, and the long-term conceptual development of the research institution RVO: 68145535. The work was partially supported also by the Ministry of Education, Youth and Sports of Czech Republic (project reg. no. SP2016/67). The authors are thankful for the support.

7 REFERENCES

[1] Li, Q., Liu, J., Xu, S. (2015). Progress in research on carbon nanotubes reinforced cementitious composites. *Advances in Materials Science and Engineering*, vol. 2015, p. 1-16, **DOI:10.1155/2015/307435**.

[2] Foldyna, J., Foldyna, V., Zeleňák, M. (2016). Dispersion of carbon nanotubes for application in cement composites. *Procedia Engineering*, vol. 149, p. 94-99, **DOI:10.1016/j.proeng.2016.06.643**.

[3] Sitek, L., Bodnarova, L., Soucek, K., Stas, L., Gurkova, L. (2015) Analysis of inner structure changes of concretes exposed to high temperatures using micro X-ray computed tomography. *Acta Geodynamica et Geomaterialia*, vol. 12, no. 1(177) p. 79-89, **DOI:10.13168/AGG.2015.0009**.

[4] Okeil, A.M., El-Tawil, S., Shahawy, M. (2001). Short-term tensile strength of carbon-fiber-reinforced polymer laminates for flexural strengthening of concrete girders. *ACI Structural Journal*, vol. 98, no. 4, p. 470–478.

[5] Lim, T.Y., Paramasivam P., Lee, S.L. (1987). Analytical model for tensile behavior of steel-fiber concrete. *ACI Materials Journal*, vol. 84, no. 4, p. 286-298.

[6] Neville, A. M.,Brooks, J.J. (1987). *Concrete Technology*. Longman Scientific & Technical, Harlow.

[7] Balaguru, N.P., Shah, S.P. (1992). *Fiber-reinforced cement composites*. McGraw-Hill, New York.

[8] Xu, S., Li, Q. (2009). Theoretical analysis on bending behaviour of functionally graded composite beam crack-controlled by ultrahigh toughness cementitious composites. *Science in China Series E: Technological Sciences*, vol. 52, no. 2, p. 363-378, **DOI:10.1007/s11431-008-0337-9**.

[9] Li, V.C., Leung, C.K.Y. (1992). Steady-state and multiple cracking of short random fiber composites. *Journal of Engineering Mechanics*, vol. 118, no. 11, p. 2246-2264, **DOI:10.1061/(ASCE)0733-9399(1992)118:11(2246)**.

[10] P.,carbon–Zweben, C. (1968). Tensile failure of fiber composites. *AIAA Journal*, vol. 6, no. 12, p. 2325-2331, **DOI:10.2514/3.4990**.

[11] Iijima, S. (1991). Helical microtubules of graphitic carbon. Nature, vol. 354, p. 56-58, **DOI:10.1038/354056a0**.

[12] Kang, S., Seo, J., Park, S. (2015). The characteristics of CNT/cement composites with acid-treated MWCNTs. *Advances in Materials Science and Engineering*, vol. 2015, p. 1-9, **DOI:10.1155/2015/308725**.

[13] Grobert, N. (2007). Carbon nanotubes – becoming clean. *Materials Today*, vol. 10, no. 1-2, p. 28-35, **DOI:10.1016/S1369-7021(06)71789-8**.

[14] Popov, V.N. (2004). Carbon nanotubes: properties and application. *Materials Science and Engineering: R: Reports*, vol. 43, no. 3, p. 61-102, **DOI:10.1016/j.mser.2003.10.001**.

[15] Sitek, L., Foldyna, J., Martinec, P., Ščučka, J., Bodnárová, L., Hela, R. (2011). Use of pulsating water jet technology for removal of concrete in repair of concrete structures. *The Baltic Journal of Road and Bridge Engineering*, vol. 6, no. 4, p. 235-242, **DOI:10.3846/bjrbe.2011.30**.

[16] EN 12350-2 Testing of fresh concrete - Part 2: Slump-test. European standard.

[17] EN 12390-3 Testing hardened concrete – Part 3: Compressive strength of test specimens. European standard.

[18] EN 12390-5 Testing hardened concrete - Part 5: Flexural strength of test specimens. European standard.

[19] Foldyna, J., Svehla, B. (2011). *Method of Generation of Pressure Pulsations and Apparatus form Implementation of This Method*. US patent no. 7,934,666, USPTO, Aleksandria.

[20] Foldyna, J., Sitek, L., Ščučka, J., Martinec, P., Valíčicek, J., Páaleníkováa, K. (2009) Effects of pulsating water jet impact on aluminium surface. *Journal of Materials Processing Technology*, vol. 209, no. 20, p. 6174-6180, **DOI:10.1016/j.jmatprotec.2009.06.004**.

Strojniški vestnik - Journal of Mechanical Engineering 63(2017)10, 590-596
DOI:10.5545/sv-jme.2017.4363
Original Scientific Paper
Received for review: 2017-01-30
Received revised form: 2017-05-22
Accepted for publication: 2017-06-27

Automatable Splicing Method for Steel Cord Conveyor Belts – Evaluation of Water Jetting as a Preparation Process

David Zaremba[1,*] – Patrick Heitzmann[2] – Ludger Overmeyer[2] – Lennart Hillerns[1] – Thomas Hassel[1]
[1] Leibniz Universität Hannover, Institute of Materials Science (IW), Germany
[2] Leibniz Universität Hannover, Institute of Transport and Automation Technology (ITA), Germany

The increased demand of mineral resources leads to worldwide application of incessantly longer conveying systems. The length between axes can amount to 15 km and more. Owing to manageable dimensions and weight, appropriate conveyor belts are produced in segments of up to 300 m. Final assembly takes place at the conveyor system, where the multitude of segments is connected to a long conveyor belt. An important point in assembly preparation is the stripping of the steel cords, which is mainly carried out manually using rudimentary techniques. The optimization potential is high, since the adoption of automatable and application-oriented preparation methods can minimize the conveyor downtime and improve the joint quality.

In this study, the application of the pure water jet is investigated, since this selective stripping method offers a lot of potential for automation and the creation of rough surfaces. The objective was to determine if an efficient, homogenous and selective removal of the rubber is possible without damaging the zinc coating of the steel cords. Following a parameter study, the generated kerf geometries and surfaces were investigated. The stripped steel cords and zinc coatings were analyzed through the preparation of micrographs. Concluding, an evaluation about the qualification of water jetting as an automatable method for joint and repair preparation is made.

Keywords: steel cord conveyor belt, splicing, repair preparation, automation, water jetting

Highlights

- *It is found that water jetting is a promising preparation method for the splicing of steel cord conveyor belts that comes along with an excellent potential for automation.*
- *A deep material removal with sharp, orthogonal and plane-parallel edges and a consistently rough surface is possible.*
- *The zinc-coated steel cords do not suffer visible damage.*

0 INTRODUCTION

The belt is one of the most important parts of a conveyor system when it comes to design and investment costs. Due to logistic reasons, the belt can only be transported in segments to the conveyor system, limited by weight or length of the individual segment. The splicing is done directly at the system. In the splice, tensile forces are transferred through the core rubber and not via tension member. This fact makes a splice the weakest point of a conveyor belt. The tension member of a belt can consist of textile fabric or steel cords, depending on the tensile strength of the belt. Steel cord conveyor belts can reach a nominal belt breaking strength up to 10.000 N/mm. Fig. 1 shows the general structure of a steel cord conveyor belt [1].

Current research to achieve a higher quality for splicing is mainly focused on optimization using FEM but neglects adhesion mechanisms and automation capability of the process [2].

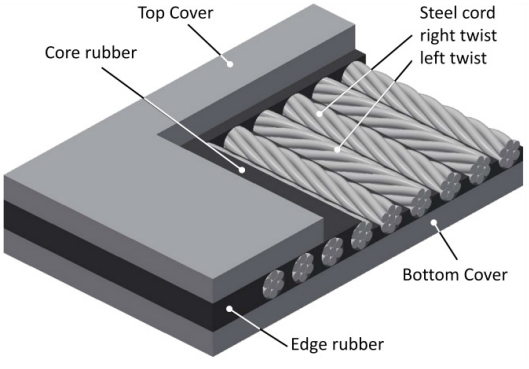

Fig. 1. *Steel cord conveyor belt*

1 STEEL CORD CONVEYOR BELT

The steel cords are covered in core rubber and form the carcass of the belt which is covered by top and bottom cover. The bottom cover transfers the driving forces from drive pulley to the belt. The top cover transports the bulk material and protects the carcass from damages caused by material impacts. The steel cords are right and left twisted and placed alternate next to each. The cords are zinc coated and have a

*Corr. Author's Address: Leibniz University of Hannover, Institute of Materials Science, An der Universität 2, D-30823 Garbsen, Germany, zaremba@iw.uni-hannover.de

zinc oxide layer on top. Zinc oxide has two effects during the belt fabrication. On the one side, it is a vulcanization accelerator and, on the other hand, it provides the basis for a zinc sulfide layer that occurs during vulcanization process between rubber and steel cords and leads to a better adhesion [3] and [4].

The splicing procedure of a steel cord conveyor belt is performed as follows. First, the splicing area needs preparation. Before assembling the vulcanization press, the new rubber has to be placed into the splice. Then the vulcanization of the splice area completes the splicing procedure. The present preparation process for splicing procedure consists of numerous manually performed steps. The steel cords of both ends of the conveyor belt have to be completely removed from rubber. Therefore, the first step is to remove top and bottom cover with an oscillating cutting edge. To cut the steel cords apart, a stripping machine is used. Then the biggest amount of the core rubber is stripped from the cords with piano wires.

Fig. 2. *Preparation process of a steel cord splice [RI-Belt Sud S.R.L]*

As last step, cutting tools are used to remove the remaining amount of rubber and shorten the steel cords to the required length if necessary. Fig. 2 shows a splicing process. Then the cords have to be placed according to the splice layout, see Fig. 3. Then new core rubber has to be put between the steel cords. The total process is very time consuming due to its low level of automation and considerable number of manual work steps. The splicing quality can be primary defined through the adhesion between steel cords and core rubber. The fact that the zinc oxide layer of the steel cords is responsible for it, the layer must not be damaged during the preparation of the splicing procedure. To avoid damaging the zinc oxide layer is almost impossible due to the removal of core rubber just by cutting tools [1].

In this study, the application of the pure water jet is investigated, since this selective stripping method offers a lot of potential for automation and the creation of rough surfaces. Machining rubber with an erosive, pure water jet is a common method for cutting, cleaning and recycling purposes [5] to [7], so the application as a splicing preparation method is obvious. The objective was to determine if an efficient, homogenous and selective removal of the rubber is possible without damaging the zinc coating of the steel cords.

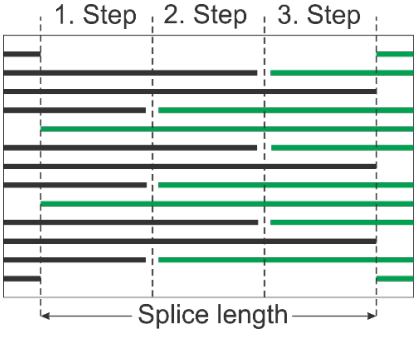

Fig. 3. *Layout of a 3-step steel cord splice*

2 MATERIALS AND METHODS

The investigations were carried out using a segment of an industrial steel cord conveyor belt with a thickness of $t = 30$ mm, in new condition.

The material was vulcanized using "STG type" primer, rubber strips and cover plates (manufacturer: "Nilos"). The cover plate had a thickness of $t = 15$ mm, the diameter of the zinc-coated steel cords was $d = 8$ mm. Fig. 4 shows a sectional view of the test material.

All jetting experiments were carried out using a "Stein Moser WS0707" gantry-style

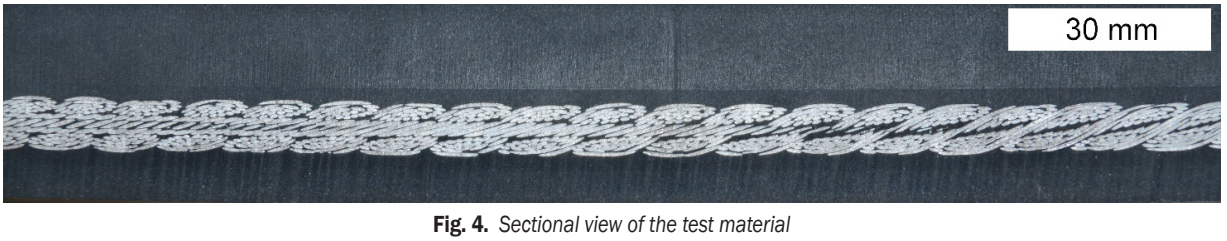

Fig. 4. *Sectional view of the test material*

(x, y, z)-guiding machine. The high-pressure pump was a "BFT Servotron 40.37" (max. operating pressure p_w = 400 MPa, max. volume flow rate Q_w = 3.8 l/min). The high-pressure valve applied was a "BFT WJ070060", modified to include a "Hammelmann" nozzle mount. Three flat-jet nozzles "Hammelmann Type R" with the jet angles $\alpha_1 = 10°$, $\alpha_2 = 20°$ and $\alpha_3 = 30°$ were used alongside with sharp-edged round-jet nozzles "Hammelmann Type I". The nozzle diameter was kept constant with $d_0 = 0.4$ mm. The nozzle coefficients were specified with $k_f = 0.67$ for the flat-jet nozzles and $k_r = 0.70$ for the round-jet nozzle by the manufacturer, respectively. The nozzles allowed for a maximum water pressure of p = 300 MPa. Because of the flexible material behavior of the rubber, the achieved kerf-depth- and surface-roughness values were measured optically using fringe projection technology (equipment manufacturer: "GF Messtechnik"), in five positions each respectively.

For a neutral comparison of the material removal profile and –efficiency, the optimum standoff distance was determined for each jet angle α to allow a material removal width of b = 10 mm. Following, surface structure and -profile were analyzed. As different jet disintegration stages are present at the same jet width when using various jet angles, an influence on the material removal profile can be expected. For the round jet nozzle, staggered tool paths were used with variation of the tool path distance. The nozzles with the most promising results were picked for a more detailed parameter investigation, also including multiple material removal iterations. After parameter and procedure optimization, the conveyor belt was stripped down to its steel cords. A micro section was prepared in order to investigate if the formerly applied zinc coating was still intact.

3 RESULTS AND DISCUSSION

Initial experiments showed that the utilized round jet nozzles did not allow a consistent material removal of the belt rubber. Similar to nozzle types used for cutting applications, they generate a coherent and narrow jet with a characteristically high energy density on a small contact area. Although this kind of nozzle is well suited for precise material removal of other composite materials (e.g. CFRP **[8]** to **[10]**), the elastic flexibility of the rubber effected a bending of the material away from the jet. This resulted in lamellar surfaces, combined with a comparatively low material removal rate. The results obtained using flat-jet nozzles were considerably better. As expected, different surface profiles were generated dependent on the jet angle. While the flat-jet nozzles with $\alpha_1 = 10°$ and $\alpha_2 = 20°$ produced a straight surface profile with a consistent surface roughness, the surface profile generated by the nozzle with $\alpha_3 = 30°$ was accentuated in the edges and less consistent. Through a furthermore lower material removal rate compared to $\alpha_1 = 10°$ and $\alpha_2 = 20°$, the jet angle of $\alpha_3 = 30°$ did not implicate applicable advantages and was therefore rejected from the following investigations. Fig. 5 shows a consistent material removal path of a flat jet nozzle with $\alpha_1 = 10°$ and p = 100 MPa.

As displayed in Fig. 6, achieved kerf depths for $\alpha_1 = 10°$ were slightly higher than for $\alpha_2 = 20°$. Measured surface roughness was significantly higher for the narrower jet angle. Since higher surface roughness goes along with an increased surface area,

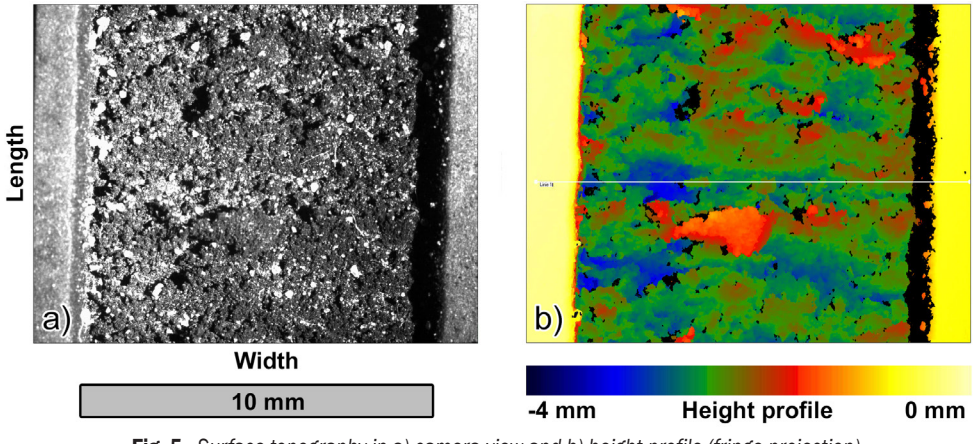

Fig. 5. *Surface topography in a) camera view and b) height profile (fringe projection) of a material removal path generated by a nozzle with $\alpha_1 = 10°$ and p = 100 MPa*

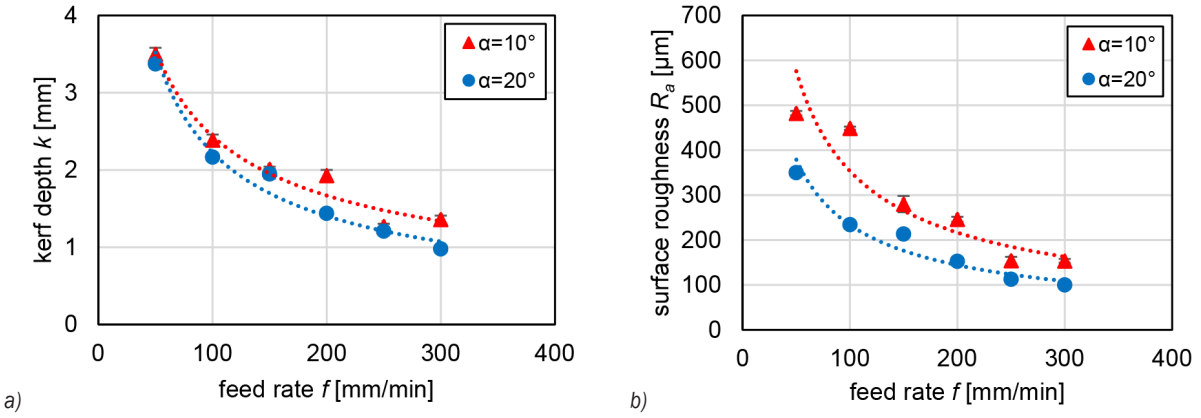

a) b)

Fig. 6. *a) Kerf depth k and b) mean surface roughness index R_a compared to the feed rate f for a kerf width of b = 10 mm*

this can be advantageous when it comes to priming and splicing. Therefore, a higher surface roughness is generally preferable. A noteworthy fact is that the utilized flat-jet nozzles required a higher water volume flow rate than the stated nozzle coefficient of 0.67 would let guess. The available water volume flow rate of Q_w = 3.8 l/min was almost consumed at p = 150 MPa (α_1 = 10°) and p = 200 MPa (α_2 = 20°). For this reason, the stated pressure levels were set as the maximum values for each test series, respectively. As expected for an appropriate parameter study, kerf depth and surface roughness increase with an elongated contact time (smaller feed rate). As displayed in Figs. 7 and 8, the achievable kerf depth increases straight proportional to the quantity of iterations for both jet angles. Using the test setup, a total of n = 4 iterations was necessary to completely remove the top cover and strip the steel cords at a feed rate of f = 100 mm/min. For α_1 = 10° a water pressure of p = 150 MPa was necessary, for α_2 = 20° a water pressure of p = 200 MPa. In both cases, the real water volume flow rate is expected to be similar close to Q_w = 3.8 l/min, recognizable by the pump's maximum workload. Furthermore, it was found that the surface roughness remains constant independent of the iteration quantity. The test equipment allowed for maximum surface roughness values of R_{a1} = 480.9 µm (σ_1 = 5.3 µm) for α_1 = 10°, p = 150 MPa and R_{a2} = 465.7 µm (σ_2 = 6.2 µm) for α_2 = 20°, p = 200 MPa, respectively. Both jet angles were likewise found suitable for the application, with advantages regarding equipment wear which can be expected for the lower necessary pressure at α_1 = 10°.

Fig. 9 shows two photographs after removal of the cover plate and stripping the steel cords by water jetting and following drying by compressed air, as

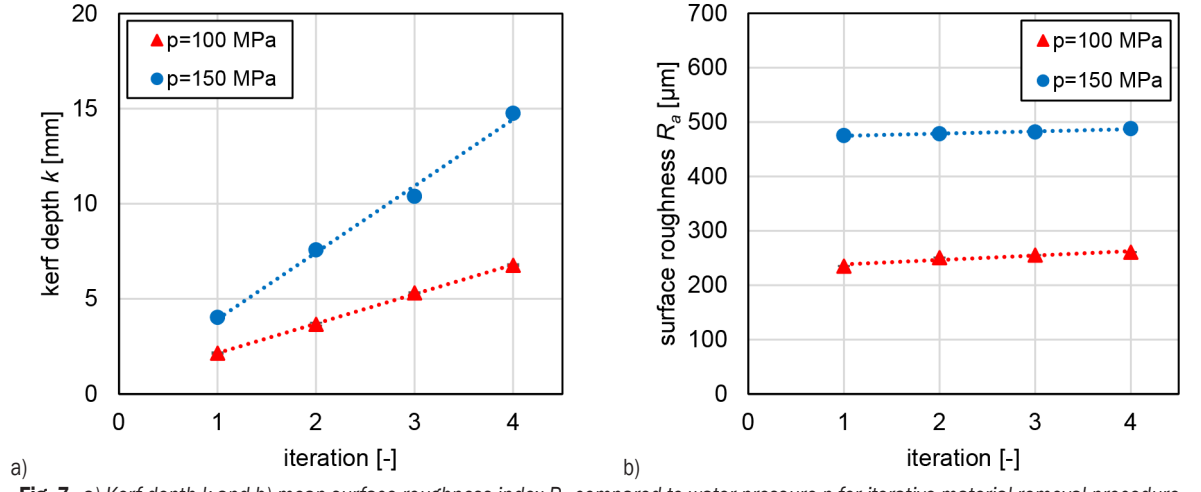

a) b)

Fig. 7. *a) Kerf depth k and b) mean surface roughness index R_a compared to water pressure p for iterative material removal procedure, a jet angle of α = 10° and a feed rate of f = 100 mm/min*

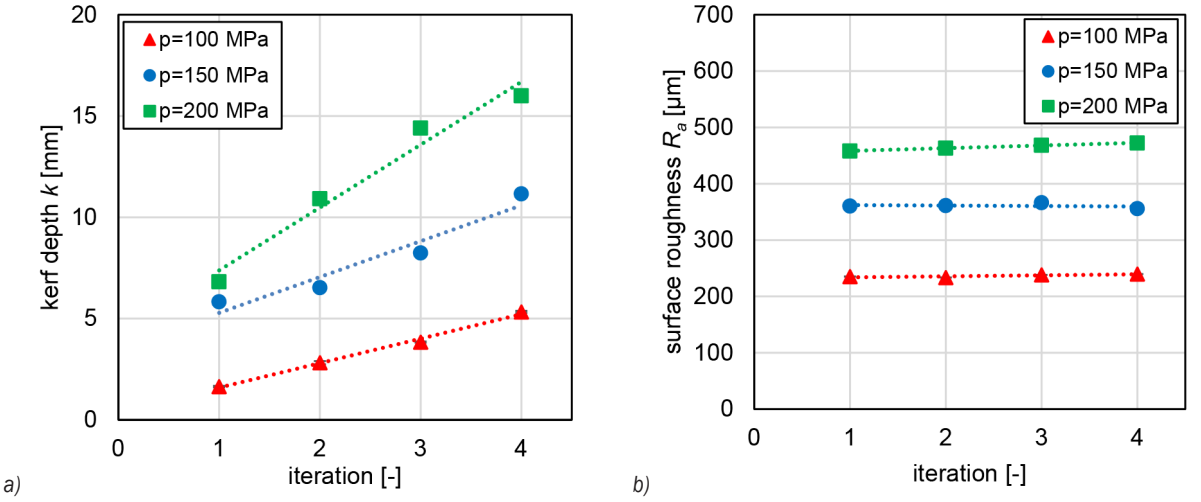

a) b)

Fig. 8. *a) Kerf depth k and b) mean surface roughness index R_a compared to water pressure p for iterative material removal procedure, a jet angle of α = 20° and a feed rate of f = 100 mm/min*

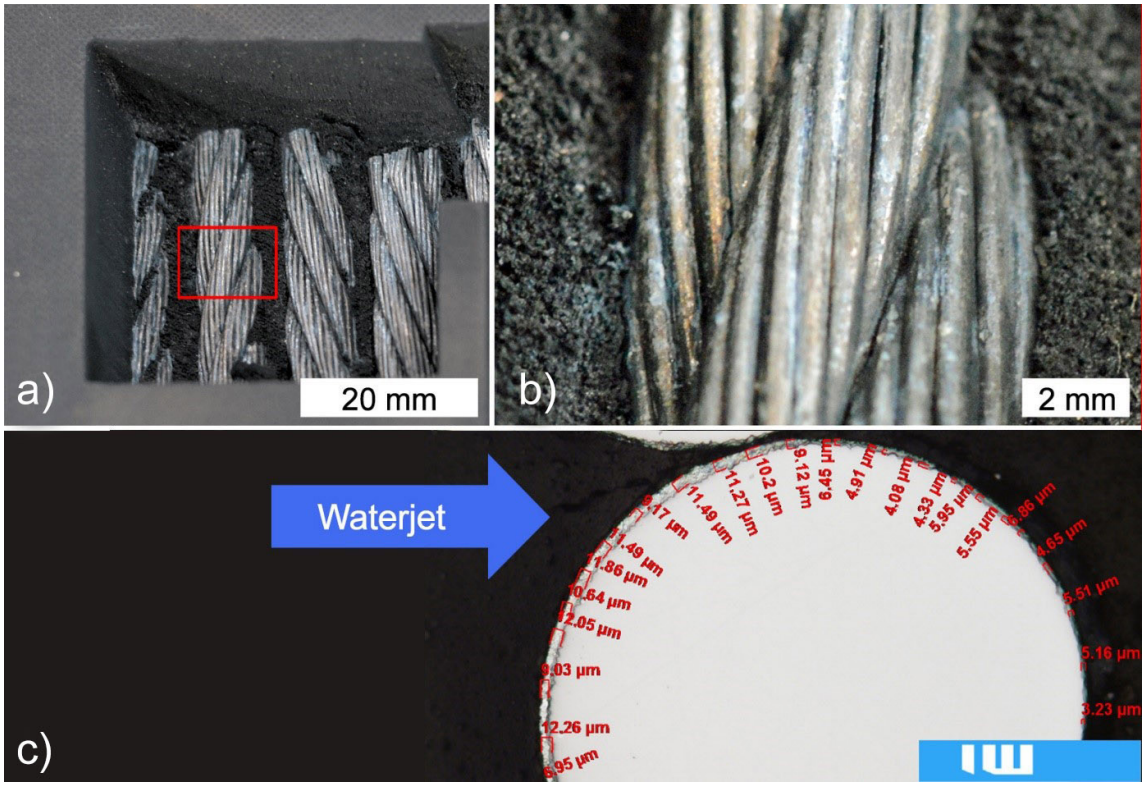

Fig. 9. *Stripped steel cords after iterative removal of the a) cover plate, b) detail view, and c) micro section of a stripped cord with measurements of the zinc coating thickness*

well as a micro-section of a single cord wire. It shows that a deep material removal with sharp, orthogonal and plane-parallel edges is possible with the utilized equipment (Fig. 9a). The exposed zinc-coated steel cords do not suffer visible damage (Fig. 9b). The prepared micro-section of a stripped cord shows that the galvanized zinc coating is still visible on the waterjet-treated side (Fig. 9c). The thinner coating on the opposite side originates from the wire production method (wire drawing); this appearance can also be found on new condition steel cords.

4 CONCLUSIONS AND OUTLOOK

Concluded, water jetting is a promising preparation method for the splicing of steel cord conveyor belts that comes along with an excellent potential for automation. Utilizing commercially available pump technology combined with flat-jet nozzles, stripping rubber of the steel cords is easily possible in high quality without visible damage of the zinc coating.

Besides the effect on splice quality, the described preparation process offers further improvement opportunities. Material removal rate and surface roughness are further expected to be increased through bigger water volume flow rates, which go along with an increase of hydraulic power. Appropriate technology is available in the market and will be utilized by the authors for further investigations. Considering the behavior of load transmission in a steel cord belt splice, it becomes apparent that it mainly takes place at the lateral cord flanks. Unlike this, the preparation method described in this paper only includes the top- and bottom machining of the belt (cf. Fig. 10a). Therefore, future investigations should also include 3D machining processes cf. Fig. 10b.

Current splicing preparation applications used in industry furthermore include both the complete stripping of the steel cords (cf. Fig. 11a), and the leaving of a residual rubber layer on the cords (cf. Fig. 11b). Some manufacturers' perception is that the first bonding between the zinc coating and the rubber offers better adhesion quality than a later bonding, other manufacturers prefer the fabrication of a clean splicing through completely stripping the cords from old rubber.

These procedures are however based on practical experiences made by the individual manufacturers. Future work should therefore include an independent investigation of both variants under consideration of the present adhesion mechanisms. The splicing preparation method presented in this paper however offers a lot of potential for both variants. Alongside the damage-free, complete stripping of the steel-cords, which offers superior quality compared to conventional cutting tools, a consistently rough rubber surface is generated when leaving a rubber layer on the steel cords. This rough rubber surface comes along with a larger contact surface for following vulcanization processes. Compared to the flat surfaces, which are generated through the conventional preparation techniques as described before, the application of this technology does not only offer a lot of potential to reduce downtime and splicing duration through automation, but also to improve the adhesion quality. As shown in Fig. 11c and d, the adaption of water jetting as a preparation process offers new layout possibilities through the integration of textures, which may further support adhesion quality. The effect on quality and reproducibility of appropriate belt splicing has to be analyzed in further investigations.

Following the described optimization of the preparation and splicing processes, an application in form of automatable preparation- and splicing machines is likely.

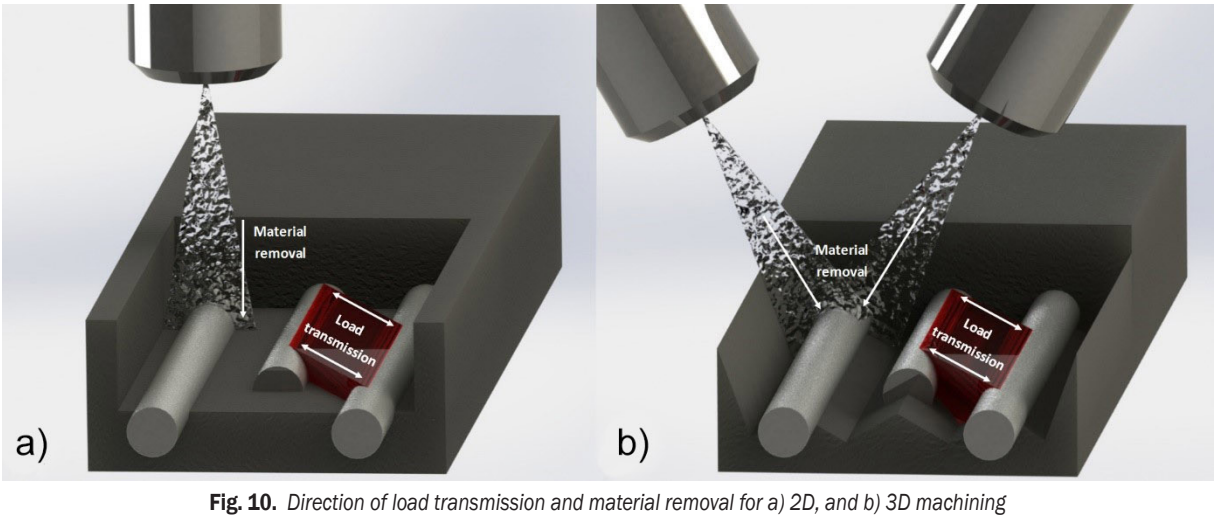

Fig. 10. *Direction of load transmission and material removal for a) 2D, and b) 3D machining*

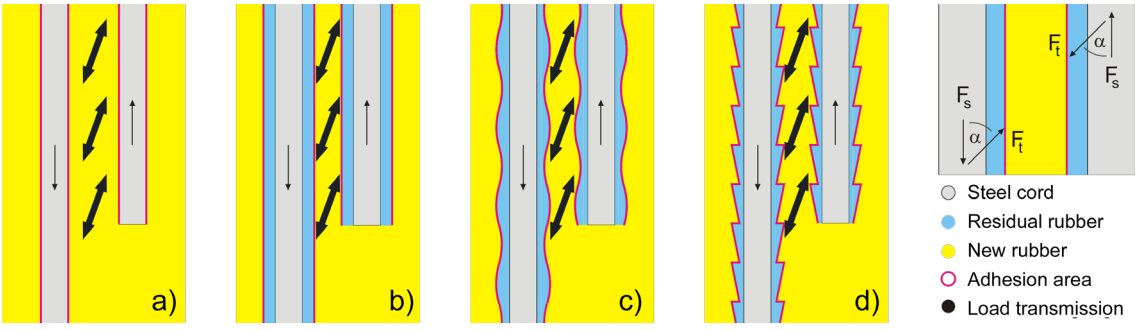

Fig. 11. *Schematic splice illustration for different splicing preparation layouts for steel cord conveyor belts; a) complete stripping of the cords, b) remaining residual rubber layer with defined thickness and c) and d) systematic texturing of the residual rubber layer*

5 ACKNOWLEDGEMENTS

The authors thank the Institute of measurement and automatic control (IMR) for providing the fringe projection instrumentation and the German working group of waterjet technology (AWT) for fruitful discussion.

6 NOMENCLATURE

α	jet angle, [°]
b	kerf width, [mm]
d	diameter, [mm]
d_0	orifice diameter, [mm]
f	tool feed rate, [mm/min]
k	kerf depth, [mm]
k_f, k_r	nozzle coefficient, [-]
n	iteration count, [-]
p	water pressure, [MPa]
Q_w	water volume flow rate, [l/min]
R_a	mean roughness index, [µm]
σ	standard deviation, [µm]
t	material thickness, [mm]

7 REFERENCES

[1] Ziller, T., Hartlieb, P. (2010). *Fördergurte in der Praxis – Know How and Know Why*. NILOS GmbH & Co. KG, VGE Verlag GmbH, Essen.

[2] Froböse, T.; Heitzmann, P.; Wakatsuki, A.; Overmeyer, L. (2014). Entwicklung eines FE-Modells zur Optimierung von Stahlseil-Fördergurtverbindungen. *Logistics Journal: Proceedings*, vol. 2014, no. 1, **DOI:10.2195/lj_Proc_froboese_de_201411_01**.

[3] Sönksen, H. (1987). *Korrosionsschutz von Seilen als Zugträger in Fördergurten*. PhD Thesis, University of Hannover, Faculty of Mechanical Engineering, Hannover.

[4] Rzymski, W., Wolska, B. (2005). Unkonventionelle Vernetzung ausgewählter Elastomere. *Gummi Fasern Kunststoffe*, vol. 58, no. 6, p. 358-363.

[5] Raghavan, C., Olsen, J.H. (1993). *Airport runway cleaning method and apparatus*. United States Patent and Trademark Office, US5228623 A.

[6] Weide, H.G., Kikels, R., Hänisch, G. (2016). Wasserkreislauf-Anhänger für Landebahnreini-gung mit Hochdruck-Reinwasserstrahl. *50. Arbeitskreis Wasserstrahltechnologie*, Hannover.

[7] Spur, G., Stöferle, T. (1987). *Handbuch der Fertigungstechnik. Band 4/1, Abtragen/ Beschichten*. Carl Hanser Verlag, München, Wien

[8] Zaremba, D., Wachsmuth, S., Schneider, P., Hufenbach, W., Maier, H.J., Hassel, T. (2014). Method for the material-specific repair preparation of carbon fiber reinforced plastic structures. *Proceedings of the 22nd International Conference on Water Jetting*, Haarlem.

[9] Zaremba, D., Biskup, C., Heber, T., Weckend, N., Hufenbach, W., Adam, F., Bach, Fr.-W., Hassel, T. (2012). Repair preparation of fiber-reinforced plastics by the machining of a stepped peripheral zone. *Strojniški vestnik - Journal of Mechanical Engineering*, vol. 58, no. 10, p. 571-577, **DOI:10.5545/sv-jme.2012.305**.

[10] Hufenbach, W., Adam, F., Heber, T., Weckend, N., Bach, Fr.-W., Hassel, T., Zaremba, D. (2011). Novel repair concept for composite materials by repetitive geometrical interlock elements. *Materials*, vol. 4, no. 12, p. 2219-2230, **DOI:10.3390/ma4122219**.

Strojniški vestnik - Journal of Mechanical Engineering 63(2017)10, 597-605

DOI:10.5545/sv-jme.2017.4424 Original Scientific Paper
Received for review: 2017-03-01
Received revised form: 2017-05-29
Accepted for publication: 2017-06-16

Determining Focusing Nozzle Wear by Measuring AWJ Diameter

Miha Prijatelj[1] – Marko Jerman[1] – Henri Orbanić[1] – Izidor Sabotin[1] – Joško Valentinčič[1] – Andrej Lebar[1,2,*]

[1] University of Ljubljana, Faculty of Mechanical Engineering, Slovenia
[2] University of Ljubljana, Faculty of Health Sciences, Slovenia

Abrasive water jet (AWJ) cutting is a versatile technology, but it is limited by relative poor accuracy. The main problem is the unknown diameter of the jet, as there is no device or instrument on the market that would enable a quick and easy measurement of it. With such an instrument the diameter could be regularly measured, nozzle wear monitored and noted offset adjusted. This would greatly improve the quality control of the process and the accuracy of the cut. This paper investigates the usage of a through-beam laser sensor for monitoring jet diameter and nozzle wear. Experiments were performed with five differently worn nozzles, with two different water pressures, with and without abrasive, at different standoff distances and with varying measuring times. Results show that the instrument is capable of monitoring the jet diameter and nozzle wear with an accuracy of ±0.03 mm, but it is very susceptible to the jet's spray and abrasive sticking to the sensor's screens. Jet diameter correlated better with the diameter of the focusing nozzle when taking measurements without the abrasive, at high water pressures and at a standoff distance of 1 mm.

Keywords: abrasive waterjet, nozzle diameter, jet diameter, nozzle wear

Highlights

- *Built an operational device for measuring jet diameter with an optical instrument.*
- *Analysed the effect of water pressure, abrasive and standoff distance on AWJ diameter.*
- *Analysed the effect of measuring time on standard deviation and measuring uncertainty.*
- *Found the correlation between nozzle diameter and jet diameter.*
- *Achieved monitoring nozzle wear.*

0 INTRODUCTION

Abrasive water jet (AWJ) technology utilizes a high velocity stream of water to accelerate abrasive particles, which then erode a narrow kerf in the material. The main advantages of this technology are the ability to cut virtually all materials without a heat affected zone, while disadvantages are mainly related to relatively poor accuracy, which is usually between 0.05 mm and 0.1 mm [1]. The source of rather poor accuracy lies in the geometrically non-defined and flexible tool which bends as it cuts and starts breaking up as it enters the air. The common result of jet break-up is a tapered and striated cut, which can only be partially solved by tilting the cutting head. Another issue to address in order to achieve high accuracy is determining tool offset, which is currently set to the radius of a new nozzle. This means that parts cut with a new nozzle can achieve accuracies of ±0.08 mm, but as the nozzle wears and diameter increases, the accuracy drops. The other method for determining offset is by cutting a test piece and measuring the dimensions of that piece. The new offset is then calculated from the measured dimensions and the set one [2]. This method is both time consuming and produces waste material. Another problem in the process is uneven nozzle wear [3], which means that at some point the offset can no longer be adjusted and the nozzle has to be replaced.

Regarding research on AWJ process several simulations were developed [4] which mostly relay on the diameter of the focusing tube as a jet diameter, while reliable measured jet diameter would provide better results.

For industrial applications, a quick and easy to use instrument for measuring jet diameter is needed. An instrument that measures jet diameter prior to machining and displays correct offset would improve cutting accuracy and provide better quality control. Several instruments for measuring jet diameter have already been developed. Orbanić et al. [5] measured AWJ diameter by passing the cutting head over a load cell while AWJ was active. The device determined the diameter by measuring the force of the jet on the load cell at a constant feed rate. The problem arising with this device is the wear to the measuring probe, which then distorts further measurements on that same spot of the probe. Folkes and Li [6] measured the jet diameter using two optical instruments. One instrument was a non-contact LED micrometre which projected a parallel line on the surface of the jet while a CCD camera then measured the contour it formed on

*Corr. Author's Address: University of Ljubljana, Faculty of Mechanical Engineering, Aškerčeva 6, 1000 Ljubljana, Slovenia, andrej.lebar@fs.uni-lj.si

the surface. The other instrument used a narrow beam laser that detected a change in intensity as the AWJ passed across the beam. The diameter was calculated by using a constant feed rate and a time difference between changes in intensity. It is questionable whether it is possible to measure AWJ diameter using a through beam laser, which is an optical instrument for measuring the solid tool diameter. Such a method could be used to monitor nozzle wear, adjust its offset and determine when the nozzle needs to be replaced.

1 FOCUSING NOZZLE WEAR

Due to the aggressiveness of AWJ, the focusing nozzle wears rather quickly. Lifetime depends on numerous AWJ system and nozzle parameters and is usually between 50 hours and 100 hours [3]. As a result of nozzle wear, the jet diameter increases, which decreases the cutting efficiency and precision while increasing its roughness. The nozzle wear principle is shown in Fig. 1. We can see that abrasive appears to erode the nozzle randomly, but eventually a typical wave-like pattern is formed. Wear also depends on orifice and focusing nozzle alignment. Any misalignment causes faster and more uneven wear and may even cause a blowout to occur, i.e. a critical failure in which the AWJ erodes through the side of the focusing nozzle [7]. Uneven wear causes significantly faster jet disintegration and makes the cut wavy, which makes reaching set tolerances impossible.

2 EXPERIMENTAL SETUP

The experimental setup was designed to enable the analysis of AWJ diameter and its correlation to nozzle diameter. In the experiments we analysed the difference between measured jet diameter while using abrasive (AWJ) and while cutting with pure water (WJ). The rationale behind this is that the jet formation mechanism is different. When abrasive is added in the mixing chamber, air is also sucked in, and consequently the jet consists of more than 90 % ambient air [8], which then causes quicker disintegration of the jet. Because of the quick divergence of the jet, it comes into contact with the focusing nozzle earlier and this causes a turbulent flow, which accelerates jet disintegration [9]. When abrasive is not added, the shape of the jet is better maintained, diverging slower, meaning that the jet without abrasive behaves quite differently.

During experiments, the effect of standoff distance on jet diameter was analysed. When the jet exits the focusing nozzle, it starts to disintegrate; here, the rate of disintegration could hold some important information about nozzle state. Experiments also included analysis of the effect of water pressure on AWJ diameter, as higher water pressures produce a more concentrated jet [10]. The last parameter we analysed was measurement time. Because of AWJ properties such as water pressure oscillations and jet oscillations, a sufficient duration of measurement is important to get a reliable reading, but at the same time it must not be too long to be economical.

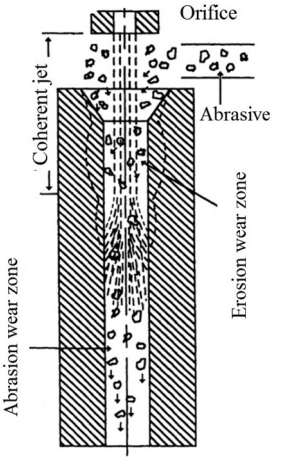

Fig. 1. *Phenomenological model of focusing nozzle wear*

2.1 Measuring Instrument

The instrument used for measuring jet diameter was a Keyence digital display compact laser through-beam sensor LX2-V10W series (Keyence, JP). The sensor was designed to measure a diameter or a gap between objects and works using a shadowing method. On one side the line laser emits light and on the other side the receiver measures the amount of light passed through an obstacle. A controller measures the amount of light received and calculates its ratio to the full signal, i.e. the signal in the case there is no obstacle between laser and receiver [11]. The principle of the through-beam sensor is shown in Fig. 2.

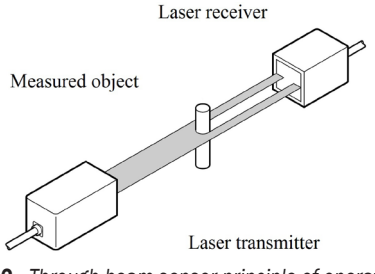

Fig. 2. *Through-beam sensor principle of operation*

The sensor uses a 5 mm wide laser beam with a wave length of 780 nm and repeatability of 10 µm. The controller has an analogue voltage output that was connected to an Arduino Uno microcontroller (Arduino LLC, USA) in order to acquire, process, present and store data.

To avoid water damage it is enclosed in a waterproof casing, as shown in Fig. 3.

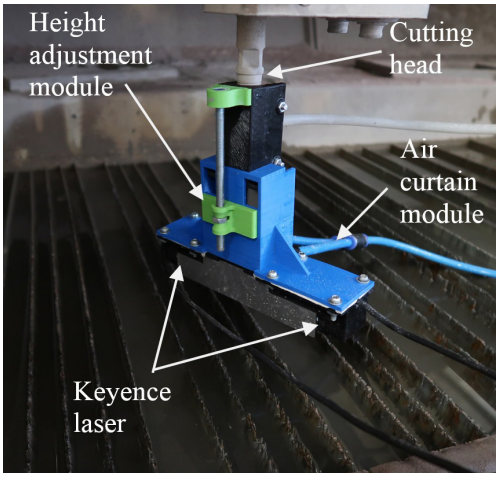

Fig. 3. *Waterproof casing designed to protect laser sensor from water*

2.2 Casing

The casing was designed to fit firmly onto the cutting head while enabling height adjustment of the sensor. This is achieved with a threaded rod and a nut. By turning the nut, the sensor is raised or lowered in order to measure the jet diameter at the desired distance from the focusing nozzle.

Both the sensor transmitter and receiver were kept in boxes that are sealed by a transparent screen made from 1 mm thick acrylic glass on one side. The sensor was calibrated using a set of stainless steel gauge blocks. The sensor characteristic is shown in Fig. 4 and shows linear characteristics with correlation coefficient R^2 equal to 0.9988.

During the initial tests, some droplets landed on screens of either the laser transmitter or receiver due to the jet spray or its splash back from the catcher tank. As expected, this caused a significant distortion in the measuring results, so a module that creates an air curtain barrier and a splash guard were designed. The air curtain module creates a stream of air at around a 20° angle away from jet to prevent interaction between the jet and air. The splash guard was designed to prevent the splashing of water back onto the screens while enabling air from air the curtain module to escape. The air curtain module and splash guard are shown in Fig. 5.

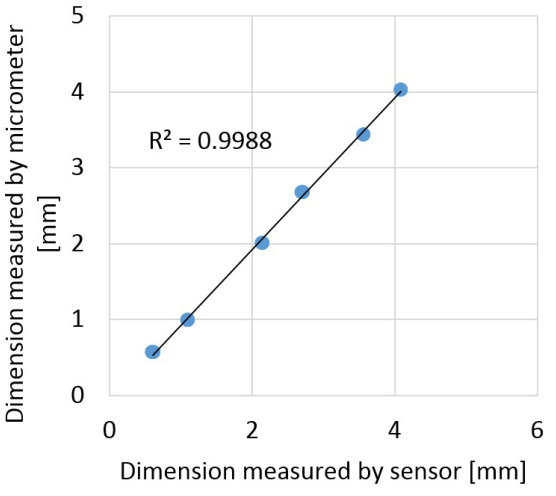

Fig. 4. *Sensor calibration characteristics*

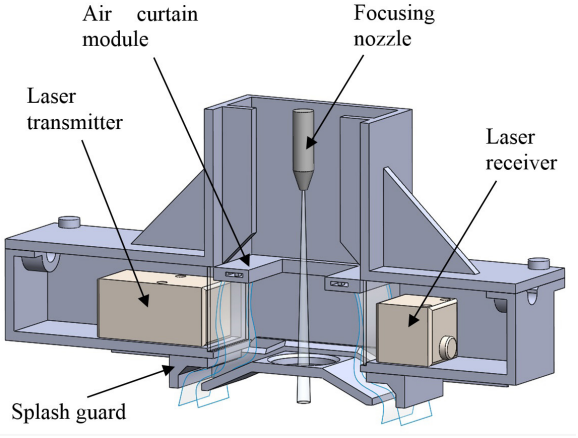

Fig. 5. *Cross section of casing showing air curtain and the splash guard*

2.3 Measuring the Focusing Nozzle Diameter

In the experiment, five focusing nozzles were used, each with different wear. Two nozzles were 0.76 mm in diameter when new and three were 1.02 mm in diameter when new. The length of all nozzles was the same, 76.20 mm. Before the experiment, the diameters of the focusing nozzle were measured using a Mitutoyo toolmakers microscope (Mitutoyo, JP). The microscope is equipped with a 2.0 Mega-pixel CCD camera and software tools from MoticImages Plus 2.0 to process the acquired pictures and measure

the diameter of the nozzles. Positioning accuracy of the microscope table is 0.001 mm.

Nozzles were observed with 30x magnification and illuminated coaxially with microscope objective from above. Nozzle diameter was measured by selecting three points on the inner edge of the nozzle, from which the program then calculated the radius. For every nozzle, the diameter was measured at least four times. The number of measurements depended on the nozzle wear. The more the nozzle was worn, the more times it was measured. Images of nozzle diameters are shown in Fig. 6, and average diameters are shown in Table 1.

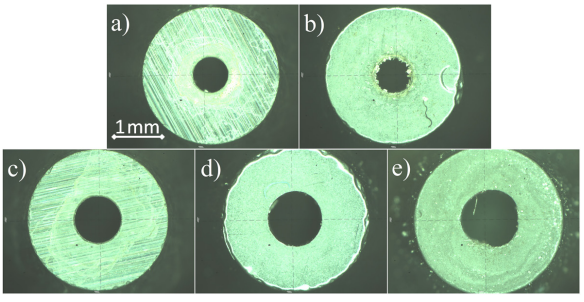

Fig. 6. *Images of focusing nozzles taken with the Mitutoyo microscope: a) 0.76 mm new, b) 0.76 mm worn, c) 1.02 mm new, d) 1.02 mm worn, e) 1.02 mm very worn*

From the images it can be observed that when the nozzle is new, the hole is almost perfectly round; however, as the wear starts to increase, the roundness slowly decreases. As a consequence, the jet becomes more unstable and loses its efficiency. For this reason, it is only economical to correct the offset up to a certain point before the nozzle needs to be replaced. Fig. 6e) shows the uneven wear on the focusing nozzle – the reason why, at some point, increasing the offset is no longer an option and the nozzle has to be replaced. That is also the reason why monitoring nozzle wear is of great importance for good quality control.

Table 1. *Average focusing nozzle diameter, measured with the microscope*

Status	Nominal nozzle diam. [mm]	Avg. meas. nozzle diam. [mm]
New	0.76	0.832
Worn	0.76	0.904
New	1.02	1.094
Worn	1.02	1.301
Very worn	1.02	1.364

2.4 Experimental Procedure

Measurements were conducted on an Omax 2652A machine (Omax, USA), equipped with an Ecotron 403 high pressure water pump (BFT GmbH, Austria) capable of reaching pressures of 400 MPa. Experiments were conducted at water pressures of 200 MPa and 275 MPa using an orifice diameter of

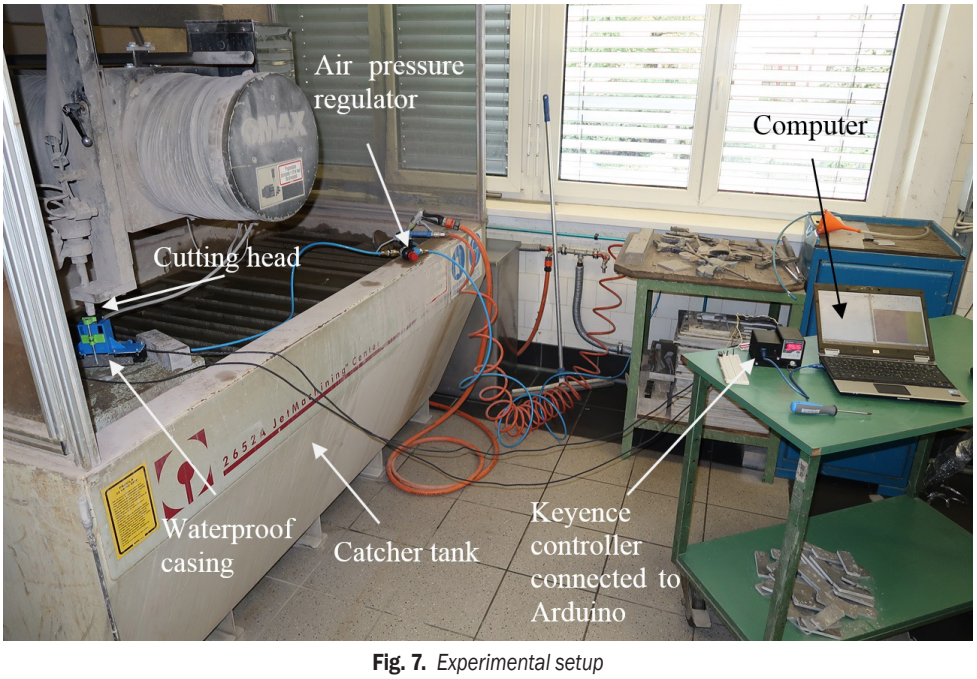

Fig. 7. *Experimental setup*

0.3 mm. Measurements were done with and without the abrasive, for which garnet mesh 80# was used. The jet diameter measurements were taken at the exit from the focusing nozzle. The experimental setup is shown in Fig. 7. First, the nozzle was mounted onto the cutting head, and then the casing of the jet diameter measurement system was attached to the cutting head. By turning the nut on the back of the casing, the sensor was raised until it reached the tip of the nozzle. After turning the jet on, the microcontroller started to acquire and interpret the analogue signal from the laser sensor. Collected data was processed offline on a PC. Acquired values were transformed to mm using a calibration equation. Three measurements were taken for each setup combination.

3 RESULTS AND DISCUSSION

3.1 Effect of Water Pressure and Abrasive on Jet Diameter

The Arduino program was set to measure the jet diameter for 3 s with a sampling rate of 100 Hz. The purpose of this test was to determine whether it is possible to get a reliable measurement in a short time and to observe the effect of abrasive and water pressure. Fig. 8 shows the measurements obtained by the device. Measurements are labelled according to the new focusing nozzle diameter - type of jet - test number. For example, 0.76 WJ 1 means that particular measurement involves a focusing nozzle 0.76 mm in diameter, without abrasive and is the first repetition. Fig. 8 shows that measurements without abrasive are relatively stable, have a good repeatability and correlate better with measurements taken with the microscope, while measurements with abrasive do not. We assume the reason for the larger jet diameter when using abrasive is that when abrasive mixes with the jet in the mixing chamber, it also sucks in air. This causes an increase in volume, which, after exiting the focusing nozzle, causes quicker dispersion.

The reason for poor repeatability lies in the spraying of the jet. In cases without abrasive, spraying involves only water, which does not stick to acrylic glass very well and is quickly blown clear by the air curtain module. When using abrasive, the tiniest particles of abrasive dissolved in water droplets tend to stay on the acrylic glass and are not effectively cleared by the air curtain module. As the residue accumulates, measurements become more and more unreliable.

Values of jet diameter labelled with 0.76 AWJ 1 and 0.76 AWJ 2 lie close together, while 0.76 AWJ 3 is notably off. This pattern was also observed in the rest of the measurements, so after preliminary AWJ tests, they were discarded.

In Fig. 8 it can also be observed that jet diameter oscillates rather significantly, which is why these measurements cannot be as accurate as measurements of solid tools.

Results from all measurements are shown in Fig. 9. Blue dots represent measured jet diameter values and orange squares represent measured focusing nozzle diameters. The experiments show that pressure has a significant effect on the correlation between jet diameter and nozzle diameter. Measurements done at 200 MPa are, on average, off by 0.18 mm, while measurements done at 275 MPa are, on average, off by 0.10 mm.

3.2 Determining Optimal Measuring Time

To determine optimal measuring time, results obtained from previous measurements and those measuring only the jet without abrasive and with water pressure of 275 MPa were used. We defined optimal measuring time as the time when either standard deviation or measuring uncertainty significantly decreases. The

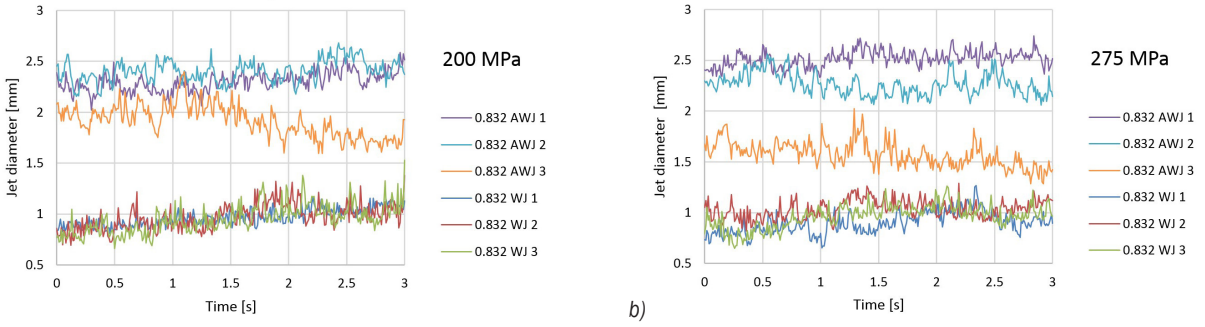

Fig. 8. *Results from measurements using a new 0.76 mm focusing nozzle at a) 200 MPa and b) 275 MPa of water pressure*

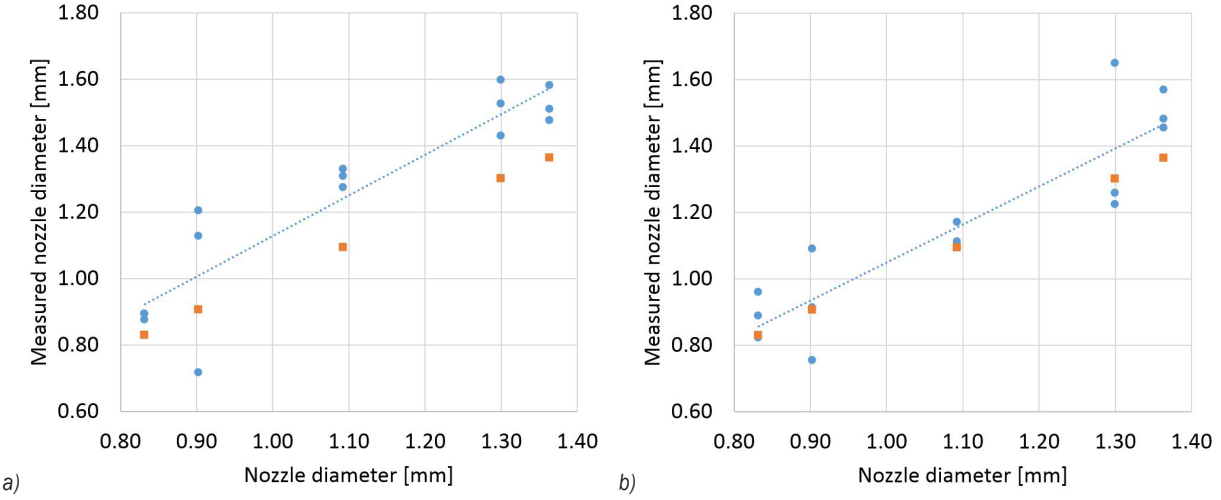

Fig. 9. *Results of measured WJ diameter at: a) 200 MPa and b) 275 MPa of water pressure*

Arduino program was reset to measure jet diameter with a sampling rate of about 3400 Hz for different lengths of time. Measuring times were (1, 2, 4, 8 and 16) s. As the device was measuring diameter, it was also calculating average diameter, standard deviation and measuring uncertainty, where it then displayed these values. Results are shown in Figs. 10 and 11. Results show that measuring time has no effect on standard deviation, so a 1 s measurement would be sufficient. Measuring uncertainty, however, is much more time dependent, as it decreases exponentially. The differences between 1 s, 2 s and 4 s are quite large, while the differences between 4 s, 8 s and 16 s are no longer significant. Another observation showed that repeatability of measurements is also much better after about 4 s compared to those measured at shorter times. Based on these results, we decided the optimal measuring time is 4 s.

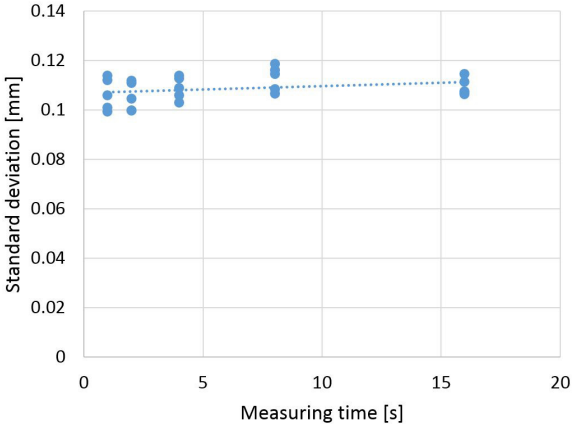

Fig. 10. *Effect of measuring time on standard deviation of measurement*

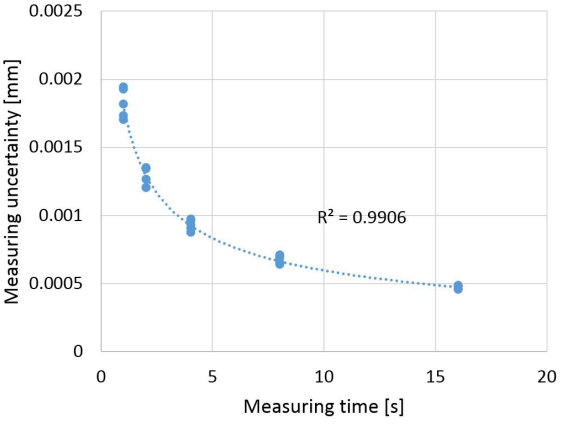

Fig. 11. *Effect of measuring time on measuring the uncertainty of measurement*

3.3 Measuring Jet Diameter at Different Standoff Distances

As the jet leaves the focusing nozzle, it starts to disintegrate. Its rate of disintegration depends on numerous parameters, such as condition of the orifice, alignment of the orifice and focusing nozzle, abrasive feed rate and focusing nozzle wear [12] and [13]. In order to measure the rate of jet disintegration below the nozzle exit, the measurement algorithm was adjusted and reloaded in the microcontroller, which acquired and processed data as long as it was needed to achieve the standard uncertainty of the mean value below 0.005 mm. In most of the measurements it took less than a second for the microcontroller to obtain the result with the desired uncertainty. Height adjustment in the present state of the prototype was adjusted manually. Results are shown in Fig. 12. The

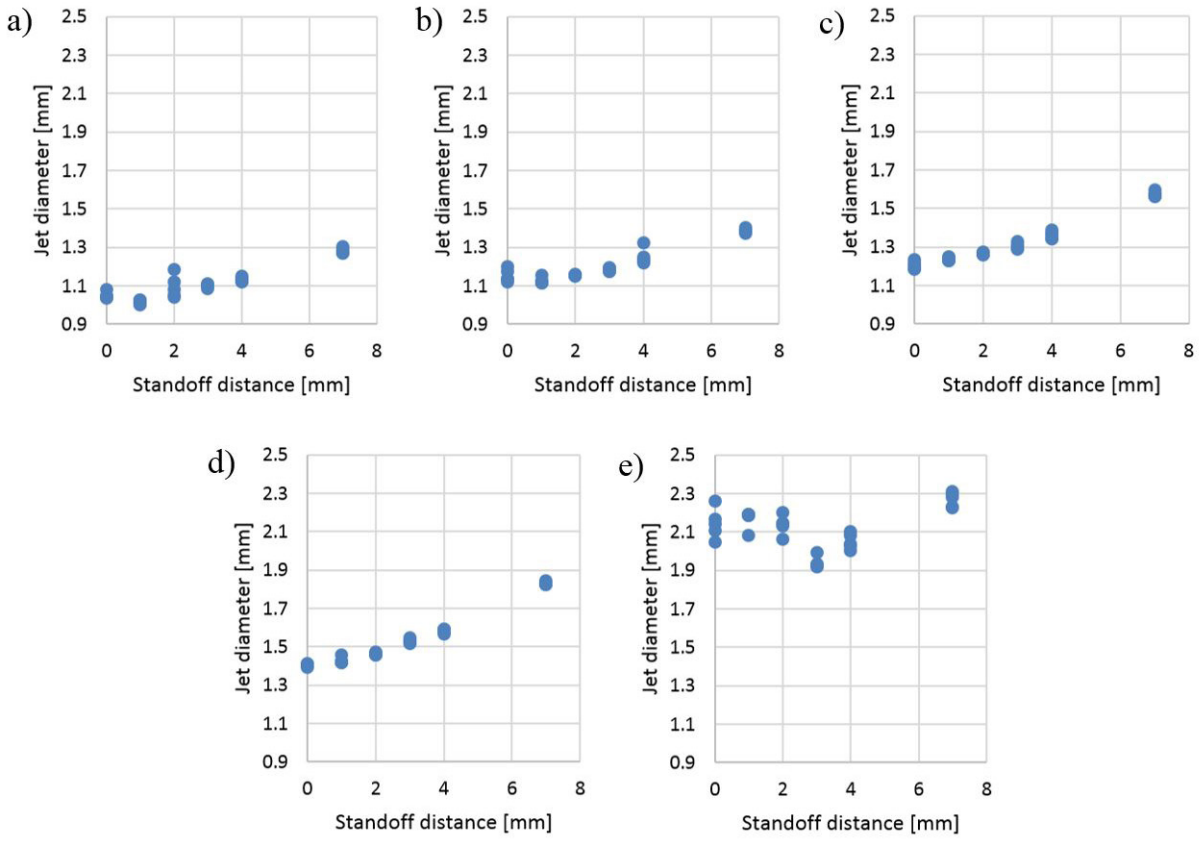

Fig. 12. *Measurements of WJ diameter at six different standoff distances for five different focusing nozzle diameters: a) 0.832 mm, b) 0.904 mm, c) 1.094 mm d) 1.300 mm and e) 1.364 mm*

program was calculating average diameter, standard deviation and measuring uncertainty in real time. Height adjustment was done by turning the nut on the back to raise or lower standoff distance. Results are shown in Fig. 12.

These results show that the jet spreads at a fixed angle; however, for the focusing nozzles with diameters of 0.832 mm and 0.904 mm an interesting phenomenon occurs. Instead of the diameter increasing proportionally with increasing standoff distance, the jet diameter shrinks at the standoff distance of 1 mm. This phenomenon is only present on the small focusing nozzle diameters, and the reason for it remains unknown. It is also possible to see that for the unevenly worn nozzle in Fig. 12e, the jet does not spread at a constant angle, but has almost constant diameter for the first 2 mm, and only afterwards it shrinks and begins to spread at an angle. This type of jet behaviour could lend useful information when determining the uniformity of nozzle wear.

We then compared the correlation between focusing nozzle diameter and WJ diameter at standoff distances of 0 mm and 1 mm. The nozzle with diameter of 1.364 mm was excluded because it was worn asymmetrically and produced a jet with much greater diameter. Results are shown in Fig. 13.

Results show that there is a much better correlation at standoff distances of 1 mm versus standoff distances of 0 mm. This is likely due to the phenomenon of the jet shrinking at a 1 mm standoff distance. The results also show better repeatability at the standoff distance of 1mm, which makes the measurements more reliable.

Using the linear equation presented in Fig. 13, the program code on the microcontroller was modified in order to calculate jet diameter in real time. With this modification of the program, measurement accuracy improved tremendously. The average difference between the predicted diameter and measured diameter of the focusing nozzle decreases to 0.02 mm, while maximum difference is only 0.07 mm. Most measurements (90 %) are within ±0.03 mm of the corresponding measured nozzle diameter. As expected, however, accuracy significantly decreases

when determining nozzle diameter of the most worn nozzle. The average difference between measured and calculated diameters is 0.80 mm.

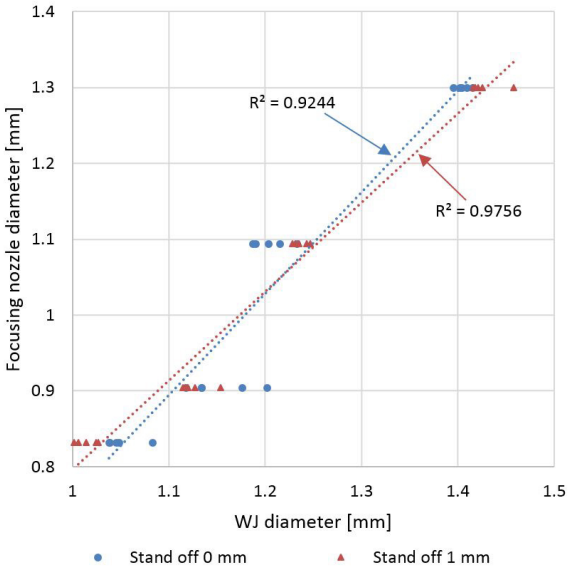

Fig. 13. *Comparison of measuring WJ diameter at 0 mm and 1 mm standoff distances*

4 CONCLUSIONS

In this paper the usage of a through-beam sensor for measuring the jet diameter and determining the focusing nozzle diameter was analysed. The results show much stronger correlation between jet diameter and focusing nozzle diameter at high water pressures, when not using abrasive and at a standoff distance of 1 mm. The main reason for measuring without adding abrasive is that as the jet sprays, residue accumulates on the screens of the instrument and measurements become distorted. Cleanliness in general is the main problem when measuring AWJ diameter. To solve this, we created an air curtain module and a splash guard, which proved to be effective, but not sufficient so as to completely eliminate cleanliness problems. Suggestions for solving this include adding a cleaning module and applying a hydrophobic coating to screens. Before every measurement, screens would be cleaned first, then the instrument calibrated, and only then could the measurement be performed.

With this instrument we managed to determine focusing nozzle diameter to ±0.03 mm. As focusing nozzle diameter is used as a tool offset when setting cutting parameters, knowing the actual diameter would enable a much more accurate cut. This instrument can also be used to monitor nozzle wear, so that the operator can replace the focusing nozzle as it gets too worn. It was shown that it is also possible to get additional information about the uniformity of nozzle wear from the variation of the measured WJ diameter at different standoff distances; however, this relation has to be researched in greater detail in the future.

The results obtained on the prototype discussed in this paper promise that the concept can be implemented into industrial practice. In order to increase the reliability of the measurement device, a cleaning module should be added and the height adjustment automated. Such an instrument would provide better quality control as well as the possibility to make the cutting process much more automated.

5 ACKNOWLEDGEMENTS

The authors would like to thank to the Slovenian Research Agency for supporting the work in the frame of the Research programme Innovative production systems (P2-0248).

8 REFERENCES

[1] OMAX Corporation (2016). Learn About Waterjets, from *https://www.omax.com/learn/waterjet-cutting*, accessed on 2016-11-19..

[2] WaterJets.org (2016). Measuring Kerf and Tool Offset, from *http://www.waterjets.org/index.php?option=com_content&task=view&id=186&Itemid=54*, accessed on 2016-11-19.

[3] Nanduri, M., Taggart, D.G., Kim, T.J. (2002). The effects of system and geometric parameters on abrasive water jet nozzle wear. *International Journal of Machine Tools and Manufacture*, vol. 42, no. 5, p. 615-623, **DOI:10.1016/S0890-6955(01)00147-X**.

[4] Jerman, M., Valentinčič, J., Lebar, A., Orbanić, A. (2015). The study of abrasive water jet cutting front development using a two-dimensional cellular automata model. *Strojniški vestnik - Journal of Mechanical Engineering*, vol. 61, no. 5, p. 292-302, **DOI:10.5545/sv-jme.2014.2179**.

[5] Orbanić, H., Junkar, M., Bajsić, I., Lebar, A. (2009). An instrument for measuring abrasive water jet diameter. *International Journal of Machine Tools and Manufacture*, vol. 49, no. 11, p. 843-849, **DOI:10.1016/j.ijmachtools.2009.05.008**.

[6] Folkes, J., Li, Z.J. (2010). Innovative method of water jet diameter measurement for process and quality control. *20th International Conference on Water Jetting*, p. 329-340.

[7] Hashish, M. (2003). Inside AWJ Nozzles. *WJTA American Waterjet Conference*, p. 1-D.

[8] Momber, A.W., Kovacevic, R. (1998). *Principles of Abrasive Water Jet Machining*. Springer, London, **DOI:10.1007/978-1-4471-1572-4**.

[9] Agrawal K.S. (2013). Breakup of liquid jets. *International Journal of Emerging Technologies in Computational and Applied Sciences*, no. 5, p. 487-496.

[10] Birouk, M., Lekic, N. (2009). Liquid jet breakup in quiescent atmosphere: a review. *Atomization and Sprays*, no. 6, p. 501-528, **DOI:10.1615/AtomizSpr.v19.i6.20**.

[11] Keyence (2016). *Laser Thrubeam Photoelectric Sensor LX2(W) Series. Instruction manual.* Keyence, Osaka,

[12] Stevenson, A.N.J., Hutchings, I.M. (1995). The influence of nozzle length on the divergence of the erodent particle stream in a gas-blast erosion rig. *Wear*, vol. 189, no. 1-2, p. 66–69, **DOI:10.1016/0043-1648(95)06641-1**.

[13] Annoni, A., Arleo, F., Malmassari, C. (2014). CFD aided design and experimental validation of an innovative air assisted pure water jet cutting system. *Journal of Materials Processing Technology*, vol. 214, no. 8, p. 1647-1657, **DOI:10.1016/j.jmatprotec.2014.01.020**.

Strojniški vestnik - Journal of Mechanical Engineering 63(2017)10, 606-613
DOI:10.5545/sv-jme.2017.4463
Original Scientific Paper
Received for review: 2017-03-20
Received revised form: 2017-06-19
Accepted for publication: 2017-07-05

Obtaining the Selected Surface Roughness by Means of Mathematical Model Based Parameter Optimization in Abrasive Waterjet Cutting

Andrzej Perec [1,2,*] – Frank Pude[1] – Michael Kaufeld[3] – Konrad Wegener[1,4]
[1]ETH Zürich, Inspire AG, Switzerland
[2]Jacob of Paradies University, Department of Technology, Poland
[3]University of Applied Sciences Ulm, Institute of Production Engineering and Materials Testing, Germany
[4]ETH Zürich, Institute of Machine Tools and Manufacturing, Switzerland

The study on the effect of abrasive water jet machining process parameters on micro alloyed steel surface roughness was described. Taguchi method to predict machining parameters of due to minimum surface roughness was used. The influence of pressure, abrasive flow rate and traverse speed on the R_z and R_{max} roughness parameters were presented. The optimum combination of processing parameters was established. Verified parameters were tested and the achieved results were compared to predicted values. This method allows limiting the amount of research needed to achieve the desired test results, thereby reducing the time as well as the cost required to carry them out. The Taguchi signal/noise (S/N) ratio enables the assessment of the relevance of the impact of various parameters on the process, which is still not well enough understood.

Keywords: abrasive water jet, design of experiment, optimization, cutting, prediction

Highlights
- *Influence of hydraulic pressure, traverse speed and abrasive flow rate on micro alloyed steel cut surface roughness was presented.*
- *An optimal set of parameters to achieve the smallest surface roughness of cut material was established.*
- *A significant reduction in the cost of the experimental work by reducing the number of necessary tests and shorten the time to carry out with high accuracy of results was achieved.*

0 INTRODUCTION

In recent years, high pressure water-jet machining has competed effectively with conventional methods of separation of materials. This is mainly because of the wide range of options it offers, including the processing of complex shapes, cutting of a large variety of materials, and its effectiveness under extreme conditions (hazard of fire or explosion, work under water up to a depth of 6000 m, etc.) and the environmental friendliness **[1]**.

Further advantages of the treatment of materials with a high-pressure fluid jet include:
- ability to cut with constant stand-off distance between the working nozzle and machined top surface of the workpieces,
- good surface structure after cutting or surface processing,
- leaves the structure of the cut material thermally unaffected,
- no internal stresses in the cutting zone,
- fluid jet can be operated very easily.

However, the application of a pure fluid jet is not very effective in cutting hard materials such as metals or rocks. The application of solutions for intensifying the erosive abilities of the fluid jet, such as the introduction of a loose abrasive is necessary for improving the effectiveness of the treatment. It should also be noted that the treatment is performed without significant increase in heat, as any heating produced as a result of the friction of the abrasive against the material and the nozzle is immediately counteracted by the water jet.

1 WATER JET CUTTING

Cutting by high-pressure water jet is an advanced method of separating materials. Processing materials using a high pressure abrasive water jet is more complex than conventional treatments. Existing models for predicting the results of cutting by water jet as presented for example in **[2]** to **[4]** cannot achieve satisfactory results in the wide area of parameter changes, especially for the large number of different materials. High pressure water is converted to a high speed jet inside a nozzle (Fig. 1a) and flows out of the nozzle at a speed of several hundred meters per second, hits a stream of abrasive particles and accelerates them to high particle speed.

*Corr. Author's Address: Department of Technology, Jacob of Paradies University, Teatralna 25, PL-66 400 Gorzow Wlkp., Poland, aperec@ajp.edu.pl

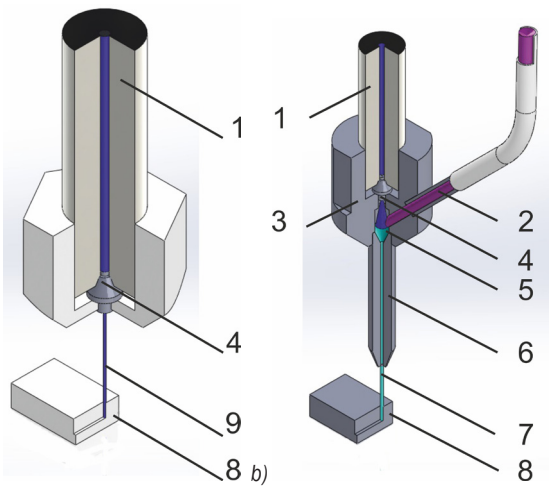

Fig. 1. *Schematic diagram of: a) water jet cutting, and b) abrasive water jet cutting; 1. high pressure water inlet, 2. abrasive inlet, 3. cutting head, 4. water nozzle, 5. mixing chamber, 6. focussing tube, 7. high speed abrasive water Jet, 8. sample, 9. high speed water jet*

Adding dry abrasive to the water jet in a special mixing chamber (Fig. 1b) increases cutting efficiency. As a result, it becomes possible to cut almost any material. Typical pressure levels used by the abrasive water jet (AWJ) system range from 400 MPa to 600 MPa. The most commonly used abrasive is garnet **[3]** and **[5]**.

2 MATERIALS AND EXPERIMENTAL SETUP

The study is conducted on the test rig shown in Fig. 2 by using a high pressure intensifier (BYPUMP 50APC) presented in Fig. 2b. The maximum working pressure is 400 MPa at a flow rate of 5 dm^3/min. This allows the use of a water nozzle with maximum diameter of 0.4 mm.

The cutting head used, as shown in Fig. 2a is equipped with a water nozzle with a diameter of 0.28 mm, and a focussing tube with a diameter of 0.76 mm and a length of 75 mm, mounted on 3-axis Siemens Sinumerik 840D CNC machine as can be seen in Fig. 2c.

The working area is 1000 mm × 1000 mm × 400 mm. The machine is equipped with an abrasive feeder from the Swiss company Allfi. During the test garnet (Almandine) 80 mesh is used, from which a sample is presented in Fig. 3. The basic properties of this abrasive are presented in Table 1.

The garnet abrasive group contains closely related, isomorphous, minerals that may contain low percentages of elements found in other members of

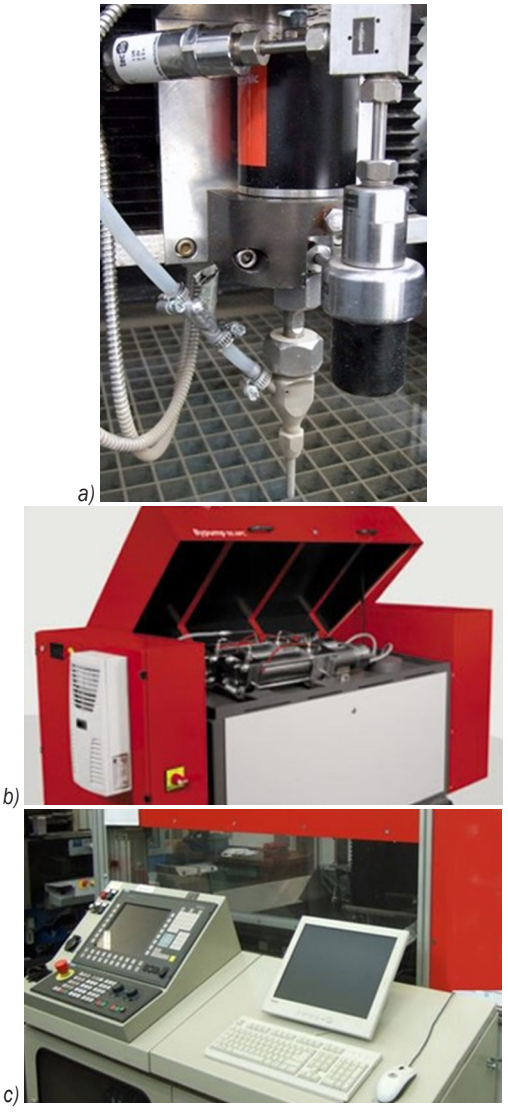

Fig. 2. *Test rig: a) cutting head, b) high pressure intensifier, and c) control module*

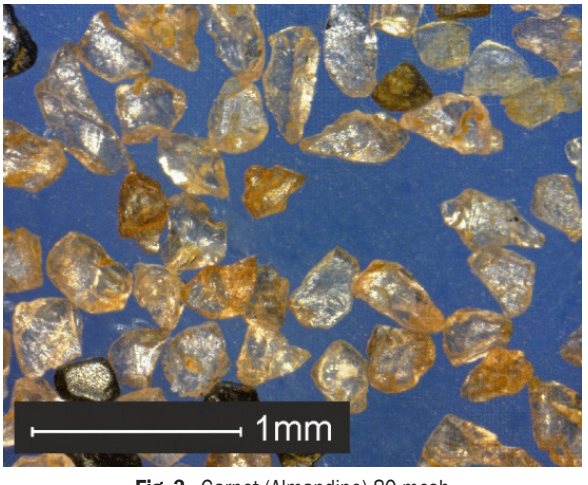

Fig. 3. Garnet (Almandine) 80 mesh

the garnet family. Garnets are isostructural, meaning that they share the same crystal structure [6].

Table 1. *Garnet (Almandine) properties* [6]

Crystal system	Cubic
Twinning	None
Unit cell	$a = 11.53$ Å
Habit	crystals usually dodecahedrons or trapezohedrons; also in combination or with hexoctahedron; massive; granular
Cleavage	1; {110} parting sometimes distinct
Fracture	conchoidal to uneven
Tenacity	Brittle
Color	deep red to reddish-brown, some-times with a violet or brown or brownish black hue
Hardness (Mohs)	6.5 to 7.5
Density	4.1 to 4.3

As sample used micro alloyed steel 27MnSiVS6 (DIN 1.5232). It is ferritic-perlitic high strength Mn-V-based, low alloy high grade steel with good machinability for controlled cooling from working heat steel for precipitation hardening.

3 THE TAGUCHI METHOD

The selection of parameters which can produce optimal results is usually a complex process. Typically this requires carrying out a number of tests, and in this way the effect of technological parameters on the properties of the final product can be determined. The Design of Experiment can be shortened by using this method. The planning of such studies is an interdisciplinary science, which lies at the intersection of metrology, applied mathematics, statistics, and computer science, allowing researchers to use the information the program has provided them with to reduce both the cost and time expended in obtaining the relevant information. This Design of Experiment enables researchers to select the input variables which significantly affect the process observed and can also build a mathematical model of the process and the mathematical relationships between input and output values. Further, it can determine the value of the input quantities which affect the most desired outcome of the process (process optimization), and determine the effect of variation in the size of the input on the variability of the whole process [7].

The Taguchi Method [8] is a technique that provides a systematic and efficient methodology for process optimization and is a useful tool for the design of high quality systems. The Taguchi approach to Design of Experiments is easy for users with less experience of statistical methods to apply , and has therefore gained wide popularity in engineering. It is used for example in surface engineering [9] and [10], turning [11], and of course in water jet machining [12].

Abrasive water jet machining allows for the cutting of almost any material with high efficiency and accuracy. Therefore Taguchi approach is successfully used in the cutting optimization of a different materials such as coal [13], ceramics [14], [15], aramid [16] and glass/epoxy composite [17], inconel [18] and aluminum [19] to [21]. The well-studied material is only mild steel [22] and stainless steel [12] and [23]. Micro-alloyed steel used in test is significantly different from mild and stainless steel, it is advisable to carry out appropriate roughness tests.

The average roughness (R_a) measurements for machined surface finishes have become the standard default representation for abrasive waterjet machined surfaces. By comparison the relative differences between R_a and R_z surfaces, it was demonstrated that R_z measurements provide a more accurate representation of the surface finish of an abrasive waterjet machined surface [24]. Therefore, the novelty of their research also applies to the use of other (R_z and R_{max}) roughness parameters, than commonly used R_a.

The Taguchi Method is an engineering methodology for obtaining optimized products and processes, which are minimally robust and which produce high-quality products with reduced development and production costs. Signal to noise ratio (S/N ratio) and orthogonal matrix are two major tools used in the planning of experiments.

The S/N ratio values can be divided into three categories when the number is continuous:

- nominal is the best,
- smaller is better,
- larger is better.

The Taguchi Method is used to generate a S/N ratio η in order to determine the current scatter of values. The signal (S) is derived from factors which are adjustable or under the control of the user, but noise (N) refers to those factors which affect the signal, but which are beyond the control of the user.

The aim of the design is to enable the selection of the parameters of the experiment (in this case the process), so as to maximize the η. Various S/N indicators can be used according to the researcher's needs [10]. Taguchi analysis observes the higher value of mean S/N ratio as better quality characteristic.

Orthogonal matrix is selected subset of combinations of multiple factors at multiple levels. Taguchi Orthogonal matrix are balanced to ensure that

all levels of all factors are considered equally. For this reason, the factors can be evaluated independently of each other despite the fractionality of the design [25].

In abrasive water jet cutting typically aims at achieving the maximal depth of cut and low roughness of the cut surface. Especially during precision cutting low roughness of the cut surface is of paramount importance. In this case the roughness of the kerf's surface should be as small as possible. This is described by the "smaller is better" equation:

$$\eta = -10 \log\left(\frac{1}{n}\sum_{i=1}^{n} y_i^2\right), \quad (1)$$

where n is the number of repetitions of measurement, y the current value of the measurement, and i the number of variables.

4 OPTIMIZATION AND PREDICTION PROCEDURE

The influence of the selected parameters of abrasive water jet cutting on the accepted optimization criterion – surface roughness of the cutting kerf – is analyzed.

A machining parameter selection process, using the L18 orthogonal array, was applied in this study (Table 2). This array is chosen because it consists of three control parameters: one (P1) with 6 levels, and the next two (P2 and P3) with three levels, as shown in Table 2.

Table 2. *Orthogonal array L18 for Taguchi design*

Test number	P1	P2	P3
1	1	1	1
2	1	2	2
3	1	3	3
4	2	1	1
5	2	2	2
6	2	3	3
7	3	1	2
8	3	2	3
9	3	3	1
10	4	1	3
11	4	2	1
12	4	3	2
13	5	1	2
14	5	2	3
15	5	3	1
16	6	1	3
17	6	2	1
18	6	3	2

In this case, the control parameter P1 is represented by the traverse speed, control parameter P2 by the pressure, while control parameter P3 by the abrasive flow rate.

The Minitab16 program is used for the calculation procedure. The variation interval of the selected cutting parameters used under optimization are presented in Table 3.

After conducting research at relevant parameters according to Taguchi array, roughness values were measured for each parameter combination.

Roughness was measured according to the most commonly used methods: R_{max}, and R_z [26] to [28].

Roughness measurements were performed on optical 3D measuring system NanoFocus mSurf (Fig. 4a).

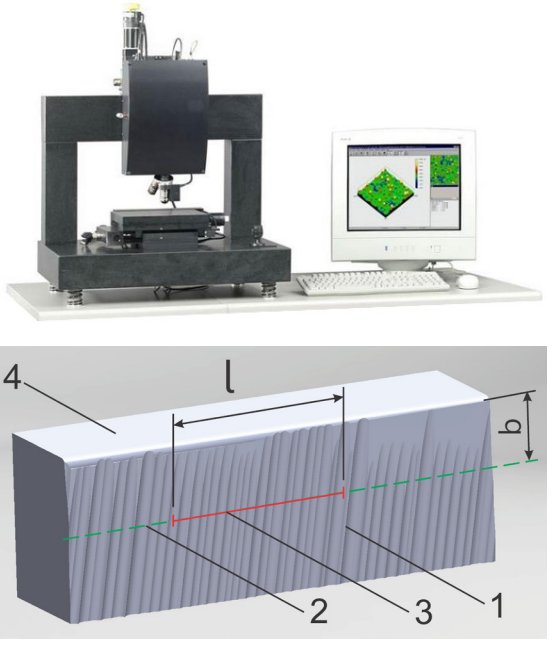

Fig. 4. *Measurement of roughness: a) NanoFocus msurf optical 3D measuring system, and b) details of measurement: 1 cutting surface, 2 sampling line, 3 sampling length, and) top plane*

The measurement principle is based on the white light confocal technique and is specially designed for quality control of technical surfaces as a completely independent 3D video measurement system, with cut-off wave length l_c filter, according to DIN EN ISO 4287 norm.

Optical system msurf allowed representation of 3D structures in the nanometer range, measurement of surfaces, microstructures and surface topographies on working area: X = 380 mm, Y= 250 mm and Z= 355 mm.

To eliminate the influence of rounded cutting edges (Fig. 4b), the sampling line was set at b = 1 mm from the top surface. The sampling length of the measurement is l = 4 mm. Each measurement of the roughness was taken five times and their arithmetic mean was calculated as to minimize the errors.

Fig. 5 presents the calculated dependency terms of the cut of the value of S/N ratios, R_z and R_{max} coefficients. The higher the signal to noise ratio, the more favorable is the effect of the input variable on the output. The impact of individual process parameters on the S/N ratio is similar for all analyzed roughness values. For each roughness coefficient, a maximal S/N ratio is reached at the smallest traverse speed value, which was 20 mm/min.

In the case of pressure, the largest value of the S/N ratio is reached at the highest pressure, which was 360 MPa. This result is obtained for all roughness coefficients. Maximal S/N ratio values are reached for the highest abrasive flow rate (100 g/min), for all roughness coefficients. By increasing the kinetic energy of the abrasive water jet a lower level of surface quality at the bottom of the cutting edge can be transferred to better quality levels.

Table 3. *Parameters of the cutting process and values of η factor*

Traverse speed	Pressure	Abrasive flow rate	R_{max}	S/N (R_{max})	R_z	S/N (R_z)
[mm/min]	[MPa]	[g/min]	[mm]	η	[mm]	η
20	360	100	15.59	-24.67	13.61	-22.68
20	300	80	17.44	-24.29	14.43	-23.19
20	240	60	19.32	-26.24	18.33	-25.26
40	360	100	21.02	-27.10	12.76	-22.12
40	300	80	18.41	-25.22	15.67	-23.90
40	240	60	15.39	-26.55	14.49	-23.22
60	360	80	22.78	-25.09	19.52	-25.81
60	300	60	25.56	-28.45	20.46	-26.22
60	240	100	19.18	-27.47	16.38	-24.29
100	360	60	20.37	-25.28	17.51	-24.87
100	300	100	18.09	-26.64	14.69	-23.34
100	240	80	19.43	-26.29	17.39	-24.81
140	360	80	21.82	-26.67	16.66	-24.43
140	300	60	31.76	-27.00	19.40	-25.76
140	240	100	29.25	-29.17	20.47	-26.22
180	360	60	22.04	-26.45	19.65	-25.87
180	300	100	21.47	-27.02	17.76	-24.99
180	240	80	24.33	-27.05	20.45	-26.21

The effect of control factors were investigated through the analysis of variance – ANOVA. Based on

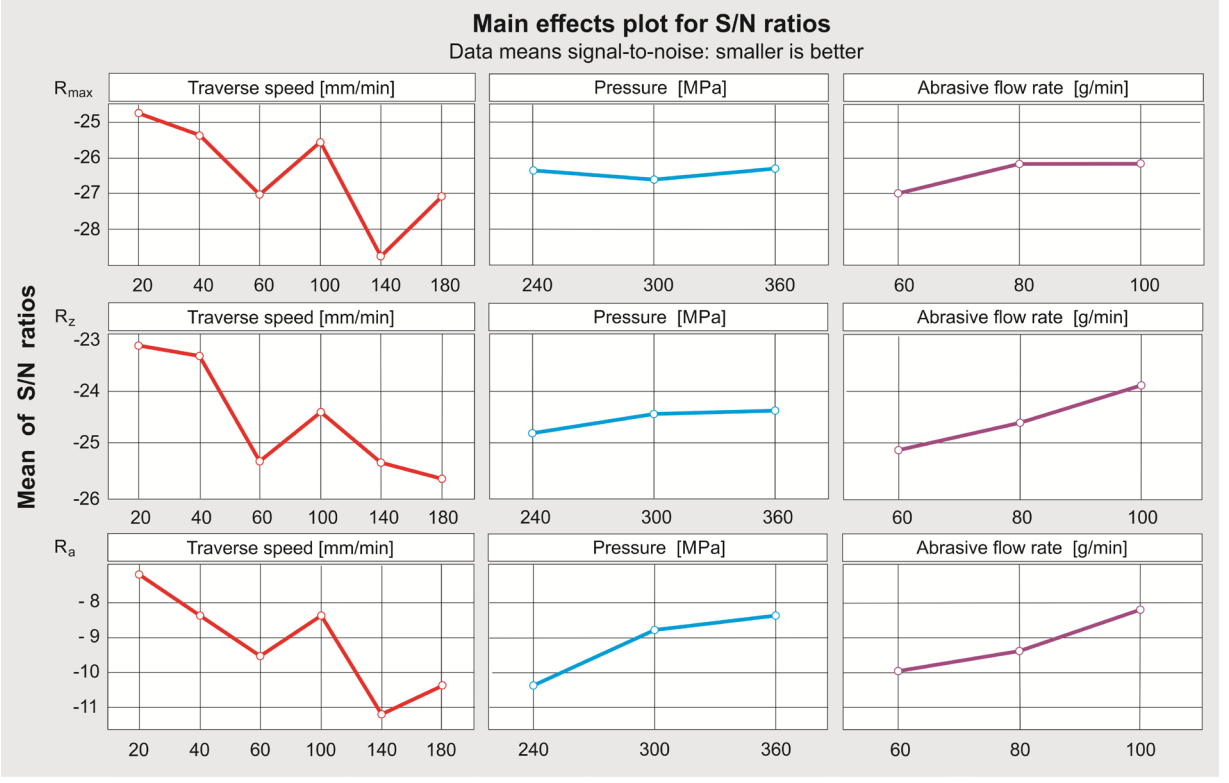

Fig. 5. *S/N ratio of roughness for each of tested parameters*

the results shown in Table 3, test the significance of machining parameters: traverse speed, pressure and abrasive flow rate on R_{max} and R_z surface roughness parameters was calculated.

Table 4. *ANOVA and F-ratio for* R_{max}

Parameter	*SS*	*Df*	*Ms*	*F*	*p*
Traverse speed	70.307	5	14.061	3.189	0.071
Pressure	28.968	2	14.484	3.285	0.091
Abrasive flow rate	30.441	2	15.220	3.452	0.083
Error	35.270	8	4.409		

SS is sum of squares, *Df* degree of freedom, *Ms* mean square, and *F* ratio of variance of a source to variance of error.

The results of machining parameters influence on R_{max} shows Table 4 and on R_z shows Table 5.

This analysis was carried out for a 95 % confidence level. It was found that traverse speed failed the test of significance at 95 % confidence level and therefore, they were pooled [29]. The factors that pass the test of significance are considered significant. They are considered insignificant if they fail the test of significance and are usually treated as if they are not present. This process is called pooling.

Pressure is the most significant factor influencing the assessment of both R_{max} and R_z. Meanwhile abrasive flow rate respectively have sub significant effect on both R_{max} and R_z. Traverse speed is the least significant in influencing both R_{max} and R_z.

Table 5. ANOVA and F-ratio for R_z

Parameter	*SS*	*Df*	*Ms*	*F*	*p*
Traverse speed	27.763	5	5.553	2.609	0.111
Pressure	8.496	2	4.248	1.996	0.198
Abrasive flow rate	10.114	2	5.057	2.376	0.155
Error	17.028	8	2.129		

SS is sum of squares, *Df* degree of freedom, *Ms* mean square, and *F* ratio of variance of a source to variance of error.

In Fig. 6 are shown the predicted and the measured roughness values reached at optimal cutting parameters: traverse speed = 20 mm/min, pressure = 360 MPa and abrasive flow rate = 80 g/min. The best prediction data is reached for the roughness coefficient R_{max}. and the worst fit is reached for the roughness coefficient R_z.

Fig. 7 shows an exemplary photorealistic shading view and profile generated by machining parameters which were optimal from the roughness point of view. It is possible to observe parallel machining traces characteristic for abrasive grain cutting.

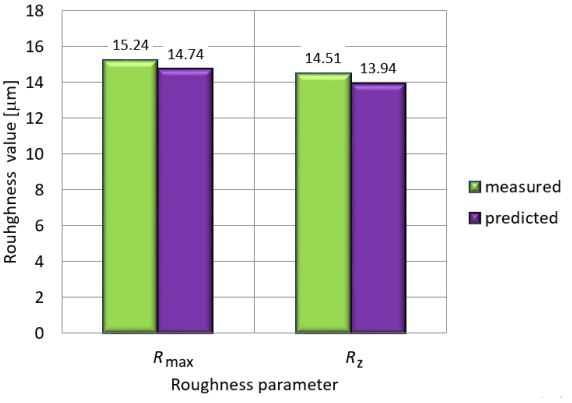

Fig. 6. *Results of predicted and measured values for different roughness parameters*

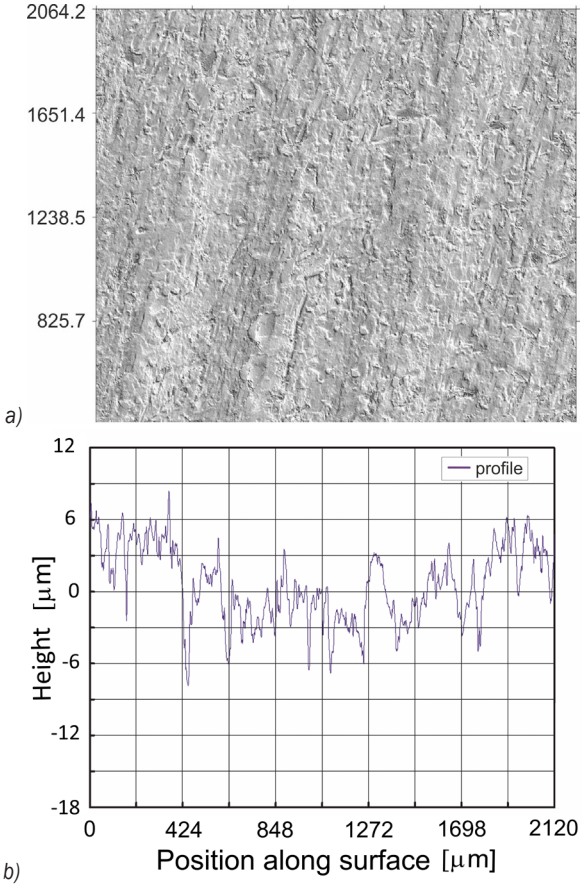

Fig. 7. *Sample of a cut steel surface at optimal parameters: traverse speed = 20 mm/min, pressure = 360 MPa, abrasive flow rate = 100 g/min, a) photorealistic shading view, b) surface profile of the sample*

5 CONCLUSIONS

On the basis of experimental results, calculation of S/N ratios and confirmation results of tested steel by Abrasive Water Jet the following conclusions can be drawn as follows:

1. Pressure is the most significant control factor on both surface roughness values R_{max} and R_z generated by AWJ machining.
2. Abrasive flow rate is a sub significant machining parameter in influencing both R_{max} and R_z surface roughness values.
3. Traverse speed is the least significant machining parameter in influencing on both R_{max} and R_z surface roughness values.
4. Increasing the hydraulic pressure results in lower R_{max} and R_z roughness values.
5. Traverse speed shows the opposite effect on both R_{max} and R_z roughness values.
6. By increasing the kinetic energy of the abrasive water jet a lower level of surface quality at the bottom of the cutting edge can be transferred to better quality levels.
7. Taguchi method turns out to be a suitable method for design and analysis of experiments. Reachable surface roughness values for the predicted optimal machining parameters are similar (differences are smaller than 4 %) than the surface roughness values obtained in experiments defined in the orthogonal array.
8. For optimum surface roughness abrasive water jet machining combination parameters is:

- pressure = 360 MPa,
- abrasive flow rate = 80 g/min,
- traverse speed = 20 mm/min.

The method may be particularly useful in planning research into the treatment of new materials regarding which there is insufficient information, about the properties. It may also be important in assessing the significance of the parameters that influence the cutting of new materials and newly developed procedures which are not yet sufficiently understood.

6 REFERENCES

[1] Kukiełka, K. (2016). Ecological aspects of the implementation of new technologies processing for machinery parts. *Annual Set the Environmental Protection*, vol. 18, no. 1, p. 137-157.

[2] Feed Rate Calculator (2017). From *http://www.wardjet.com/downloads.html* accessed on 17-01-2017.

[3] Perec, A., Pude, F., Stirnimann, J., Wegener, K. (2015). Feasibility study on the use of the fractal analysis method for evaluating the surface quality generated by high pressure waterjet machining. *Tehnički vjesnik - Technical Gazette*, vol. 22, no. 4, 879-883, **DOI:10.17559/TV-20140128231244**.

[4] Strnadel, B., Hlaváč, L., Gembalová, L. (2013). Effect of steel structure on the declination angle in AWJ cutting. *International Journal of Machine Tools and Manufacture*, vol. 64, p. 12-19, **DOI:10.1016/j.ijmachtools.2012.07.015**.

[5] Valíček, J., Harničárová, M., Hlavatý, I., Grznárik, R., Kušnerová, M., Hutyrová, Z., Panda, A. (2016). A new approach for the determination of technological parameters for hydroabrasive cutting of materials. *Materialwissenschaft und Werkstoff-technik*, vol. 47, no. 5-6, p. 462-471, **DOI:10.1002/mawe.201600522**.

[6] Martinec, P., Foldyna, J., Sitek, L., Ščučka, J. Vašek, J. (2002). *Abrasives for AWJ Cutting*. Institute of Geonics, Ostrava.

[7] Perec, A., Ťavodova, M. (2016). Abrasive water jet cutting depth optimization by taguchi approach. *Manufacturing Technology*, vol. 16, no. 3, p. 590-595, **DOI:10.1016/j.proeng.2016.06.680**.

[8] Taguchi, G. (1989). *Quality Engineering in Production Systems*. McGraw-Hill, New York.

[9] Macodiyo, D.O., Soyama, H. (2006). Optimization of cavitation peening parameters for fatigue performance of carburized steel using Taguchi methods. *Journal of Materials Processing Technology*, vol. 178, no. 1-3, p. 234-240, **DOI:10.1016/j.jmatprotec.2006.03.172**.

[10] Olik, R., Warcholinski, B., Ratajski, J., Michalski, J. (2011). Application of Taguchi Method to Optimize process Parameters of Gas Nitriding. *Surface Engineering*, vol 4, p. 3-7.

[11] Krishankant, J.T., Bector, M., Kumar R. (2012). Application of Taguchi method for optimizing turning process by the effects of machining parameters. *International Journal of Engineering and Advanced Technology*, vol. 2, no. 1, p. 263-274.

[12] Badgujar, P.P., Rathi, M.G. (2014). Taguchi method implementation in abrasive waterjet machining process optimization. *International Journal of Engineering and Advanced Technology*, vol. 3, no. 5, p. 66-70.

[13] Sharma, V., Chattopadhyaya, S.A., Hloch, S. (2011). Multi response optimization of process parameters based on Taguchi–Fuzzy model for coal cutting by water jet technology. *International Journal of Advanced Manufacturing Technology*, vol. 56, no. 9-12, p. 1019-1025, **DOI:10.1007/s00170-011-3258-x**.

[14] Santhanakumar, M., Adalarasan, R., Rajmohan, M. (2015). Experimental modelling and analysis in abrasive waterjet cutting of ceramic tiles using grey-based response surface methodology. *Arabian Journal for Science & Engineering*, vol. 40, no. 11, p. 3299-3311, **DOI:10.1007/s13369-015-1775-x**.

[15] Srikanth, D.V., Sreenivasa, Rao, M.S. (2015). Application of Taguchi & response surface methodology in optimization for machining of ceramics with abrasive jet machining. *Materials Today: Proceedings*, vol. 2, no. 4-5, p. 3308-3317, **DOI:10.1016/j.matpr.2015.07.149**.

[16] Azmir, M.A., Ahsan, A.K., Rahmah, A. (2009). Effect of abrasive water jet machining parameters on aramid fibre reinforced plastics composite. *International Journal of Material Forming*, vol. 2, no 1, p. 3744, **DOI:10.1007/s12289-008-0388-2**.

[17] Azmir, M.A., Ahsan, A.K. (2008). Investigation on glass/epoxy composite surfaces machined by abrasive water jet machining.

Journal of Materials Processing Technology, vol. 198, no. 1-3, p. 122-128, **DOI:10.1016/j.jmatprotec.2007.07.014**.

[18] Yünlü, L., Çolak, O., Kurbanoglu, C. (2014). Taguchi DOE analysis of surface integrity for high pressure jet assisted machining of Inconel 718. *Procedia CIRP*, vol. 13, p. 333-338, **DOI:10.1016/j.procir.2014.04.056**.

[19] Kolahan, F., Khajavi, H. (2009). Modeling and optimization of abrasive waterjet parameters using regression analysis. *International Journal of Mechanical, Industrial, Mechatronic and Manufacturing Engineering*, vol. 3, no. 11 p. 1425-1430.

[20] Nagdeve, L., Chaturvedi, V., Vimal, J. (2012). Implementation of Taguchi approach for optimisation of abrasive water jet machining. *International Journal of Instrumentation, Control and Automation*, vol. 1, no. 3-4, p. 9-13.

[21] Shukla, R, Singh, D. (2017). Experimentation investigation of abrasive water jet machining parameters using Taguchi and Evolutionary optimization techniques. *Swarm and Evolutionary Computation*, vol. 32 p. 167-183, **DOI:10.1016/j.swevo.2016.07.002**.

[22] Rao, M.S., Ravinder, S., Kumar, A.S. (2014). Parametric optimization of abrasive waterjet machining for mild steel: Taguchi approach. *International Journal of Current Engineering and Technology*, no. 2, p. 28-30, **DOI:10.14741/ijcet/spl.2.2014.06**.

[23] Ramprasad, Upadhyay, G., Hassan, K. (2015). Optimization MRR of stainless steel 403 in abrasive water jet machining using Anova and Taguchi method. *Journal of Engineering Research and Applications*, vol. 5, no. 5, p. 86-91.

[24] Miles, P., Henning, A. (2013) Rz: A better measurement of abrasive waterjet cut surface finishes. *WJTA-IMCA Conference Proceedings*. Houston, paper C2.

[25] Weibull Reliability Hot Wire from *http://www.weibull.com/hotwire/issue111/tooltips111.htm* accessed on 16-01-2017.

[26] Hreha, P., Hloch, S. (2013). Potential use of vibration for metrology and detection of surface topography created by abrasive waterjet. *International Journal of Surface Science and Engineering*, vol. 7, no. 2, p. 135-150, **DOI:10.1504/IJSURFSE.2013.053699**.

[27] Perec, A. (2016). Abrasive suspension water jet cutting optimization using orthogonal array design. *Procedia Engineering*, vol. 149, p. 366-373, **DOI:10.1016/j.proeng.2016.06.680**.

[28] Suszynski, Z., Majchrzak, P., Musial, W. (2005). Detection and analysis of subsurface cracks in ground ceramics using thermal wave method. *34th Winter School on Wave and Quantum Acoustics. Journal de Physique IV Proceedings*, vol. 129, p. 275-279, **DOI:10.1051/jp4:2005129056**.

[29] Roy, R.K. (2001). *Design of Experiments Using the Taguchi Approach: 16 Steps to Product and Process Improvement.* John Wiley & Sons Inc., New York.

Vsebina

Strojniški vestnik - Journal of Mechanical Engineering
letnik 63, (2017), številka 10
Ljubljana, oktober 2017
ISSN 0039-2480

Izhaja mesečno

Razširjeni povzetki (extended abstracts)

Strojniški vestnik - Journal of Mechanical Engineering 63(2017)10, SI 81

Prejeto v recenzijo: 2017-01-31
Prejeto popravljeno: 2017-05-18
Odobreno za objavo: 2017-05-29

Homogenost delovnega območja aditivnih tehnologij Primer taljenja z elektronskim snopom

Alexandre Piaget – Matthieu Museau* – Henri Paris
Univerza Alpes v Grenoblu, Francija

Uporaba aditivnih tehnologij (AM - angl. *Additive Manufacturing*) vse bolj narašča. Aditivne tehnologije postajajo ključna orodja v sodobni industriji. V omenjeno skupino sodi taljenje z elektronskim snopom (EBM - angl. *Electron Beam Melting*). Pri tem postopku se za izdelavo izdelkov uporablja elektronski snop kot vir energije za taljenje kovinskega prašnega materiala nanešenega po slojih. Študija se osredotoča na homogenost delovnega območja pri postopku taljenja z elektronskim snopom. S preizkusi je bilo ugotovljeno, da se dva podobna testna izdelka, izdelana na različnih lokacijah delovnega območja, med seboj razlikujeta po obliki, lastnostih in dimenzijah. Ker homogenost delovnega območja v literaturi o slojevitih tehnologijah ni obravnavana, v tej študiji predstavljamo, preizkušamo in razpravljamo o metodah za karakterizacijo delovnega območja.

Preizkus je bil izveden na stroju Arcam AB A1. Uporabljen je bil material Ti-6Al-4V. Delovno območje je bilo okarakterizirano z večkratno izdelavo testnega kosa na različnih lokacijah in opazovanjem odstopanj med izdelanimi testnimi kosi. Za prikaz in merjenje geometrijskih in dimenzijskih napak sta bili pri izdelavi testnega kosa uporabljeni dve različni strukturi (mrežasta in polna). Izmerjene napake so bile karakterizirane in povezane z lokacijo delovnega območja, na katerem je bil izdelan testni kos.

Rezultati preizkusa so pokazali močno povezavo med lokacijo izdelave in izmerjenimi geometrijskimi in dimenzijskimi napakami. Ugotovljeno je bilo, da se z oddaljevanjem od središčne točke delovnega območja, po Z-ravnini slabša kakovost izdelave. Meritve so pokazale do 10 % odstopanja dimenzij zaradi izgube materiala. Napake so se v začetnih slojih pojavljale do višine 8 mm.

Ena od rešitev za omenjene napake je implementacija 8 mm visokih podpornih ravnin, na katere se nanese začetne sloje. S tem se prenesejo napake iz začetnih slojev na podpore. Druga možnost, s katero se izognemo napakam je zmanjšanje delovnega območja na valj z radijem 86 mm. Preizkusi so namreč pokazali, da se napake pojavljajo preko omenjene velikosti radija.

Za boljše razumevanje pojava, ki vodi do heterogenosti delovne površine so bile izvedene podrobnejše analize. Rezultati so pokazali razliko v gostoti prašnega materiala (3,5 % med središčem delovne površine in robovi), kar še dodatno potrjuje heterogenost delovne površine. Sintranje je na robnih območjih delovne površine šibkejše. Zaradi tega so kosi slabše pritrjeni in se med postopkom izdelave premikajo. Ta pojav povzroči izgubo materiala v slojih. Poleg tega prašni material na robovih delovnega območja prevaja manj toplotne energije, dovedene z elektronskim snopom. Manjša odvedena toplota povzroča geometrijske deformacije.

Obravnavana metodologija je prvi korak za karakterizacijo homogenosti delovne površine v primeru uporabe tehnologije EBM. Zanimivo dopolnilo bi bila primerjava z drugimi tehnologijami. V študiji je bil ugotovljen izvor napak, toda resnični pojav in načini za odpravo le-teh niso bili potrjeni. Kljub temu sta bili predstavljeni, preizkušeni in validirani dve rešitvi, s katerimi se lahko delno izogibamo pojavu napak.

Ključne besede: Aditivne tehnologije, upravljanje kakovosti, homogenost delovnega območja

*Naslov avtorja za dopisovanje: Inženirski iinštitut, Univerza Alpes v Grenoblu, Laboratorij G-SCOP, 46 Félix Viallet, Grenoble, Francija, matthieu.museau@g-scop.fr

Strojniški vestnik - Journal of Mechanical Engineering 63(2017)10, SI 82

Prejeto v recenzijo: 2017-05-19
Prejeto popravljeno: 2017-06-29
Odobreno za objavo: 2017-07-19

Cenovno ugodna naprava za DLP stereolitografijo

Joško Valentinčič[1,*] – Matej Peroša[1] – Marko Jerman[1] – Izidor Sabotin[1] – Andrej Lebar[1,2]
[1]Univerza v Ljubljani, Fakulteta za strojništvo, Slovenija
[2]Univerza v Ljubljani, Zdravstvena fakulteta, Slovenia

Smer razvoja stereolitografije temelječe na digitalnem procesiranju svetlobe (angl. Digital Light Processing, DLP) je krajšanje izdelovalnih časov in večanje natančnosti izdelave. V primerjavi s tehnologijo ciljnega nalaganja (angl. Fused Deposition Modelling, FDM) je izdelava z DLP- stereolitografijo bistveno bolj natančna in površine izdelkov imajo boljšo hrapavost. Vendar so naprave za stereolitografijo bistveno dražje in prav zato se ne tako množično uporabljajo kot naprave za ciljno nalaganje.

V prispevku obravnavamo tri glavne izzive cenovno ugodne DLP-stereolitografije: neenakomerno jakost osvetlitve komercialnih DLP-projektorjev, smer osvetlitve in izbiro optimalnih izdelovalnih parametrov. V ta namen smo izdelali dve prototipni napravi za DLP-stereolitografijo; ena osvetljuje gladino fotopolimerne tekočine in izdelek se med nastajanjem potaplja v bazen, druga osvetljuje dno bazena in izdelek se dviga iz dna bazena običajno tudi nad gladino fotopolimera. Obe napravi uporabljata enako programsko in strojno opremo. NC-kodo za izdelavo se pripravi v programski opremi Creation Workshop (DataTree3D Ltd., USA) na osebnem računalniku, ki je povezan z mikrokrmilnikom Arduino Mega 2560. Slednji posreduje ukaze gonilniku Gecko (Geckodrive Inc., USA), ki poganja koračni motor z ločljivostjo 1,8°. Ker ima vreteno korak navoja 2 mm, je ločljivost osi z enaka 0,01 mm. Obe napravi uporabljata DLP-projektor Acer P1500 z ločljivostjo 1920 × 1080 točk in svetilnostjo 3000 lumnov. Uporabljali smo fotopolimer Deep Black (Fun ToDo, Netherlands).

S fotografiranjem izvora svetlobe in ustrezno obdelavo slike v programskem okolju Matlab smo ugotovili, da je jakost svetlobe občutno manjša na robovih projicirane svetlobe, kar je verjetno posledica optičnega sistema DLP-projektorja. Zato smo v programskem okolju Microsoft Visual studio C++ izdelali masko in jo uporabili v programu Creation Workshop (DataTree3D Ltd., USA) pri pripravi NC-kode. Masko smo uporabili pri obeh načinih osvetljevanja fotopolimera, izdelali testne izdelke in jih primerjali tako vizualno kot tudi s stališča natančnosti izdelave. Izkaže se, da se boljše rezultate doseže pri osvetljevanju dna bazena, kjer polimerizacija poteka brez prisotnosti kisika. Za ta primer DLP-stereolitografije smo določili optimalne izdelovalne parametre. Pri planiranju preizkusov smo uporabili ortogonalne matrike in rezultate obdelali po Taguchiju z metodo odzivnih površin (angl. Surface Response Methodology).

Materialni stroški izdelave naprave za DLP stereolitografijo niso presegali 1500 €. Z uporabo maske smo dosegli enako kvaliteto tiskanja po celotni izdelovalni površini. Maska deluje tako, da zmanjša jakost osvetlitve na mestih, kjer je osvetlitev močnejša. S tem so se izdelovalni časi močno povečali; čas potreben za osvetljevanje enega sloja je 16,5 s. Ostala optimalna izdelovalna parametra sta: debelina sloja 0,06 mm in čas med dvema osvetlitvama 4 s. Pri osvetljevanju dna bazena smo s temi parametri dosegli natančnosti izdelave 30 µm v smeri x, 10 µm v smeri y in 80 µm v smeri z. Zaradi dolgih časov osvetljevanja sloja razvita naprava ni primerna za profesionalno uporabo. Za ta namen je treba uporabiti boljši sistem osvetljevanja, kar bistveno poveča ceno naprave. Poleg tega so še tudi druge možnosti za izboljšanje naprave: povečanje ločljivosti osvetljevanja (zmanjšanje velikosti pike) z uporabo optičnega sistema, ki pomanjša sliko projiciranja, in izboljšanje vzporednosti med platformo, kjer nastaja izdelek in dnom bazena.

Ključne besede: DLP-stereolitografija, maska, osvetljevanje, ortogonalne matrike, metoda odzivnih površin

*Naslov avtorja za dopisovanje: Univerza v Ljubljani, Fakulteta za strojništvo, Aškerčeva 6, 1000 Ljubljana, Slovenija, jv@fs.uni-lj.si

Strojniški vestnik - Journal of Mechanical Engineering 63(2017)10, SI 83

Prejeto v recenzijo: 2017-02-14
Prejeto popravljeno: 2017-06-27
Odobreno za objavo: 2017-09-14

Optimizacija hibridne izdelave za izboljšanje kakovosti površine, porabe materiala in produktivnosti

Damir Grguraš, Davorin Kramar
Univerza v Ljubljani, Fakulteta za strojništvo, Slovenija

Hibridna izdelava (ang. *hybrid manufacturing*) je izdelava enega izdelka z dvema ali več različnimi izdelovalnimi tehnologijami. Značilnost hibridne izdelave je, da združi dobre lastnosti vseh uporabljenih izdelovalnih tehnologij in obenem odstrani slabe lastnosti posamezne izdelovalne tehnologije.

V tej raziskavi je predstavljena hibridna izdelava s postopkom ciljnega nalaganja taljenega polimera (ang. *Fused Deposition Modeling – FDM)* in frezanja. Vzorčni izdelki, kocke dimenzij 22 mm × 22 mm × 22 mm, so bili izdelani s postopkom FDM iz materiala PLA, hrapavost zunanjih površin izdelka pa je bila izboljšana s postopkom frezanja.

FDM je najbolj pogost postopek dodajanja materiala po plasteh, kjer material prihaja v neprekinjen toku skozi ekstrudorsko šobo. Material je običajno termoplastični polimer (najpogosteje PLA ali ABS), ki ga naprava segreje do določene temperature in v obliki tanke nitke nalaga na podlago, ter na ta način gradi izdelek. Material prihaja skozi ekstrudorsko šobo, ki je pri večini FDM sistemov standardnega premera $D_1 = 0{,}4$ mm. S ciljem skrajšanja proizvodnega časa in povečanja produktivnosti, je v tej raziskavi bila uporabljena tudi ekstrudorska šoba večjega premera $D_2 = 1{,}1$ mm.

Cilj raziskave je bil poiskati optimalne vhodne – tehnološke parametre hibridne izdelave (višina plasti nalaganja materiala, kompenzacijski pretok materiala, hitrost nalaganja materiala, vrtilna hitrost frezala, podajalna hitrost frezala in globina frezanja) za dosego maksimalne produktivnosti ob minimalni porabi materiala in najboljši kakovosti obdelane površine. Zato so bili kot izhodni parametri izbrani naslednji: hrapavost obdelane površine, poraba materiala in čas hibridne izdelave.

S pomočjo Taguchijeve ortogonalne matrike L_{27} (3^{13}) sta bila oblikovana dva ločena načrta eksperimentov (za ekstrudorski šobi premera D_1 in D_2). Vpliv vhodnih parametrov na izhodne je bil popisan s pomočjo empiričnega modeliranja in pridobljenih regresijskih modelov. Pridobljeni regresijski modeli so bili ovrednoteni preko vrednosti R^2, prilagojenega in predvidenega R^2, ter preko razmerja signal/šum in so bili označeni kot zanesljivi.

Pridobljene rezultate in ugotovitve za obe ekstrudorski šobi premera D_1 in D_2 je možno interpretirati na enak način, kakor sledi. Ugotovljeno je bilo, da ima na hrapavost površine po hibridni izdelavi največji vpliv višina plasti nalaganja materiala. In sicer, za dosego minimalne hrapavosti obdelane površine je potrebno izbrati največjo višino plasti nalaganja materiala. Da se prepreči ovijanje materiala na frezalo in posledično poslabšanje hrapavosti obdelane površine, je potrebno izbrati najmanjšo vrtilno hitrost, ter največjo podajalno hitrost frezala. Minimalna globina frezanja zagotavlja najmanjšo hrapavost obdelane površine v primeru uporabe ekstrudorske šobe standardnega premera D_1. V primeru uporabe ekstrudorske šobe večjega premera D_2 pa globina frezanja nima signifikantnega vpliva na hrapavost površine. Na porabo materiala ima največji vpliv kompenzacijski pretok materiala, ki vpliva premosorazmerna. Ta parameter je tudi ne vpliven na hrapavost obdelane površine, zato je kot optimalna vrednost tega parametra izbrana minimalna vrednost. Na čas potreben za hibridno izdelavo premosorazmerna vplivata višina plasti nalaganja materiala in hitrost nalaganja materiala. Ugotovljeno je bilo, da je pri obeh ekstrudorskih šobah možno doseči enako hrapavost površine po hibridni izdelavi, le da pri uporabi ekstrudorske šobe večjega premera D_2 dosežemo trikratni časovni prihranek. Torej, trikratno povečanje produktivnosti ob ne poslabšani kakovosti površine, je možno doseči ob uporabi ekstrudorske šobe večjega premera $D_2 = 1{,}1$ mm namesto standardne ekstrudorske šobe premera $D_1 = 0{,}4$ mm.

Za nadaljnje raziskave na tem področju avtorji predlagajo optimizacijo istih tehnoloških parametrov takšne hibridne izdelave za primer uporabe materiala ABS, ki je poleg uporabljenega materiala PLA v tej raziskavi, najpogosteje uporabljen polimer pri postopku FDM.

Ključne besede: hibridna izdelava, ciljno nalaganje taljenega polimera, frezanje, material PLA, načrtovanje eksperimentov, empirično modeliranje in optimizacija, metodologija odzivne površine

*Naslov avtorja za dopisovanje: Univerza v Ljubljani, Fakulteta za strojništvo, Aškerčeva 6, 1000 Ljubljana, Slovenija, damir.grguras@fs.uni-lj.si

Strojniški vestnik - Journal of Mechanical Engineering 63(2017)10, SI 84

Prejeto v recenzijo: 2017-01-26
Prejeto popravljeno: 2017-04-14
Odobreno za objavo: 2017-06-06

Vpliv obdelave površine aluminijevih zlitin na lastnosti obdelave s pulzirajočim vodnim curkom

Jiri Klich* – Dagmar Klichova – Vladimir Foldyna – Petr Hlavacek – Josef Foldyna
Inštitut za geoniko Češke akademije znanosti, Republika Češka

Članek obravnava vpliv erozije pulzirajočega vodnega curka (PVC) na površino aluminijevih zlitin, ki so bile predhodno obdelane z različnimi obdelovalnimi postopki. Raziskava obravnava vpliv začetne topografije površine na končno topografijo vzorca izpostavljenega PVC. Dimenzije vzorcev so bile 10 x 60 x 100 mm. Hrapavost vzorcev je bila merjena z optičnim profilometrom pred izpostavitvijo PVC. Za primerjavo hrapavosti površin pred in po obdelavi s PVC je bil uporabljen parameter Ra_{ratio}, ki predstavlja razmerje med hrapavostjo površine po obdelavi s PVC (Ra) in hrapavostjo površine pred obdelavo s PVC (Ra_{ini}).

Za potrebe izvajanja eksperimentov je bil razvit sledeči postopek. Robotska roka je zagotavljala premik šobe PVC po točno določeni trajektoriji. V eksperimentih so bile uporabljene hitrosti prehoda 0,5 mm·s^{-1}; 0,75 mm·s^{-1}; 1 mm·s^{-1}; 2 mm·s^{-1} in 4 mm·s^{-1} ter odmik šobe PVC od površine vzorca 55 mm. Razdalja odmika je bila določena kot optimalna v prejšnjih poizkusih. Kot vpada PVC na površino vzorca je bil 90°. Poizkusi so bili izvedeni pri tlaku črpalke 20 MPa. Nihanja tlaka so bila ustvarjena v generatorju PVC s frekvenco 20,09 kHz. Vsak vzorec je bil izpostavljen PVC na petih območjih, glede na predhodno določen potek eksperimentov, ki je bil osnovan na različnih hitrostih prehoda PVC. Po obdelavi s PVC so bile površine pravtako merjene z optičnim profilometrom.

Iz rezultatov je razvidno, da se pri hitrosti prehoda 4 mm·s^{-1} hrapavost Ra bistveno ne razlikije od začetne hrapavosti. Hrapavosti vzorcev po obdelavi s PVC si, glede na začetno obdelavo, sledijo od največje proti najmanjši: grobo frezana površina, valjana površina in fino frezana površina. Pri hitrosti prehoda 2 mm·s^{-1} ima PVC še večji učinek na hrapavost, kar se najbolj izrazi pri povečanju hrapavosti valjane površine. Pri hitrosti prehoda 1 mm·s^{-1} je učinek PVC še večji in hrapavost valjane površine skokovito naraste v primerjavi s hitrostjo prehoda 2 mm·s^{-1}. V nasprotju z valjano površino se na frezanih površinah hrapavosti ne povečata izrazito. Pri hitrosti prehoda 0,75 mm·s^{-1} se hrapavost vseh površin, razen fino frezane, izrazito poveča. Pri najnižji hitrosti prehoda se pojavi zelo veliko odnašanje materiala na vseh površinah, kar se odraža tudi v izrazitem povečanju hrapavosti.

Glede na parameter hrapavosti površinskih slojev Ra, v odvisnosti od hitrosti prehoda, je analiziran učinek erozije PVC. Ugotovljeno je, da ima obdelovalni postopek površine pred izpostavitvijo PVC velik vpliv na topografijo površine po obdelavi s PVC.

Površine, katerim obdelovalni postopek izrazito spremeni lastnosti (frezanje), izkazujejo mnogo večjo odpornost na PVC kot preoblikovane površine (valjane) in imajo posledično manjšo hrapavost. Medtem ko je povečanje hrapavosti frezanim (grobo ali fino) približno enako, se valjanim površinam, po obdelavi s PVC, hrapavost poveča do 150 krat. Tako povečanje hrapavosti valjanih površin je posledica manjšega utrjevanja in posledično manjše odpornosti površine na PVC. Najvišja hrapavost je bila dosežena pri najnižji hitrosti prehoda, saj ima tako PVC največ časa za erozijo površine.

Praktični pomen teh eksperimentov je določitev optimalne tehnologije izdelave površine za nadaljnjo obdelavo s PVC. Ta podatek bi lahko pripomogel k optimizaciji postopka obdelave s PVC in zmanjšal stroške proizvodnje.
Keywords: pulsating water jet, surface topography, material erosion

*Naslov avtorja za dopisovanje: Inštitut za geoniko Češke akademije znanosti, Ostrava, 70800, Republika Češka, jiri.klich@ugn.cas.cz

Strojniški vestnik - Journal of Mechanical Engineering 63(2017)10, SI 85

Prejeto v recenzijo: 2017-01-26
Prejeto popravljeno: 2017-05-19
Odobreno za objavo: 2017-06-13

Vplivi kontinuiranega in pulzirajočega vodnega curka na kompozit CNT/beton

Vladimir Foldyna[1, 2,*] – Josef Foldyna[2] – Dagmar Klichova[2] – Jiri Klich[2] – Petr Hlavacek[2] – Lenka Bodnarova[3] – Tomas Jarolim[3] – Katerina Mamulova Kutlakova[1]

[1] Tehniška Univerza v Ostravi, Nanotehnološki center, Republika Češka
[2] Inštitut za geoniko na ASCR, Oddelek za razpad materialov, Republika Češka
[3] Tehnološka Univerza v Brnu, Fakulteta za gradbeništvo, Republika Češka

V članku predstavljamo prve rezultate raziskave na temo odpornosti kompozita ogljikove nanocevke/beton (CNT/beton) na vpliv kontinuiranega in pulzirajočega vodnega curka. CNT predstavljajo eno izmed najbolj obetajočih polnil za izboljšanje lastnosti nanokompozitnega betona. Možne izboljšave fizikalnih in mehanskih lastnosti nanokompozitov s cementno osnovo bi lahko vodile do nove generacije ultra-visoko zmogljivega betona. Izboljšane lastnosti vodijo v zmanjšane dimenzij strukturnih betonskih elementov, kar ima ugodne ekonomske in okoljske vplive. Lastnosti visokohitrostnega vodnega curka lahko uporabimo za določevanje kakovosti betona. Opravljeni preizkusi so usmerjeni v določevanje erozijskega učinka pulzirajočega (PVC) in kontinuiranega vodnega curka (KVC), ki udarja ob površino referenčnega materiala (beton) in kompozita CNT/beton.

V splošnem opazimo večje razlike v odpornosti preizkušancev na vpliv PVC in KVC pri delovnih tlakih višine 20 MPa. Hitrost odnašanja materiala pri CNT/beton kompozitnih preizkušancih v primerjavi z referenčnim materialom je bila v razmerju od 69 % do 94 % v primeru PVC in v razmerju 27 % do 83 % v primeru uporabe KVC. Pri tem smo upoštevali hitrost odnašanja materiala za referenčni material kot 100 %. Pri prehodu preizkušanca s PVC opazimo globlje brazde, kjer so bila odstranjena tudi večja kamnita zrna iz cementne matrice. Po drugi strani pa je KVC odstranil le zgornjo plast cementne matrice in samo majhna kamnita zrna.

Podobne rezultate opazimo pri delovnem tlaku 40 MPa. Hitrost odnašanja materiala pri vzorcih iz kompozita CNT/beton v primerjavi z referenčnim preizkusom je bila izmerjena v intervalu od 78 % do 99 % za PVC in med 25 % do 93 % za KVC.

Rezultati kažejo, da izkazuje kompozit CNT/beton višjo odpornost glede na referenčni beton tako pri uporabi PVC kot KVC v območju preizkušenih parametrov. Omenjeno lahko pripišemo dejstvu, da dodajanje CNT cementni matrici spremeni lastnosti rezultirajočega betona v smislu večje obrabne obstojnosti na delovanje tako PVC kot KVC. Pri ostalih merjenih lastnostih nismo opazili signifikantnih razlik med kompozitom CNT/beton in referenčnim betonom. Iz tega razloga je v prihodnosti potrebno izvesti dodatne preizkuse pri uporabi cementne paste z in brez dodatka CNT.

Prvi rezultati raziskave na temo obstojnosti betona z dodatkom CNT glede na udar s PVC in KVC vodijo do sledečih zaključkov:

- fizikalne in mehanske lastnosti referenčnega betona in kompozita CNT/beton se niso signifikantno razlikovale po 7 dnevnem obdobju. Preiskava preizkušancev z rentgensko praškovno difrakcijo in vrstičnim elektronskim mikroskopom ni pokazala signifikantnih razlik v strukturi referenčnega in kompozitnega betona;
- navkljub zgornjemu zaključku rezultati kažejo na večjo odpornost kompozita CNT/beton v primerjavi z referenčnim materialom na delovanje PVC in KVC. To dokazuje, da dodajanje CNT cementni matrici spremeni lastnosti, ki povečajo odpornost rezultirajočega betona;
- za namen razlage opaženega učinka je potrebno opraviti dodatne raziskave v smeri določanja vpliva CNT na proces hidracije cementne paste z rentgensko praškovno difrakcijo ter vrstičnim in transmisijskim elektronskim mikroskopom neposredno pred opravljanjem preizkusov po 28 dnevih sušenja. Dodatno je potrebno raziskati tudi vpliv VC na vzorce iz paste CNT/cement.

Ključne besede: pulzirajoči vodni curek, kontinuirani vodni curek, ogljikove nanocevke (CNT), betonski kompozit, odnašanje materiala

*Naslov avtorja za dopisovanje: Tehniška Univerza v Ostravi, Nanotehnološki center, 17. listopadu 15/2172, 70833 Ostrava-Poruba, Republika Češka, vladimir.foldyna@vsb.cz

Strojniški vestnik - Journal of Mechanical Engineering 63(2017)10, SI 86

Prejeto v recenzijo: 2017-01-30
Prejeto popravljeno: 2017-05-22
Odobreno za objavo: 2017-06-27

Avtomatizirana metoda združevanja tekočega traku z armaturo iz jeklenic – ovrednotenje uporabe vodnega curka za proces predpriprave

David Zaremba[1,*] – Patrick Heitzmann[2] – Ludger Overmeyer[2] – Lennart Hillerns[1] – Thomas Hassel[1]
[1]Leibniz Univerza v Hannovru, Inštitut za materiale, Nemčija
[2]Leibniz Univerza v Hannovru, Inštitut za transportne tehnologije in avtomatizacijo, Nemčija

Povečane potrebe svetovnega trga po mineralih vodijo do novih aplikacij čedalje daljših transportnih trakov in sistemov. Razdalja med gnanimi osmi lahko doseže tudi 15 km in več. V ta namen so transportni trakovi predhodno izdelani v segmentih po 300 m, saj je take segmente še možno dostaviti na mesto uporabe. Montaža transportnega traku poteka na mestu same uporabe, kjer se več segmentov poveže v en dolg tekoči trak. Pomemben del sestavljanja je odstranjevanje odvečne gume okrog armature iz jeklenih vrvi na konceh segmenta tekočega traku. Trenutno je to opravilo izvedeno s preprostimi metodami, kot je uporaba tanke žice. Izboljšava omenjenega postopka je nujna, saj lahko avtomatizirana in uporabniško orientirana metoda pomembno zmanjša čas popravila tekočega traku in omogoči kvalitetnejšo združevanje segmentov.

V našem delu predstavljamo raziskavo na temo uporabe visokohitrostnega vodnega curka za namen selektivnega odstranjevanja gume, ki omogoča avtomatizacijo postopka predpriprave za učinkovito združevanje. Cilj raziskave je ovrednotiti učinkovitost, homogenost in selektivnost odstranjevanja gume, pri čemer ne sme priti do poškodb s cinkom oplaščenih jeklenic. Izvedena je bila študija vpliva procesnih parametrov na obliko reza in nastalih površin. Oluščene jeklene vrvi s cinkovim oplaščenjem so bile analizirane z mikrografijo. Ugotovitve kažejo na primernost uporabe vodnega curka za predpripravo segmentov tekočega traku za združevanje in obetajo možnost avtomatizacije. Uporaba komercialno dostopnih črpalk v kombinaciji s ploščato vodno šobo omogoča odstranjevanje gume pri čemer ne pride do poškodb armature iz pocinkanih jeklenic.

Trenutne metode predpriprave za združevanje segmentov tekočega traku, ki se uporabljajo v industriji, vključujejo popolno odstranitev gume iz jeklenic ali pa puščanje tanke plasti gume na jeklenicah. Obe varianti je možno izvesti z uporabo visokohitrostnega vodnega curka. Poleg naštetih prednosti predstavljene metode pred konvencionalnimi pristopi je potrebno izpostaviti možnost izdelave enakomerno hrapave površine na preostali plasti gume na jeklenici. Enakomerno grobo hrapava površina izboljša spajanje segmentov s procesom vulkanizacije zaradi povečane adhezivnosti, ki je posledica povečane kontaktne površine. Predstavljena optimizacija in predpriprava segmenta tekočega traku omogoča razvoj stroja za avtomatizirano predpripravo in združevanje.

Ključne besede: transportni trak, jeklena armatura, spajanje jeklenice, sanacija, avtomatizacija, vodni curek

*Naslov avtorja za dopisovanje: Leibniz Univerza v Hannovru, Inštitut za materiale, An der Universität 2, D-30823 Garbsen, Nemčija. zaremba@iw.uni-hannover.de

Strojniški vestnik - Journal of Mechanical Engineering 63(2017)10, SI 87

Prejeto v recenzijo: 2017-03-01
Prejeto popravljeno: 2017-05-29
Odobreno za objavo: 2017-06-16

Določevanje obrabe fokusirne šobe z merjenjem premera abrazivnega vodnega curka

Miha Prijatelj[1] – Marko Jerman[1] – Henri Orbanić[1] – Izidor Sabotin[1] – Joško Valentinčič[1] – Andrej Lebar[1,2,*]

[1] Univerza v Ljubljani, Fakulteta za strojništvo, Slovenija
[2] Univerza v Ljubljani, Zdravstvena fakulteta, Slovenija

Obdelava z abrazivnim vodnim curkom (AVC) je postopek rezanja, ki uporablja visoko-hitrostni vodni curek za pospeševanje trdih abrazivnih zrn, ki odnašajo material obdelovanca. Tehnologija omogoča rezanje praktično vseh vrst materialov, s to prednostjo, da se med procesom rezanja material ne segreva bistveno, vendar je omejena z dokaj slabo natančnostjo. Izvor slabe natančnosti leži v nedefinirani rezalni geometriji, fleksibilnem orodju, ki ob vstopu v atmosfero začne razpadati in se med rezanjem ukrivi ter v nenadzorovani obrabi fokusirne šobe. Razpad curka v atmosferi povzroča koničen rez, kar se delno odpravlja z nagibom rezalne glave. Drugi del problema zagotavljanja natančnosti reza je določanje širine reza. Trenutno se za širino reza privzame premer nove fokusirne šobe, kar pomeni, da so kosi odrezani z novo šobo relativno natančni, ko pa se fokusirna šoba začne obrabljati in se širina curka poveča, se tudi natančnost reza zmanjša. Članek obravnava nov pristop k izboljšanju natančnosti reza in zagotavljanju kakovosti procesa z merjenjem premera AVC z linijskim laserjem ter ugotavljanjem povezave širine curka z obrabljenostjo fokusirne šobe.

V eksperimentih je bil uporabljen preprost laserski mikrometer s širino žarka 5 mm, valovno dolžino 780 nm in natančnostjo merjenja 0,01 mm, ter pet različno obrabljenih fokusirnih šob. Dve fokusirni šobi sta bili novi, tri fokusirne šobe pa so bile obrabljene, kar je omogočalo merjenje AVC različnih širin in geometrijskih lastnosti. Premeri fokusirnih šob so bili merjeni z orodjarskim merilnim mikroskopom Mitutoyo TM z natančnostjo 0,001 mm. Merjenje širine AVC je potekalo pri dveh tlakih črpalke, z in brez dodajanja abraziva, pri različnih časih merjenja ter na različnih oddaljenostih od fokusirne šobe. Pri merjenju premera AVC je velik problem predstavljalo pršenje curka, ki je popačilo meritve in pljuskanje vode iz bazena ob vstopu AVC v bazen. Za odpravo tega problema je bilo razvito ohišje, ki mehansko ščiti zaslon laserja pred pljuskanjem in izpihovalni modul, ki je ustvarja zračno zaveso ob zaslonu laserja in s tem odpihuje drobne kapljice. Ohišje omogoča tudi nastavljanje višine merjenja.

Rezultati meritev kažejo, da premer curka izrazito niha, zaradi česar je nemogoče določiti obrabo fokusirne šobe tako natančno kot obrabo trdnih orodij kot je primer pri struženju. Pri primerjavi premera curka z abrazivom in brez abraziva je opaziti, da je premer curka z abrazivom izrazito večji. To je posledica dogajanja v mešalni komori, ko abraziv vstopi v vodni curek in s seboj potegne tudi okoliški zrak, zaradi česar se poveča volumen curka in s tem posledično tudi njegov premer. Opaženo je bilo tudi, da imajo rezultati meritev z abrazivom slabšo ponovljivost in stabilnost. To je rezultat majhnih delcev abraziva, ki priletijo na zaslon laserja in se s časom tam akumulirajo, ker jih izpihovalni modul ne odpihne stran dovolj učinkovito. Zaradi nalaganja te plasti laserski senzor zaznava postopno večanje premera, kar vodi v napačne rezultate. Zaradi teh težav so bile meritve z abrazivom zavržene. Meritve premera pri različnih tlakih so pokazale, da so meritve premera curka bližje premeru fokusirne šobe pri nižjih tlakih, t.j. pri 200 MPa. Meritve pri različno dolgih časih so pokazale, da čas merjenja nima vpliva na standardno deviacijo meritev, ima pa izrazit vpliv na merilno negotovost. Iz eksperimentov je bil določen optimalni čas merjenja 4 s. Meritve na različnih oddaljenostih od konca fokusirne šobe so pokazale, da je dosežena najboljša korelacija med premerom curka in premerom fokusirne šobe pri 1 mm. Opaziti je bilo tudi, da je divergentni kot curka zelo odvisen od obrabe fokusirne šobe. Ob upoštevanju vseh zgoraj naštetih ugotovitev, je merilni modul sposoben izmeriti premer fokusirne šobe z negotovostjo ±0,03 mm. Ker je premer fokusirne šobe uporabljen za nastavitev odmika rezalne glave od konture rezanja, tak podatek zanesljivo pripomore k izboljšanju natančnosti reza. Z rednim merjenjem premera curka je mogoče tudi spremljati obrabo fokusirne šobe in določiti čas, ko je potrebno fokusirno šobo zamenjati. Z implementacijo takega modula v sam stroj za rezanje z AVC in merjenjem premera curka pred vsakim rezanjem ter naknadno korekcijo odmika rezalne glave od konture reza, bi se povečala tudi stopnja avtomatizacije procesa. S tem bi se izboljšala zanesljivost procesa in skrajšal čas, ki ga operater nameni preverjanju ustreznosti komponent.

Ključne besede: abrazivni vodni curek, premer šobe, premer curka, obraba šobe

*Naslov avtorja za dopisovanje: Univerza v Ljubljani, Fakulteta za strojništvo, Aškerčeva 6, 1000 Ljubljana, Slovenija, andrej.lebar@fs.uni-lj.si

Strojniški vestnik - Journal of Mechanical Engineering 63(2017)10, SI 88

Prejeto v recenzijo: 2017-03-20
Prejeto popravljeno: 2017-06-19
Odobreno za objavo: 2017-07-05

Eksperimentalni parametrični matematični model za napovedovanje hrapavosti površine pri rezanju z abrazivnim vodnim curkom

Andrzej Perec [1,2,*] – Frank Pude[1] – Michael Kaufeld[3] – Konrad Wegener[1,4]

[1]ETH Zürich, Inspire AG, Švica
[2]Univerza Jacob of Paradies, Tehnološki oddelek, Poljska
[3]Univerza za uporabne znanosti Ulm, Inštitut za proizvodno strojništvo in preskušanje materialov, Nemčija
[4]ETH Zürich, Inštitut za obdelovalne stroje in izdelavo, Švica

Rezanje z visokotlačnim vodnim curkom je nekonvencionalni postopek obdelave. Rezanje z visokotlačnim abrazivnim vodnim curkom je kompleksnejši proces od konvencionalnih postopkov. Obstoječi modeli za napovedovanje rezultatov rezanja ne podajajo zadovoljivih napovedi na širšem območju procesnih parametrov, še posebej za raznolike materiale. Ena izmed metod modeliranja vpliva procesnih parametrov je metoda Taguchi. Metoda omogoča sistematični pristop k optimizaciji procesa in je uporabno orodje za načrtovanje visoko kakovostnih sistemov. Pri rezanju z abrazivnim vodnim curkom sta tipična optimizacijska kriterija čim večja globina rezanja in čim manjša hrapavost odrezanih površin. V primeru preciznega rezanja je nižja hrapavost rezalne površine ključnega pomena.

V članku je predstavljena uporaba metode Taguchi za napovedovanje obdelovalnih parametrov za doseganje minimalne hrapavosti pri rezanju mikrolegiranega jekla. Predstavljen je vpliv tlaka, masnega pretoka abraziva in podajalne hitrosti na parametra hrapavosti R_z in R_{max}. S pomočjo uporabljene metode so bile določene optimalne vrednosti procesnih parametrov. Izveden je bil tudi verifikacijski preizkus. Z uporabo metode Taguchi smo preko zmanjšanja potrebnega števila eksperimentov in posledično eksperimentalnega časa dosegli signifikantno znižanje stroškov eksperimentalnega dela.

Raziskava je bila opravljena s pomočjo visokotlačne črpalke z ojačevalnikom tipa BYPUMP 50APC. Največji testiran tlak je bil 400 MPa pri volumskem pretoku vode 5 dm^3/min. Uporabljen abraziv je bil Garnet (Almadine) z zrnatostjo 80. Kot material obdelovanca je bilo uporabljeno mikrolegirano jeklo 27MnSiVS6 (DIN 1.5232). To je feritno-perlitno visoko trdnostno jeklo, nizko legirano z manganom in vanadijem.

Izbira optimalnih obdelovalnih parametrov je kompleksen proces. Običajno je potrebno izvesti veliko število eksperimentov s pomočjo katerih je moč oceniti njihov vpliv na željeno karakteristiko končnega izdelka. Načrtovanje eksperimentov se z uporabljeno metodo poenostavi. Za implementacijo metode Taguchi je bil uporabljen program Minitab 16. Vpliv kontrolnih faktorjev je bil analiziran z metodo analize variance – ANOVA.

Na podlagi eksperimentalnih rezultatov, izračuna razmerja signal/šum in potrditve verifikacijskega preizkusa zaključujemo, da so optimalne vrednosti procesnih parametrov sledeče:

- tlak = 360 MPa,
- masni pretok abraziva = 80 g/min,
- podajalna hitrost = 20 mm/min.

Uporabljena metodologija je primerna za raziskave za rezanje novih materialov, s katero je moč pridobiti vpogled v vplive posameznih procesnih parametrov na rezanje.

Ključne besede: abrazivni vodni curek, načrtovanje eksperimentov, optimizacija, rezanje, napovedovanje

*Naslov avtorja za dopisovanje: Univerza Jacob of Paradies, Tehnološki oddelek, Teatralna 25, PL-66 400 Gorzow Wlkp., Poljska, aperec@ajp.edu.pl

DOKTORSKE DISERTACIJE

Na Fakulteti za strojništvo Univerze v Ljubljani je obranil svojo doktorsko disertacijo:

- dne *22. septembra 2017* **Andrej LOTRIČ** z naslovom: »Sistem sočasne proizvodnje toplote in električne energije z visokotemperaturnimi gorivnimi celicami s protonsko prevodnimi membranami« (mentor: prof. dr. Mihael Sekavčnik);

V doktorskem delu smo razvili koncept prototipa majhnega, močnostnega prenosnega sistema, v katerem sta integrirana parni reformer metanola (MSR) in sklad visokotemperaturnih gorivnih celic s protonsko prevodnimi membranami (HT PEMFC). Razvili in izdelali smo reaktor, v katerem je bil uporabljen inovativen katalizator z veliko aktivnostjo za reakcijo MSR. Na osnovi eksperimentalnih podatkov, dobljenih z ločenimi meritvami karakteristik MSR in HT PEMFC sklada, smo izdelali inovativen hibridni numerični model za določitev masnih in energijskih tokov ter energijskega izkoristka integriranega sistema. Eksperimentalni in numerični rezultati potrjujejo izvedljivost avtotermnega energetskega sistema. Podane so smernice za izdelavo prototipa integriranega sistema.

Information for Authors

All manuscripts must be in English. Pages should be numbered sequentially. The manuscript should be composed in accordance with the Article Template given above. The maximum length of contributions is 10 pages. Longer contributions will only be accepted if authors provide juastification in a cover letter. For full instructions see the Information for Authors section on the journal's website: http://en.sv-jme.eu .

SUBMISSION:

Submission to SV-JME is made with the implicit understanding that neither the manuscript nor the essence of its content has been published previously either in whole or in part and that it is not being considered for publication elsewhere. All the listed authors should have agreed on the content and the corresponding (submitting) author is responsible for having ensured that this agreement has been reached. The acceptance of an article is based entirely on its scientific merit, as judged by peer review. Scientific articles comprising simulations only will not be accepted for publication; simulations must be accompanied by experimental results carried out to confirm or deny the accuracy of the simulation. Every manuscript submitted to the SV-JME undergoes a peer-review process.

The authors are kindly invited to submit the paper through our web site: http://ojs.sv-jme.eu. The Author is able to track the submission through the editorial process - as well as participate in the copyediting and proofreading of submissions accepted for publication - by logging in, and using the username and password provided.

SUBMISSION CONTENT:

The typical submission material consists of:

- A **manuscript** (A PDF file, with title, all authors with affiliations, abstract, keywords, highlights, inserted figures and tables and references),
- Supplementary files:
  - a **manuscript** in a WORD file format
  - a **cover letter** (please see instructions for composing the cover letter)
  - a ZIP file containing **figures** in high resolution in one of the graphical formats (please see instructions for preparing the figure files)
  - possible **appendicies** (optional), cover materials, video materials, etc.

Incomplete or improperly prepared submissions will be rejected with explanatory comments provided. In this case we will kindly ask the authors to carefully read the Information for Authors and to resubmit their manuscripts taking into consideration our comments.

COVER LETTER INSTRUCTIONS:

Please add a **cover letter** stating the following information about the submitted paper:

1. Paper **title**, list of **authors** and their **affiliations**.
2. **Type of paper**: original scientific paper (1.01), review scientific paper (1.02) or short scientific paper (1.03).
3. A **declaration** that neither the manuscript nor the essence of its content has been published in whole or in part previously and that it is not being considered for publication elsewhere.
4. State the **value of the paper** or its practical, theoretical and scientific implications. What is new in the paper with respect to the state-of-the-art in the published papers? Do not repeat the content of your abstract for this purpose.
5. We kindly ask you to suggest at least two **reviewers** for your paper and give us their names, their full affiliation and contact information, and their scientific research interest. The suggested reviewers should have at least two relevant references (with an impact factor) to the scientific field concerned; they should not be from the same country as the authors and should have no close connection with the authors.

FORMAT OF THE MANUSCRIPT:

The manuscript should be composed in accordance with the Article Template. The manuscript should be written in the following format:

- A **Title** that adequately describes the content of the manuscript.
- A list of **Authors** and their **affiliations**.
- An **Abstract** that should not exceed 250 words. The Abstract should state the principal objectives and the scope of the investigation, as well as the methodology employed. It should summarize the results and state the principal conclusions.
- 4 to 6 significant **key words** should follow the abstract to aid indexing.
- 4 to 6 **highlights;** a short collection of bullet points that convey the core findings and provide readers with a quick textual overview of the article. These four to six bullet points should describe the essence of the research (e.g. results or conclusions) and highlight what is distinctive about it.
- An **Introduction** that should provide a review of recent literature and sufficient background information to allow the results of the article to be understood and evaluated.
- A **Methods** section detailing the theoretical or experimental methods used.
- An **Experimental section** that should provide details of the experimental set-up and the methods used to obtain the results.
- A **Results** section that should clearly and concisely present the data, using figures and tables where appropriate.
- A **Discussion** section that should describe the relationships and generalizations shown by the results and discuss the significance of the results, making comparisons with previously published work. (It may be appropriate to combine the Results and Discussion sections into a single section to improve clarity.)
- A **Conclusions** section that should present one or more conclusions drawn from the results and subsequent discussion and should not duplicate the Abstract.
- **Acknowledgement** (optional) of collaboration or preparation assistance may be included. Please note the source of funding for the research.
- **Nomenclature** (optional). Papers with many symbols should have a nomenclature that defines all symbols with units, inserted above the references. If one is used, it must contain all the symbols used in the manuscript and the definitions should not be repeated in the text. In all cases, identify the symbols used if they are not widely recognized in the profession. Define acronyms in the text, not in the nomenclature.
- **References** must be cited consecutively in the text using square brackets [1] and collected together in a reference list at the end of the manuscript.
- **Appendix(-icies)** if any.

SPECIAL NOTES

Units: The SI system of units for nomenclature, symbols and abbreviations should be followed closely. Symbols for physical quantities in the text should be written in italics (e.g. *v*, *T*, *n*, etc.). Symbols for units that consist of letters should be in plain text (e.g. ms^{-1}, K, min, mm, etc.). Please also see: http://physics.nist.gov/cuu/pdf/sp811.pdf .

Abbreviations should be spelt out in full on first appearance followed by the abbreviation in parentheses, e.g. variable time geometry (VTG). The meaning of symbols and units belonging to symbols should be explained in each case or cited in a **nomenclature** section at the end of the manuscript before the References.

Figures (figures, graphs, illustrations digital images, photographs) must be cited in consecutive numerical order in the text and referred to in both the text and the captions as Fig. 1, Fig. 2, etc. Figures should be prepared without borders and on white grounding and should be sent separately in their original formats. If a figure is composed of several parts, please mark each part with a), b), c), etc. and provide an explanation for each part in Figure caption. The caption should be self-explanatory. Letters and numbers should be readable (Arial or Times New Roman, min 6 pt with equal sizes and fonts in all figures). Graphics (submitted as supplementary files) may be exported in resolution good enough for printing (min. 300 dpi) in any common format, e.g. TIFF, BMP or JPG, PDF and should be named Fig1.jpg, Fig2.tif, etc. However, graphs and line drawings should be prepared as vector images, e.g. CDR, AI. Multi-curve graphs should have individual curves marked with a symbol or otherwise provide distinguishing differences using, for example, different thicknesses or dashing.

Tables should carry separate titles and must be numbered in consecutive numerical order in the text and referred to in both the text and the captions as Table 1, Table 2, etc. In addition to the physical quantities, such as *t* (in italics), the units [s] (normal text) should be added in square brackets. Tables should not duplicate data found elsewhere in the manuscript. Tables should be prepared using a table editor and not inserted as a graphic.

REFERENCES:

A reference list must be included using the following information as a guide. Only cited text references are to be included. Each reference is to be referred to in the text by a number enclosed in a square bracket (i.e. [3] or [2] to [4] for more references; do not combine more than 3 references, explain each). No reference to the author is necessary.

References must be numbered and ordered according to where they are first mentioned in the paper, not alphabetically. All references must be complete and accurate. Please add DOI code when available. Examples follow.

Journal Papers:

Surname 1, Initials, Surname 2, Initials (year). Title. Journal, volume, number, pages, DOI code.

[1] Hackenschmidt, R., Alber-Laukant, B., Rieg, F. (2010). Simulating nonlinear materials under centrifugal forces by using intelligent cross-linked simulations. *Strojniški vestnik - Journal of Mechanical Engineering,* vol. 57, no. 7-8, p. 531-538, DOI:10.5545/sv-jme.2011.013.

Journal titles should not be abbreviated. Note that journal title is set in italics.

Books:

Surname 1, Initials, Surname 2, Initials (year). Title. Publisher, place of publication.

[2] Groover, M.P. (2007). *Fundamentals of Modern Manufacturing*. John Wiley & Sons, Hoboken.

Note that the title of the book is italicized.

Chapters in Books:

Surname 1, Initials, Surname 2, Initials (year). Chapter title. Editor(s) of book, book title. Publisher, place of publication, pages.

[3] Carbone, G., Ceccarelli, M. (2005). Legged robotic systems. Kordić, V., Lazinica, A., Merdan, M. (Eds.), Cutting Edge Robotics. Pro literatur Verlag, Mammendorf, p. 553-576.

Proceedings Papers:

Surname 1, Initials, Surname 2, Initials (year). Paper title. Proceedings title, pages.

[4] Štefanić, N., Martinčević-Mikić, S., Tošanović, N. (2009). Applied lean system in process industry. *MOTSP Conference Proceedings*, p. 422-427.

Standards:

Standard-Code (year). Title. Organisation. Place.

[5] ISO/DIS 16000-6.2:2002. *Indoor Air – Part 6: Determination of Volatile Organic Compounds in Indoor and Chamber Air by Active Sampling on TENAX TA Sorbent, Thermal Desorption and Gas Chromatography using MSD/FID.* International Organization for Standardization. Geneva.

WWW pages:

Surname, Initials or Company name. Title, from http://address, date of access.

[6] Rockwell Automation. Arena, from *http://www.arenasimulation.com,* accessed on 2009-09-07.

EXTENDED ABSTRACT:

When the paper is accepted for publishing, the authors will be requested to send an **extended abstract** (approx. one A4 page or 3500 to 4000 characters). The instruction for composing the extended abstract are published on-line: http://www.sv-jme.eu/information-for-authors/ .

COPYRIGHT:

Authors submitting a manuscript do so on the understanding that the work has not been published before, is not being considered for publication elsewhere and has been read and approved by all authors. The submission of the manuscript by the authors means that the authors automatically agree to transfer copyright to SV-JME when the manuscript is accepted for publication. All accepted manuscripts must be accompanied by a Copyright Transfer Agreement, which should be sent to the editor. The work should be original work by the authors and not be published elsewhere in any language without the written consent of the publisher. The proof will be sent to the author showing the final layout of the article. Proof correction must be minimal and executed quickly. Thus it is essential that manuscripts are accurate when submitted. Authors can track the status of their accepted articles on http://en.sv-jme.eu/.

PUBLICATION FEE:

Authors will be asked to pay a publication fee for each article prior to the article appearing in the journal. However, this fee only needs to be paid after the article has been accepted for publishing. The fee is 240.00 EUR (for articles with maximum of 6 pages), 300.00 EUR (for articles with maximum of 10 pages), plus 30.00 EUR for each additional page. The additional cost for a color page is 90.00 EUR. These fees do not include tax.

Strojniški vestnik -Journal of Mechanical Engineering
Aškerčeva 6, 1000 Ljubljana, Slovenia,
e-mail: info@sv-jme.eu

9 770039 248001
ISSN 0039-2480

http://www.sv-jme.eu

Contents

Papers